

DOTTORATO DI RICERCA IN BIOLOGIA CELLULARE E MOLECOLARE

Ciclo 37

Settore Concorsuale: 05/E1 - BIOCHIMICA GENERALE

Settore Scientifico Disciplinare: BIO/10 - BIOCHIMICA

USE OF BIOENERGETICALLY ACTIVE MEMBRANES FOR THE STUDY OF GREEN CHEMICALS

Presentata da: Tancredi Bin

Coordinatore Dottorato Supervisore

Anna Maria Porcelli Francesco Francia

Co-supervisore

Anna Maria Ghelli

Abstract

lonic liquids (ILs) represent promising, more sustainable substitutes for canonical volatile organic compounds in many industries. Yet, their toxicity is still debated. While their impact on ecotoxicological model organisms has been extensively studied, and though it is known how their ability to interact with biological membranes is the determining factor at the base of their toxicity, a detailed understanding of ILs interaction with native membranes is still missing. In this context, we investigated ILs effect on bioenergetically active membranes using chromatophores, photosynthetic vesicles isolated from the purple non-sulfur bacteria Rhodobacter capsulatus. and bovine-heart derived submitochondrial particles. Chromatophores bear carotenoids associated to the light-harvesting complex II whose visible spectrum of absorbance responds linearly to the membrane electrical potential ($\Delta\Psi$), acting as an intramembrane voltmeter. We utilised this carotenoid shift to obtain information on the $\Delta\Psi$ dissipation in the presence of ILs. Moreover, we tested the compounds effect on the electron transfer reactions occurring within the cytochrome bc1 and the light-driven ATP synthesis of chromatophores, and in vivo on the photosynthetic growth of Rb. capsulatus. Subsequently, we tested ILs on submitochondrial particles, investigating their effect on the electron transport, and on the activity of complexes I, III and IV of the mitochondrial electron transport chain.

ILs were able to collapse the $\Delta\Psi$ at micromolar concentrations by increasing the ionic current across the chromatophores lipid bilayer, with bis(trifluoromethylsulfonyl)amide (Ntf₂-) containing ILs being particularly effective. The compounds did not significantly inhibit cytochrome bc_1 electron transfer reactions. Still, Ntf₂ caused a drammatic decrease in light-driven ATP synthesis, and was able to inhibit the bacterium growth at millimolar concentrations.

Finally, we found the ILs tested on submitochondrial particles to exert a primary effect of inhibition of the electron transport chain complexes at concentrations of tens of millimolar, with a secondary effect on the membrane electrochemical potential.

Table of contents

1. Introduction	1
1.1 Ionic liquids: structure and properties	2
1.2 Ionic liquids applications	5
1.3 Ionic liquids toxicity	8
1.4 Chromatophores as a model for bioenergetically active membranes	10
1.5 Bovine heart submitochondrial particles	14
2. Aims of the study	19
3. Materials and Methods	21
3.1 Materials	21
3.2 Bacterial growth and chromatophores isolation	21
3.3 Chromatophores visible absorption spectrum characterisation	22
3.4 Time-resolved evolution of the carotenoid shift and ILs titration	22
3.5 Spectrophotometric assay of Cytochrome bc_1 electron transfer reactions	23
3.6 Quantitative bioluminescence assay of chromatophores ATP synthesis	24
3.7 Rb. Capsulatus photosynthetic growth	25
3.8 Isolation of submitochondrial particles from bovine heart tissue	26
3.9 Reverse electron transfer assay	28
3.10 NADH:O₂ assay	28
3.11 Complex I activity assay	28
3.12 Complex III activity assay	28
3.13 Complex IV activity assay	29
4. Results	31
4.1 Isolated chormatophores characterisation	31
4.2 Kinetics of the carotenoid shift decay in the presence of ILs	33
4.3 Interpretation model and data analysis	35
4.4 ILs effect on membrane ionic current	43
4.5 Reversibility of the Ntf ₂ ⁻ anion effect on carotenoid shift	46
4.6 Ntf ₂ ⁻ anion effect on cytochrome <i>bc</i> ₁	47
4.7 ILs effect on chromatophores light-driven ATP synthesis	48
4.8 Ionic liquids effect on <i>Rb</i> . <i>Capsulatus</i> photosynthetic growth	50
4.9 Effect of ionic liquids on mitochondrial reverse electron transfer	54
4.10 ILs effect on ETPH NADH consumption in phosphorylating conditions	55
4.11 Effect of ILs on Complex I activity	57

	4.12 ILs effect on CIII and CIV activities	59
5.	Discussion	61
6.	Bibliography	65

1. Introduction

Over the last twenty years, *green* chemistry has put increasing effort into researching new, more sustainable compounds of both academic and industrial interest, aiming on reducing the impact of human activities on the environment. In this context, Ionic liquids (ILs) have gained growing interest as possible substitutes for canonical volatile organic compounds (VOC) in many fields, thanks to their unique physical and chemical features. This is well displayed by the number of publications regarding ILs (Fig. 1.1), which has raised substantially over the last two decades, stabilising at around 5000 scientific papers being published every year over the last ten years (Li & Chu, 2023). This trend is mirrored by the increase in patents, which has stabilised to around 800 applications every year in the late 2010's (Morton & Hamer, 2018). Yet, their presence on the market is still quite limited. Up until 2020, it was estimated that over 500 ILs were commercially available in quantitites below 10 kg, tens in the 10-1000 kg range, and about 10 in quantitites over one metric ton (Tullo, 2020). Although these numbers are destined to grow in the next few years, more than one point of concern has been raised regarding ILs sustainability, most importantly about their effect on living organisms. In this context, understanding the mechanism of ILs toxicity is a primary necessity for their synthesis and application.

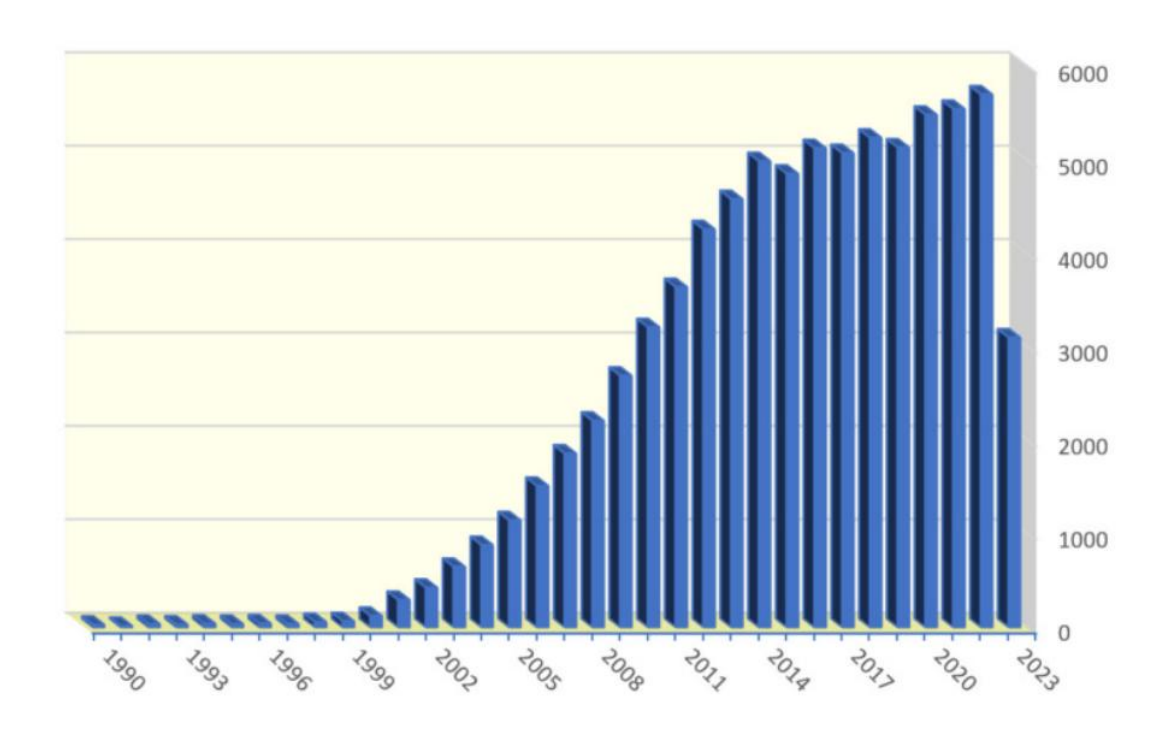


Figure 1.1 Number of scientific publications over the years on the subject "lonic liquids" up until 14th July 2023, determined by a search carried out using SciFinderⁿ (Li & Chu, 2023).

1.1 Ionic liquids: structure and properties

ILs are salts composed of an organic cation and an organic or inorganic anion, with a melting point below 100°C (Wilkes, 2002). Among the commonly used cations, we find mostly bulky and non-symmetric moieties such as *N,N'*-substituted imidazolium, *N*-substituted pyrrolidinium and pyridinium, and tetra-alkylated ammonium and phosphonium (Khoo et al., 2024), while anions span from simple halides to more complex organic ions (**Fig. 1.2**). ILs synthesis is generally straight forward: first, the cation core (amine, phosphine, etc.) is functionalised by heating and stirring in the presence of the desired haloalkane, leading to quaternization, then the anion is added through anion exchange or anion metathesis (Gujjala et al., 2024). Alternatively, microwave irradiation and ultrasound-assisted reactions have been reported as efficient, fast and solvent-free methods for ILs synthesis (Martínez-Palou, 2010; Chatel & Macfarlane, 2014).

The vast realm of possible combinations of ions, together with the great variety of substituent groups and the length and degree of functionalization of the alkyl chains (Welton, 2018), allows for a remarkable theoretical number of synthesizable compounds. In this sense, the sole binary mixtures are estimated to be at least one million (Rogers & Seddon, 2003). This intrinsic combinatorial broadness reflects in the considerable qualitative plasticity of these compounds, whose chemical and physical properties can be tailored to specific tasks by simply chosing the right combination of ions, gaining ILs the reputation of "designer solvents" (Plechkova & Seddon, 2007; Giernoth, 2010).

The physical and chemical features of ILs are determined by the nature and size of the ions, as well as by the balance of Coulomb, Van der Waals and π - π interactions and hydrogen bonds (Angell et al., 2007; Hu & Peng, 2014; Hayes et al., 2015). Their low melting point is due to the high degree of asymmetry of the ions molecular structure, a feature that is common to all ILs (Welton, 1999). In this regard, the length of the cation alkyl chain has an important role and it has been observed that, for a number of carbon atoms lower than 12, a longer chain correlates to a lower melting point. Yet, for longer alkyl chain, the melting point tends to rise (Hu & Peng, 2014; Hayes et al., 2015). Imidazolium-based ILs are generally more thermally stable than tetralkylammonium ones, with variations depending on the specific cation (Ngo et al., 2000). Dicationic imidazolium-based ILs usually show a higher stability than monocationic ones, while the thermal degradation of both does not seem to correlate linearly to the alkyl chain length (Bender et al., 2019).

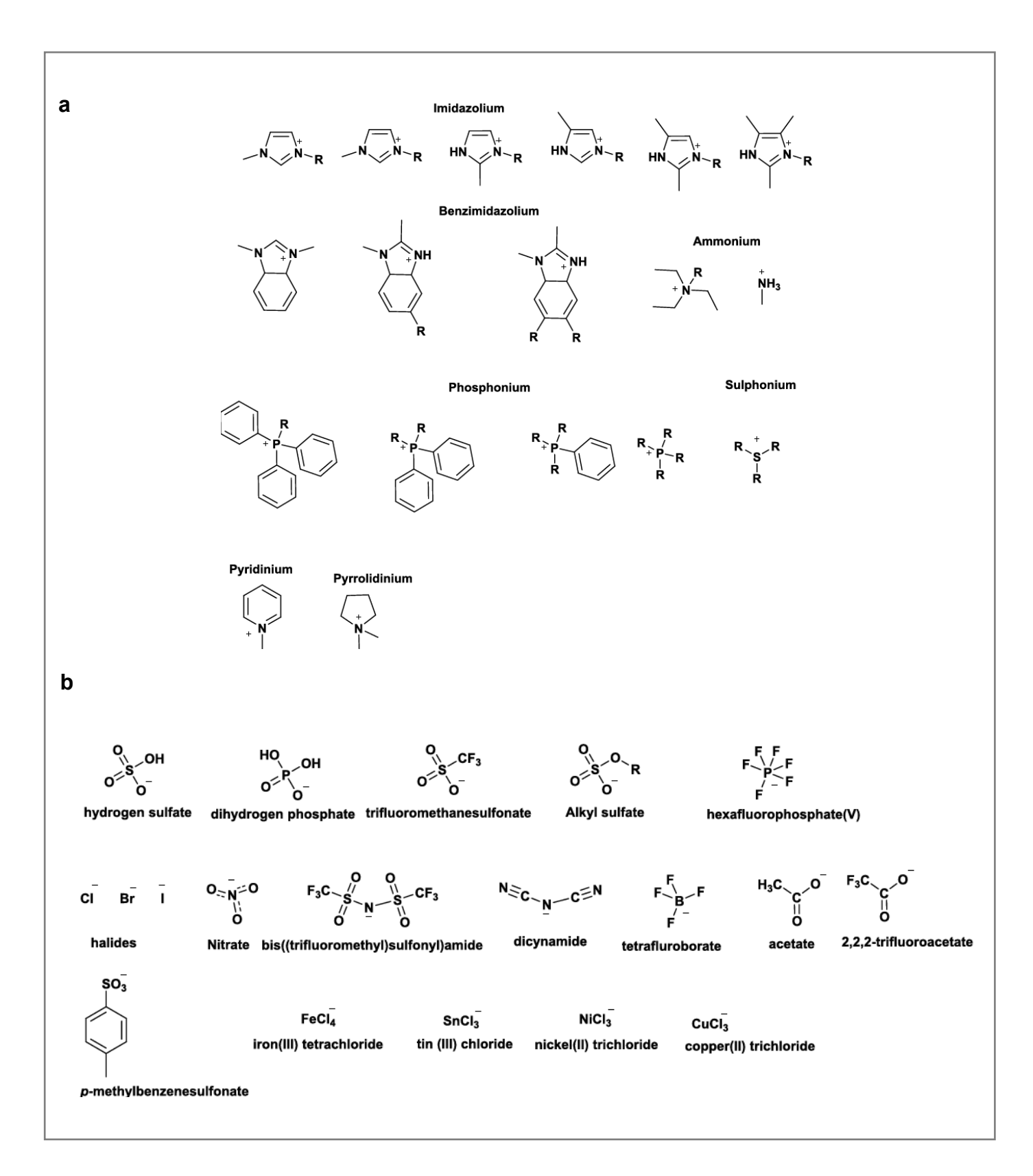


Figure 1.2 A few cations (a) and anions (b) commonly used in the preparation of ILs (Singh and Savoy, 2019).

Anions also have a huge influence on the thermal stability, with a drammatic reduction in halides-based ILs (Ngo et al., 2000; Hu & Peng, 2014). Bis(trifluoromethylsulfonyl)amide (Ntf₂-) and triflate (Otf-) anions were reported as among the most stable, while dicyanamide (N(CN)2⁻) and acetate- or nitrate-based ones were indicated as the least stable (Parajó et al., 2019). ILs density spans from 0.9 to 1.7 g · cm⁻³ (Mu & Han, 2014; Bhattacharjee et al., 2015; Zhou et al., 2019), and it is possible to determine their variation in density over a vast range of temperature and pressure, since there is a linear correlation (Paduszyński & Domańska, 2012), while their range of viscosity extends from 0.7 to 257000 mPa · S, even if, generally, they present a mild to high viscosity (Paduszyński, 2019). Although a high viscosity can be useful in lubricant and polymers dissolution (Bhattacharjee et al., 2015; Lazzús & Pulgar-Villarroel, 2015), it can represent a problem for the application of ILs in other fields, since it can impair mass transfer and conductivity (Magina et al., 2021). Yet, a slight increase in temperature or the addition of a small quantity of organic solvent is sufficient in reducing ILs viscosity (Okoturo & VanderNoot, 2004; S. Zhang et al., 2006). As far as electrical conductivity is concerned, being pure ionic compounds, ILs are ideal conductors. The ability to conduct electricity through the movement of charged ions across a liquid phase is essentially inherent to ILs, while canonical ionic compounds are usually solid at room temperature and need to be dissolved in a solvent first in order to become electrolytes (Q. Li & Ardebili, 2016). ILs conductivity compares easily to the one of the standard electrolytes used in electrochemistry and it is influenced both by the cationic and anionic component. Recently, Nancarrow and collaborators thoroughly examined the data available in literature and reported that shortchained imidazolium-, pyridinium- and pyrrolidinium-based ILs show high conductivity, while longer alkyl chains tend to increase viscosity, with detrimental effects on conductivity (Nancarrow et al., 2021). The order of conductivity reported, as a function of the cation type, was: pyrrolidinium > pyridinium > imidazolium > "others" > ammonium, with pyrrolidiniumbased ILs showing a median quartile of conductivity of 0.742 S · m⁻¹. The anionic component, which also appears to influence conductivity depending on viscosity, was found to be as important. The order for ILs conductivity as a function of the anion type reported was: $[N(CN)_2] > [OTf] > [BF_4] > [NTf_2] > [PF_6] > "others".$

Other important physical and chemical features of ILs are the good thermal conductivity, which spans from 1 to 100 mS · cm⁻¹ (Hu & Peng, 2014; Tomida, 2018) and the ability to selectively absorb gas, which is especially useful for capturing CO₂ present in flue gas (Faisal Elmobarak et al., 2023). In this context, it has been observed that some ILs are able to

outperform canonical organic compounds, while still remaining less corrosive and volatile (Carvalho et al., 2009; Wu et al., 2020).

Finally, ILs show low flammability and a negligible vapour pressure, which makes them essentially non volatile, (Aschenbrenner et al., 2009). These features are key factors in the replacement of VOCs. The non-volatility of ILs makes them especially safer for humans, since VOCs are well-known to cause serious irritation of eyes and mucous membranes and, in the long term, damages to liver, kidneys and central nervous system (Crinnion, 2010). Moreover, the low vapour pressure can also be extremely helpful in ILs recycling. In fact, ILs can be recovered through distillation, which vaporizes other volatile substances, and it has been observed that the retrieved ILs are still able to function as desired after this process (King et al., 2011; Xu et al., 2017; Hossain et al., 2019; Huang et al., 2020). Nonetheless, the high temperatures required for distillation can be detrimental for some ILs, causing their degradation (B. Li et al., 2010). This, together with the high energy requirement for distillation, has driven researchers towards alternative methods of recycling (Singh & Savoy, 2020). Membrane separation has been reported as a promising technology for ILs recovery, with nanofiltration resulting especially efficient, thanks to its ability to separate neutral and charged compounds, often outperforming distillation (Hinchliffe & Porter, 2000; Mai et al., 2014; Kuzmina, 2016), while aqueous two-phase system (ATPS) and adsorption have been taken in consideration for separating ILs from aqueous solutions (Anthony et al., 2001; C. Li et al., 2010; Lemus et al., 2012; H. Yang et al., 2018; Wei et al., 2021)

Taken together, the unique and various properties of ILs makes them suitable for their application in many fields.

1.2 Ionic liquids applications

ILs cover many areas of both academic and industrial interest, from electrochemistry to enzymatic catalysis, from extraction of secondary metabolites and dissolution of natural polymers to the coating of metal structures to protect them from corrosion (G. Kaur et al., 2022). Although discussing any aspect of ionic liquids in its entirety is basically impossible, it is important to give a general idea of the manifold areas in which these prodigious compounds can be employed (**Fig. 1.3**).

In the electrochemical field, ILs have been proposed as solvents and supporting electrolytes for electrodeposition of metals, such as zinc and zinc-nickel, silver and chromium, helping in the development of metal coatings of great interest for the aerospace and automotive industry (Maniam & Paul, 2020; Molodkina et al., 2020; Rahali et al., 2020). ILs have found an application also in the construction of better performing, safer batteries, due to their excellent

conductivity and thermal stability. In lithium-based batteries, ILs have been proposed both as liquid and as polymer/inorganic hybrid electrolytes (Isikli & Ryan, 2020; Rüther et al., 2020; G. Yang et al., 2020). On the same premises, ILs can be employed as electrolytes in aluminum-based batteries (M. Angell et al., 2020) and as supportive electrolytes and additives in different types of redox flow batteries (Ortiz-Martínez et al., 2020).

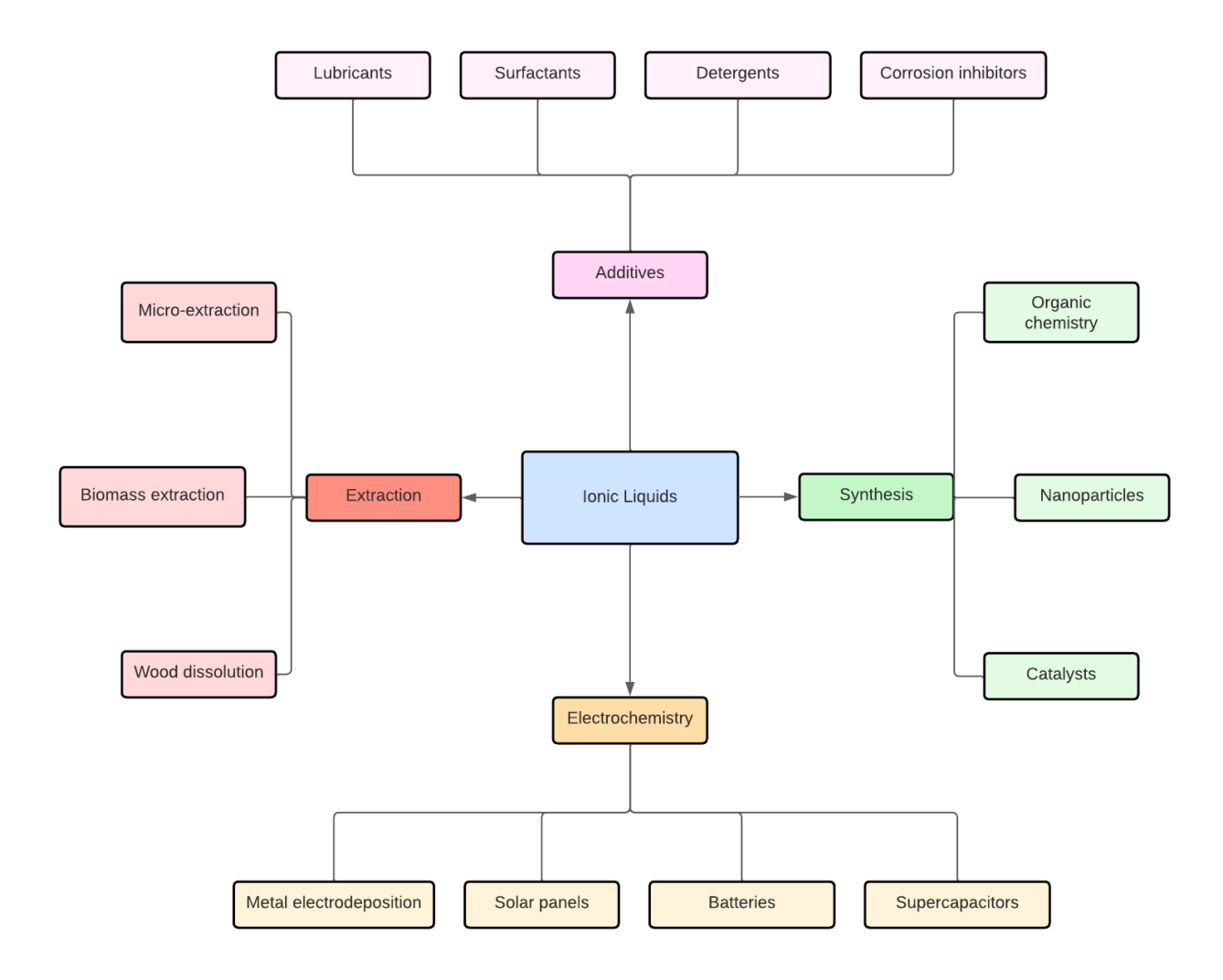


Figure 1.3 Some of the manifold applications of ionic liquids.

ILs can be employed as electrolytes in the development of photovoltaic devices, and especially in the construction of dye-sensitized solar cells (DSSC), thanks to their conductivity, electrochemical stability and low vapour pressure (Abu Talip et al., 2020; Kumarasinghe et al., 2020), sometimes even by combining different ILs, as in the case reported by Hilmy and

collaborators, where eutectic mixtures of a few iodide-based ILs were successfully used in the construction of a DSSC (Mohd Faridz Hilmy et al., 2020).

ILs ability to retain a functional conductivity even at high temperatures allows for their employment in proton exchange membrane fuel cells and thermo-electrochemical cells (Sosnowska et al., 2020; Zanchet et al., 2020) and, taken together with their low flammability, makes them suitable for supercapacitors (Pan et al., 2020).

From lubricating agents and corrosion inhibitors to shampoos and fabric softeners, ILs can be used as additives thanks to their tunable viscosity. It was observed that imadozolium-based are able to reduce friction at the interface between both films of tetrahedral amorphous carbon and multilayers of graphene oxide (Gan et al., 2020; Kawada et al., 2020), while pyrrolidinium-, phosphonium-, sulfonium- and ammonium-based ILs can reduce corrosion of desalination units and petroleum industries (Deyab, 2019, 2020). Cations with long alkyl chains can be easily employed as surfactants in paints, conditioners and household products (Pal & Punia, 2019; El Seoud et al., 2021), although anionic surface-active ILs are also being thoroughly studied (Y. Sun et al., 2019; Qin et al., 2020).

The wide range of tuneability of ILs makes them excellent solvents for different extraction processes, from the micro-extraction of drugs, secondary metabolites, metals and pesticides (Shah et al., 2020; Zante et al., 2020; Shah & Malek, 2021; L. Zhang et al., 2021) to the extraction of algal biomass (Weldemhret et al., 2020) and the dissolution of wood and cellulose for biofuel production (Abushammala & Mao, 2020; Belesov et al., 2020).

Moreover, ILs can partake in various chemical synthesis processes, improving yield and selectivity of organic reactions that produce chemicals of pharmaceutical interest (Bhongale et al., 2020; Kore et al., 2020; Yin et al., 2020), helping as solvents and stabilizers in the synthesis of nanoparticles for medical, engineering and environmental remediation applications (G. Kaur et al., 2022), and working as catalyists in enzymatic reactions for the synthesis of clothing polymers (H. Zhao & Toe, 2020) and sugar fatty acid esters for pharmaceutical, agricultural and food industries (Z. Yang & Huang, 2012; Zheng et al., 2015). Other fields of application are drug delivery (Esson & Mecozzi, 2020; Matczuk et al., 2024), CO₂ conversion technologies, such as CO₂ electrochemical reduction (Cui et al., 2020), and CO₂ sequestration (Y.-Y. Lee et al., 2020), thermal energy storage devices (Shi et al., 2021), petroleum purification from polluting agents such as sulfur and nitrogen compounds (Butt et al., 2020; Malolan et al., 2021) and many more.

Now, although for many of these applications a few obstacles are encountered, such as the still elevated cost of synthesis or the high viscosity of some ILs, the main problem of ILs resides in their controversial ecotoxicity, which has been studied for over twenty years and is still largely debated. ILs impact on living organism is considered by many to be the real challenge for their application, to the point where it has started to influence their design itself (Magina et al., 2021; Ventura et al., 2013; Weyhing-Zerrer et al., 2017)

1.3 Ionic liquids toxicity

Although at first ionic liquids were presented as harmless for living organisms, this idea has been consistently dismantled over years of studies about their toxicity. The prospect of a greater use of ILs on an industrial scale comes with the high probability, almost close to a certainty, of their emission into the environment (Dołżonek et al., 2017). The great thermal stability and non-volatility of ILs, taken together with their resistance to photodegradation (Stepnowski & Zaleska, 2005), their chemical stability (Armand et al., 2009) and their water solubility and stability (Freire et al., 2008, 2010), suggests the concrete eventuality of their persistence in the environment, once they are released. This knowledge becomes especially worrying when considering that literature shows how a great number of ILs are poorly biodegradable., as shown in a comprehensive study of 2022, where Amsel and coworkers thoroughly analysed over one hundred papers about ILs biodegradation in aerobic conditions in water, seawater or soil and in anaerobic conditions in water (Amsel et al., 2022). Moreover, the authors pointed out the difficulty in comparing different studies because of a general lack of homogeneity in conducting biodegradation experiments, calling for a standardization of the methods and a higher clarity in their communication.

In this context, the study of ILs toxicity to living organism, in its extent and mechanisms, gains even more importance. There is a vast literature about ILs toxicity towards many ecotoxicological model organisms, representative of both aquatic and land environment inhabiting beings. *Aliviibrio fischeri* is the most studied among bacteria, and possibly among marine organisms, the most common test being the bioluminescence assay, that informs about *A. fischeri* cellular metabolism, although *Staphylococcus aureus* has also been employed as a representative of Gram-positive bacteria (Gonçalves et al., 2021). ILs ability to inhibit the growth of green algae has been tested on organism such as *Scenedesmus obliquus* and the microalga *Raphidocelis subcapita* (formerly known as *Selenastrum capricornutum*)(Cho et al., 2008; Pretti et al., 2009; Y. Liu et al., 2018; Xia et al., 2018), while their toxicity was extensively studied with experiments on reproduction inhibition of *Scenedesmus vacuolatus* (Matzke et al., 2007; Steudte et al., 2012). For marine animals, a great amount of work has been carried out on the crustacean *Daphnia magna*, through the standardized acute immobilisation test (Pretti et al., 2009; Cho & Yun, 2016; C. Zhang et al.,

2017), and the fish *Danio rerio*, where lethality in adult fish was determined through the acute toxicity test (Pretti et al., 2009; T. Liu et al., 2016; C. Zhang et al., 2018). Regarding terrestrial plants, ILs toxicity has been tested on a variety of organism such as *Lepidium sativum* (crass), *Triticum aestivum* (wheat), *Raphanus sativus* (common radish) and *Zea mays* (maize), with analyses spanning from the effect on seedlings and germination to growth inhibition and chlorophyll content (Matzke et al., 2007, 2008; L.-S. Wang et al., 2009; Biczak et al., 2017; Y. Li et al., 2018). For mammals, a good number of studies has focused on the effect of ILs on different cell lines, both of human and non-human origin (X. Wang et al., 2007; García-Lorenzo et al., 2008; McLaughlin et al., 2011; Egorova & Ananikov, 2014).

The huge amount of data accumulated by the plethora of ecotoxicological papers published over the last two decades shows how the effect of ILs can vary, often also drammatically, depending on the organism tested and on the time of exposition to the compounds. Moreover, ILs toxicity is evidently dependent on their composition (Ventura et al., 2013; Egorova & Ananikov, 2014; Gonçalves et al., 2021). Nonetheless, while it is undoubtedly difficult to fully unravel such bulk of informations, over time it has become clear that the cation alkyl chain lenght consistently correlates to ILs toxicity, with longer chains inducing stronger toxic effects that are ecotoxicologically relevant and worrying. This has been mainly attributed to the ability of long-chained cations to intercalate into biological membranes, ultimately destabilizing and disgregating them, with the logical consequence of impairing fundamental biological processes (Gonçalves et al., 2021; N. Kaur et al., 2021; Magina et al., 2021). Such phenomenon has also been proved by experiments carried out on liposomes, i.e. phospholipidic vesicles, where it has been observed that cations bearing long alkyl chains are able to affect membrane stability in a concentration-dependent manner (Galletti et al., 2015; Kontro et al., 2016; Ruokonen et al., 2018; N. Kaur et al., 2021). It has also been observed that the insertion of one or more oxygen atoms in the alkyl chain causes a drastic decrease in ILs toxicity, although this also negatively impacts their biodegradability (Samorì et al., 2010, 2015; Vraneš et al., 2016). In general, the functionalization of the alkyl chain seems to correlate with a lesser toxicity (Egorova & Ananikov, 2014)

Conversely, when considering the anion role in the toxic effect of ILs, things become more nebulous. Initially, the idea of a contribution from the anionic component was underestimated, if not discarded. In time however, the awareness about the importance of the anions has grown. To this day, anions are regarded as an integral part of ILs toxicity and, as for cations, there seems to be a correlation between anions lipophilicity and their toxicity, reinforcing the idea that ILs toxicity is mainly associated with their ability to interact with biological

membranes (Matzke et al., 2007; Ventura et al., 2013; Dołżonek et al., 2017; N. Kaur et al., 2024). Yet, there really are no clear models of interpretation that explain the mechanism of anion toxicity, since they usually do not bear long alkyl chains, with experiments carried out on lipid membrane models being mainly focused on the cationic component (Mitra et al., 2023), and, to our knowledge, there only are a couple of publications regarding ILs interaction with native biological membranes that can properly represent cell membranes, both investigating the effects of cation alkyl chain lenght on bioenergetically active membranes (Malferrari et al., 2015; X. Liu et al., 2023).

In this work, the interaction between ILs and native membranes has been studied using two different model for native bioenergetically active membranes, which will be presented in the next chapters: chromatophores, isolated from *Rhodobacter capsulatus* cells, and submitochondrial particles, isolated from bovine heart tissue.

1.4 Chromatophores as a model for bioenergetically active membranes

Chromatophores are bioenergetically active vesicles that can be easily isolated from a variety of photosynthetic purple non-sulfur bacteria (Baccarini-Melandri & Melandri, 1971). The depiction of a model for a chromatophore vesicle isolated from *Rhodobacter sphaeroides*, based upon AFM, transmission electron microscopy, X-ray crystallography, mass spectroscopy, proteomics and optical spectroscopy methods (Cartron et al., 2014), is reported in **Figure 1.4**.

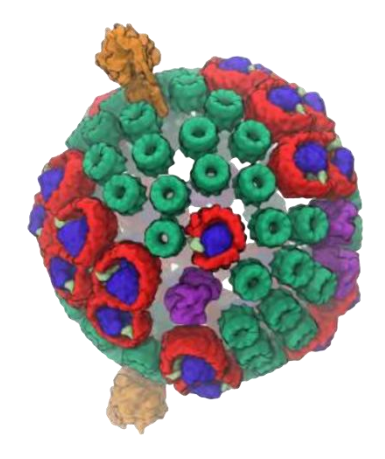


Figure 1.4 Structural model of a chromatophore isolated from *Rb. sphaeroides*. LH2 is depicted in green; LH1, red; RC, blue; cytochrom *bc*₁, magenta; ATPase, ochre. (Cartron, 2014).

Chromatophores bear all the functional elements of the photosynthetic apparatus capable of transducing the radiant energy of light into chemical energy and have been thoroughly characterised both functionally, at a molecular level, and structurally at atomic resolution (Deisenhofer et al., 1984; Allen et al., 1987; Ermler et al., 1994; Cogdell et al., 1997; Esser et al., 2008; Morales-Rios et al., 2015; Qian et al., 2021; Bracun et al., 2023).

In Rhodobacter capsulatus, a photosynthetic bacterium closely related to Rb. sphaeroides, the primary photochemistry that sets the cyclic electron transport chain in motion is mainly activated by the absorption of a photon at the level of the light-harvesting complex LH2, which picks up radiant energy and transfers the resulting excitons to the LH1 core antenna. Within 20 to 40 picoseconds, the excitation energy is then funnelled to the Reaction Center (RC) (Blankenship, 2014). LH2 and LH1 share a similar structure, consisting of αβ-heterodimers of single transmembrane helices binding carotenoids and molecules of bacteriochlorophyll (Niederman, 2017). These heterodimers form circular structures that arrange the photosynthetic pigment in the most efficient orientation to transfer the excitation energy, with LH2 being located peripherally to LH1, which forms a larger structure around the RC. The RC consists of the H subunit, which presents a large cytoplasmatic domain and that is anchored by a single hydrophobic helix to two pseudo-symmetric membrane subunits, L and M. The RC protein moiety holds together the pigment cofactor tree, which consists of two symmetrical branches, each originating from the special pair of bacteriochlorophylls (P) placed near the membrane periplasmic side, and sequentially continues with accessory monomeric bacteriochlorophylls (BChl), two bacteriopheophytins (BPheo) and two quinone binding sites, Q_A and Q_B, located near the cytoplasmic side of the membrane (Jackson, 1988; Crofts, 2021). Overall, the P-BPheo-Quinone complex is the system responsible for the photoinduced charge separation that occurs within the RC. The excitation induced by the energy coming from LH1 results in the oxidation of the special pair P, which delivers one electron to a BPheo, leading to the sequential reduction of a quinone molecule located in the QA site, which in turn reduces a second quinone situated in the QB site (Fig. 1.5). After the double reduction of the quinone, and its double protonation, the formed quinol leaves the Q_B site and it is oxidized by the quinol-cytochrome c oxido-reductase (cytochrome bc_1) in its Qo site. From here, while the protons from quinol are released in the periplasm, the electrons from the quinol reduce a quinone in the cytochrome bc_1 Qi site, which faces the cytoplasmic side, and a soluble cytochrome c_2 molecule in the periplasm, following the well-characterised Q-cycle mechanism. The now reduced cytochrome c_2 is the electron donor for the special pair P photoxidized in the RC (Jackson 1988; Crofts, 2021).

The light-driven cyclic electron transfer, according to Mitchell's chemiosmotic theory, is coupled to the formation of ATP, which is synthesised by the ATP synthase (ATPase) (Mitchell, 1961). In fact, the protons that are moved from the cytoplasm to the periplasm, entering the Q-cycle at the level of the Q_B and the Qi sites and leaving at the level of the Qo site, generate an electrochemical concentration gradient of protons accross the membrane ($\Delta\mu_{H+}$), known as proton motive force, consisting of an electrical ($\Delta\Psi$) and a pH component (Δ pH), which is eventually used by the ATPase dissipating the proton gradient and generating ATP (Mitchell, 2011; Nicholas & Ferguson, 2013).

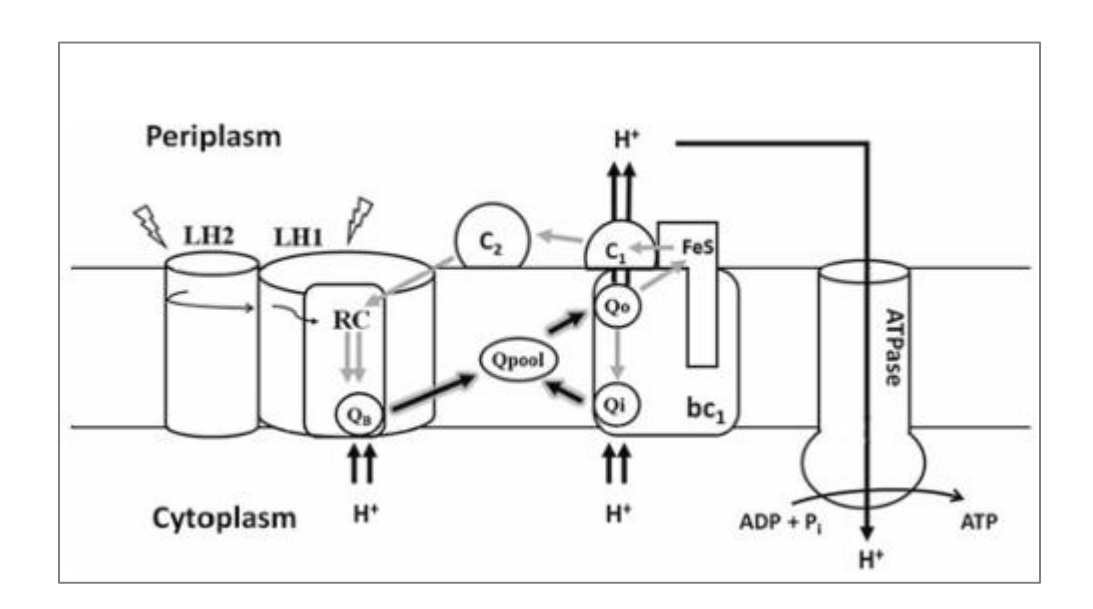


Figure 1.5 Schematic representation of the light-driven cyclic electron transfer of *Rb. capsulatus* photosynthetic membrane. LH2 and LH1 are, respectively, the light-harvesting complexes II and I; RC, reaction center; Q_B , quinone binding site of RC; bc_1 , cytochrome bc_1 ; Qo and Qi are, respectively, the quinol oxidation and quinone reduction sites of cytochrome bc_1 ; C₁ and C₂, cytochrome c_1 and c_2 ; FeS, Rieske protein iron-sulfur cluster; ATPase, ATP synthase complex. Thin black arrows represent the energy transfer from LH2, through LH1 to RC; Thick black arrows represent the protons movement; Thick grey arrows represent the electron transfer. (Bin et al., 2024).

Chromatophores retain all the functional elements needed to perform the light-driven Q-cycle, inserted in a closed and sealed membrane in their native conformation. The membrane integrity is a fundamental prerequisite for the transduction of the proton gradient into chemical energy, in the form of ATP, since an increase in ion diffusion would dissipate the $\Delta\Psi$, and a proton leakage would affect both the $\Delta\Psi$ and the ΔpH , leading to a decrease in the proton motive force. Moreover, chromatophores also retain the carotenoids associated to the LH2, which act as endogenous spectral probes and function as intramembrane voltmeters for the $\Delta\Psi$ (Jackson & Crofts, 1969; Witt, 1974). In fact, the photoinduced charge separation within the RC and the other electrogenic events that take place along the electron transfer chain, cause a vectorial displacement of electric charges across the membrane bilayer dielectric,

generating an intramembrane electric field that affects the carotenoids visible spectrum of absorbance, causing it to shift towards red light (Holmes et al., 1980). Since the amplitude of this electrochromic shift, also called carotenoid shift, linearly correlates to the $\Delta\Psi$, by spectrophotometrically monitoring at appropriate wavelenghts the variation of carotenoids absorbance, real time informations about the dissipation of the $\Delta\Psi$ can be obtained.

In particular, when the the RC is photoxidized by a single flash of light, lasting only a few microseconds, the carotenoid shift signal rises in three kinetic phases: phase I, which reflects the vectorial electron transfer from the special pair P to the primary acceptor, a quinone molecule located in the RC Q_A site (Jackson & Dutton, 1973); phase II, which is due to the sum of the vectorial displacement of charges caused by the electron transfer from cytochrome c_2 to the photoxidized P^+ and the protonation of the quinone acceptor in Q_B (Jackson & Dutton, 1973; Drachev et al., 1988); phase III which reflects the charge displacements of electron and proton transfer occuring within the cytochrome bc_1 complex (Saphon et al., 1975; Jackson, 1988). Phase I and II, which inform on the charge displacement events occuring in the RC, are completed within tens of microseconds, while phase III has a slower build up that takes a few milliseconds. When monitoring the absorbance of carotenoids past this first three phases, the decay of the signal informs on the dissipation of the $\Delta\Psi$ in the dark, which is entirely caused by ionic fluxes across the membrane (Saphon et al., 1975).

Thanks to the possibility of spectrophotometrically monitoring the dissipation of the $\Delta\Psi$, chromatophores have been widely employed in the study of the effect of different compounds on the membrane integrity (Escher et al., 1997; Schweigert et al., 2001), and recently have also been used to study the interaction between native biological membranes and ionic liquids in a couple of papers, where it was observed that cations with long alkyl chain effectively collapse the carotenoid shift signal even at low concentrations (Malferrari et al., 2015; X. L. Liu et al., 2023;). Moreover, in the work of Malferrari and coworkers, it was observed that the hydrophobic $N(CN)_2$ anion, even when paired with a short-chained cation, was able to increase ionic current across the chromatophore membrane, negatively affetting the $\Delta\Psi$, though at concentration in the millimolar range. On these premises, we decided to employ this model to test five ILs of possible application in the electrochemical industry (highlighted in Fig. 1.6), three of which containing the lipophilic Ntf_2 anion, while all containing cations with relatively short alkyl chain. We also tested the effect of the same cations, orginally paired with the Ntf_2 , once they were paired with the chloride (Cl⁻) as a counter anion.

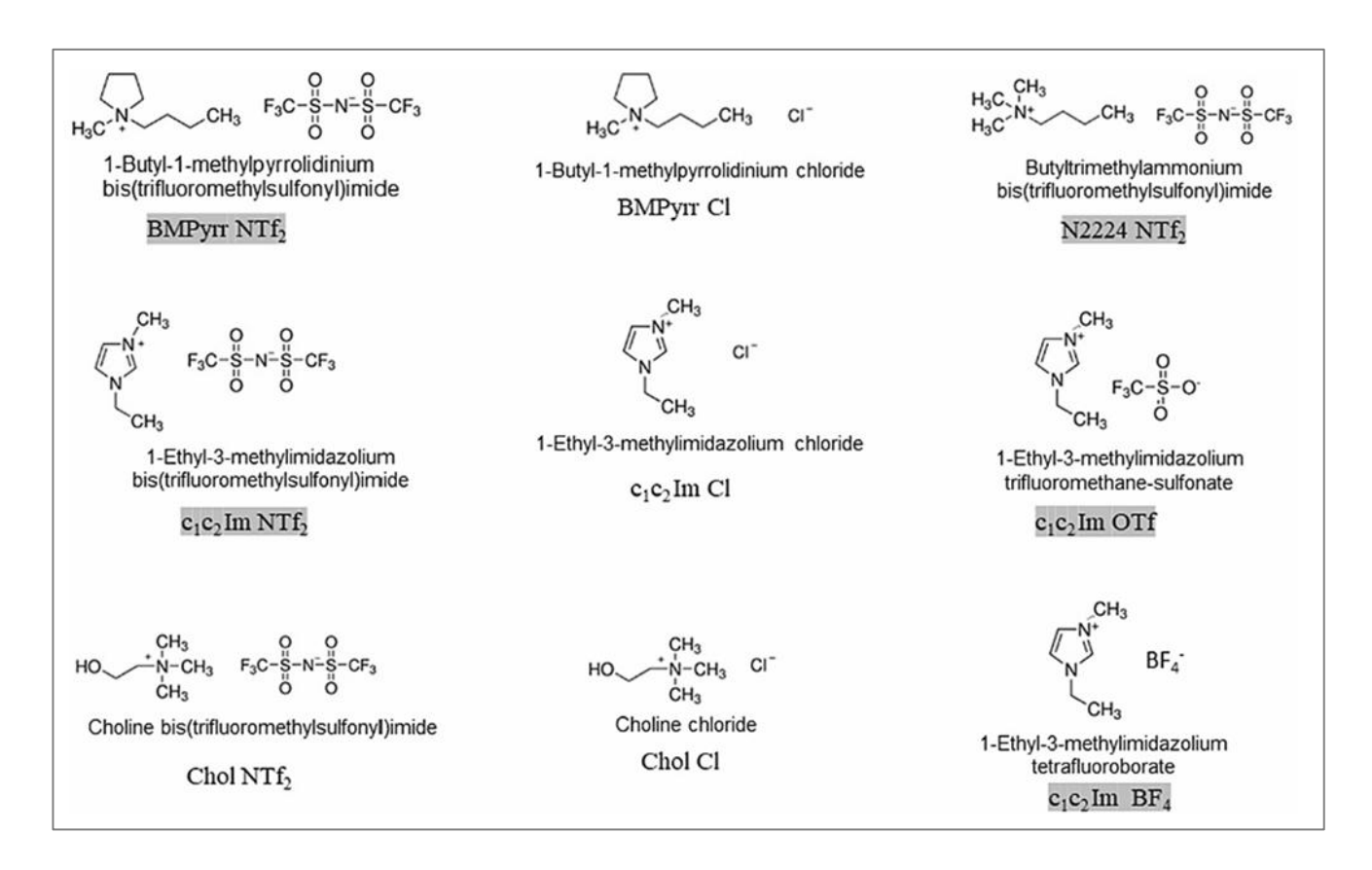


Figure 1.6 Ionic liquids tested on chromatophores.

1.5 Bovine heart submitochondrial particles

Submitochondrial particles (SMP) are vesicles that can be isolated from mitochondria derived from a great variety of organisms and tissues and have been widely used for studying fundamental bioenergetical processes, as well as mitchondrial diseases, and the effects of heavy metals, detergents and uncouplers (Katre & Wilson, 1978; Degli Esposti & Lenaz, 1982; Fato et al., 1993; Degli Esposti et al., 1994; Argese et al., 1996; Baracca et al., 2000; Bragadin et al., 2002). Moreover, bovine heart-derived mitochondria present the advantage of being particularly preservable over long periods of time (Pallotti & Lenaz, 2001).

Among the various types of submitochondrial particles that can be isolated, opportune protocols can yield phosphorylating electron transfer particles (ETPH), obtained through fragmentation of the mitochondria membranes, after which the membrane fragments, containing all the functional elements of the thoroughly characterised mitochondrial electron transport chain, reseal in closed vesicles fully capable of performing coupled oxidative phosphorylation (Hansen & Smith, 1964; Beyer, 1967;).

The electron transport chain is composed of transmembrane protein complexes (complex I-V), inserted in folded sections of the mitochondrial inner membrane known as cristae, and the

mobile electron carriers ubiquinone (Q) and cytochrome c (cyt c) (R. Zhao et al., 2019). Being ETPH inside-out vesicles, the complexes are accessible to their substrates, while cytochrome c is included in the vesicles lumen (Hansen & Smith, 1964; Beyer, 1967). Electrons are injected into the mitochondrial electron transport chain either at the level of the NADHubiquinone oxidoreductase (complex I, CI) which oxidizes NADH to NAD+, or at the level of the succinate dehydrogenase (complex II, CII), which oxidizes succinate to fumarate, in both instances injecting two electrons at a time (Fig. 1.7). Complex I has been well characterized in its structure and functioning (Carroll et al., 2006; Sazanov & Hinchliffe, 2006; Efremov & Sazanov, 2011; Vinothkumar et al., 2014; Jones et al., 2017; Kampjut & Sazanov, 2022). Cl has an "L-shaped" structure, with one arm fully embedded into the membrane and a second arm protruding into the matrix. These two domains are composed of fourteen highly conserved subunits and form the core for the enzymatic reaction. NADH donates a pair of electrons to a flavine mononucleotide molecule (FMN) situate in the distal subunit of the matrix arm, reducing it to FMNH₂ (Kampjut & Sazanov, 2022). From here, the electrons are passed down the matrix arm through a series of 8 Fe-S clusters, in sequential redox potentialdriven reactions, to the N2 cluster at the intersection between the membrane and the matrix arms, where the ubiquinone (Q) is reduced to ubiquinol (QH₂) (Sazanov & Hinchliffe, 2006; Verkhovskaya et al., 2008). The energy released by the reduction of Q is associated to the pumping of four protons across the membrane at the level of the membrane arm distal subunits (Kampjut & Sazanov, 2022).

On the other hand, CII is a relatively small complex, which is also part of the Krebs cycle, composed of two hydrophobic subunits that anchors it to the membrane and two subunits protruding in the matrix. At the level of CII peripheral subunits a molecule of flavin adenine dinucleotide (FAD), covalently bound to a flavoprotein located in the peripheral arm, accepts two electrons from succinate and is reduced to FADH₂ (Cecchini, 2003; F. Sun et al., 2005; R. Zhao et al., 2019). From here, the electrons are moved through three Fe-S clusters to Q (Iverson, 2013). Importantly, the CII catalyzed reduction of Q is not associated to the pumping of protons across the membrane.

Either way, the reduced ubiquinone, now ubiquinol, migrates towards CIII, a symmetrical dimer of monomers composed of eleven subunits each (Schägger et al., 1986). QH₂ is oxidized to ubisemiquinone (QH⁻) in the Qo site of CIII, on the intermembrane side, transferring an electron to a 2Fe-2S cluster, and two protons are pumped into the intermembrane space (Trumpower, 2002). From here, the electron is transferred to cytochrome c₁ and, subsequently, to the mobile cytochrome c, reducing it. The second

electron is swiftly transferred from the highly reductive QH⁻, formed in Qo, to the low potential subunit cytochrome b_L and, from here, to the high potential cytochrome b_H, in turn arriving at the Q_i site, on the cytoplasmic side of the membrane, where it reduces a ubiquinone molecule to QH⁻. This process is half of the well-known Q-cycle, which is completed when a second QH₂ is oxidized in Q_o (Mitchell, 1972, 1976; X. H. Yang & Trumpower, 1986; Gao et al., 2003).

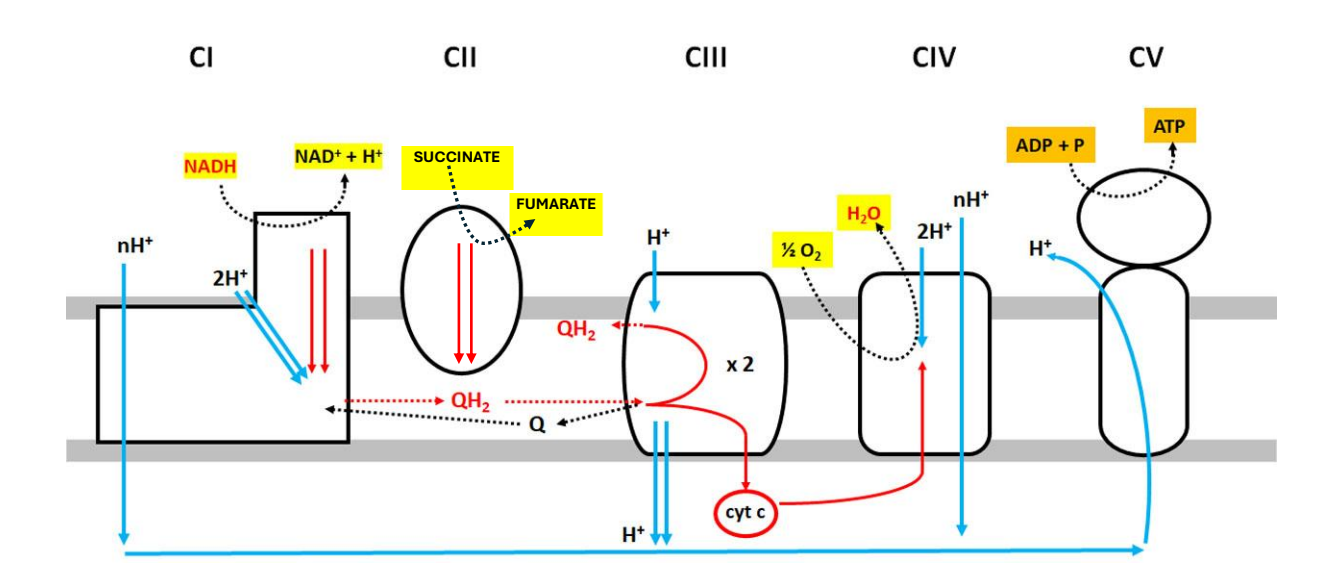


Figure 1.7 Schematic representation of the mitochondria electron transport chain. NADH-ubiquinone oxidoreductase, CI; Succinate dehydrogenase, CII; CoQ-chtochrome c reductase, or cytochrome bc_1 , CIII; Cytochrome c oxidase, CIV; ATP synthase, CV; Cytochrome c, cyt c. Blue arrows show the protons movement; Red arrows depict the electron transport. Dashed black arrows represent the redox reactions and the movement of ubiquinone molecules (Q). Dashed red lines depict movement of ubiquinol molecules (QH₂)

Cytochrome c_{red} migrates to CIV, moving along the membrane through electrostatic interactions, where it interacts with subunit II of the CIV, transferring electrons to the first of four redox-active metal centers, Cu_A. The electrons are then transferred through the other centers to O₂, reducing it to H₂O. A total of four electrons are required for the reduction of a molecule of O₂, the transferring of which is coupled to the pumping of four protons across the membrane (Wikstrom, 1977; Shimada et al., 2017;). As for the photosynthetic electron transport chain described in the previous chapter, the proton gradient formed during the electron transfer is dissipated by the ATP synthase for the production of ATP, according to Mitchell's chemiosmotic theory (Mitchell, 1961).

In ETPH, the overall activity of the respiratory chain can be observed spectrophotometrically by monitoring NADH consumption over time. Usually, although the ATPase dissipates the proton gradient, the protons pumped across the membrane create a back pressure that does not allow the maximal speed of the electron transport chain, known as respiratory control, and

it has been observed that the addition of an uncoupler, such as carbonyl-cyanide-4-(trifluoromethoxy)phenylhydrazone (FCCP), causes the release of such pressure, increasing the speed of the electron transport chain (Mitchell & Moyle, 1967). In this context, ETPH can be used to assess whether a molecule of interest is able to affect the membrane electrochemical potential formed during the electron transfer (Brand & Nicholls, 2011). Moreover, the effect of exogenous compounds on the membrane electrochemical potential can be tested observing their effect on ETPH ability to perform reverse electron transfer (RET,

Fig. 1.8).

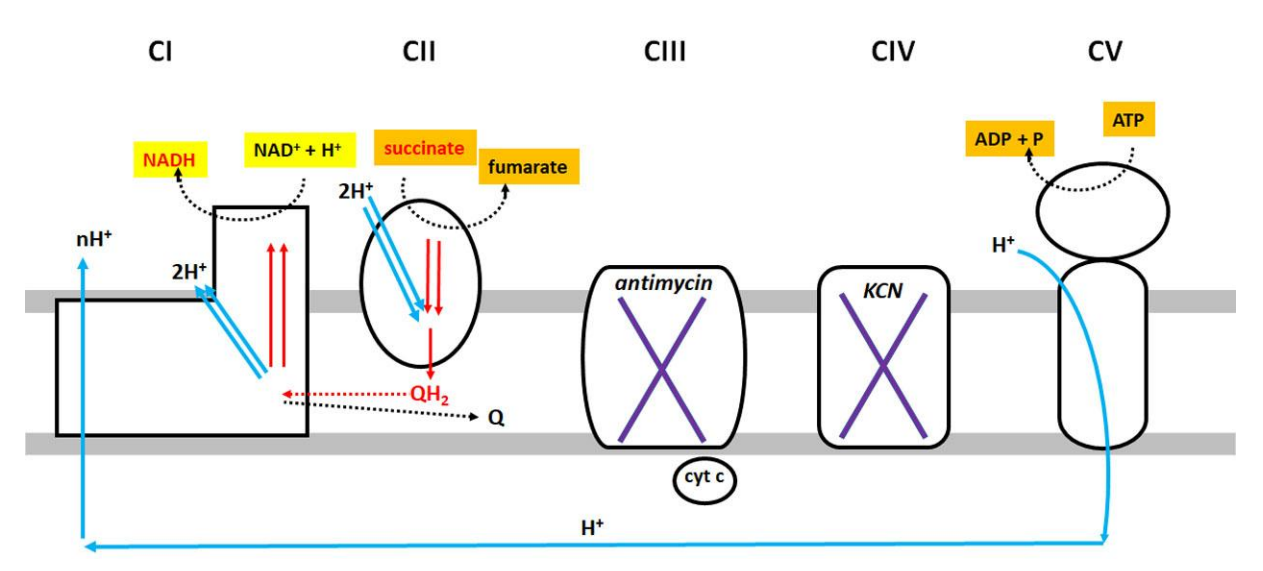


Figure 1.8 Schematic representation of ETPH reverse electron transfer. NADH-ubiquinone oxidoreductase, CI; Succinate dehydrogenase, CII; CoQ-chtochrome c reductase, or cytochrome bc_1 , CIII; Cytochrome c oxidase, CIV; ATP synthase, CV; Cytochrome c, cyt c. Ubiquinone, Q; Ubiquinol, QH₂. Blue arrows show the protons movement; Red arrows depict the electron transport. Purple cross signs represent complexes inhibition.

RET is the rotenone-sensitive process of NAD⁺ reduction catalysed by CI, supported by succinate, where the ATPase, by hydrolyzing ATP to ADP and P_i, translocates protons inside the lumen of the veiscles. The proton motive force generated drives the electron flow from the ubiquinol pool, reduced by CII activity in the presence of succinate, to CI and, eventually, to NAD⁺, reducing it. For ETPH to perform RET, CIII and CIV activity needs to be completely shut down by specific inhibitors, to preserve the forming pool of QH₂. RET was first discovered in isolated mitochondria, and subsequently demonstrated in submitochondrial particles (Klingberg & Slenczka, 1959; Hommes, 1963; Hinkle et al., 1967). Here, the dissipation of one or more component of the electrochemical potential, deprives the system of the driving force for NAD⁺ reduction (Brand & Nicholls, 2011).

We decided to employ this system to test three ILs, reported in **Fig. 1.9**, whose effect on chromatophores was already described in Malferrari and colleagues 2015 work, to evaluate the effect of such compounds on a different model for native bioenergetically active membranes, and, possibly, to find a correlation between the two models.

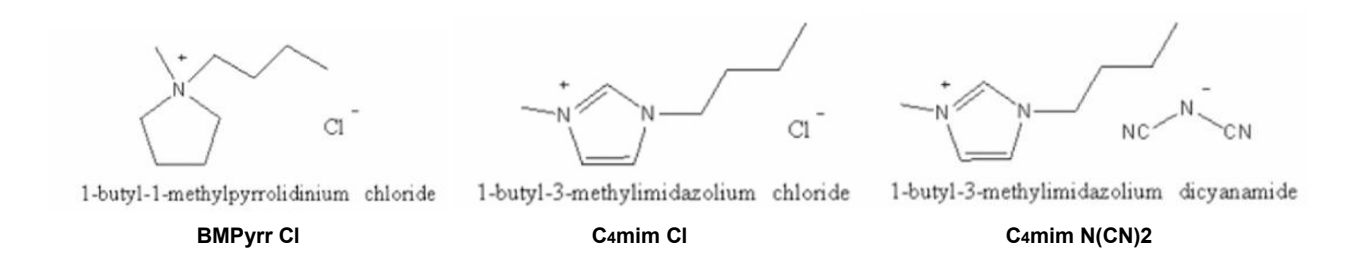


Figure 1.9 Ionic liquids tested on submitochondrial particles.

2. Aims of the study

lonic liquids toxicity has been tested extensively on a variety of ecotoxicological model organisms over the last two decades. Although there is a general consensus attributing their toxicity to their ability to interact with biological membranes, a meaningful understanding of such relationship is still missing. Therefore, this project aimed to study the interactions occurring between ionic liquids and native bioenergetically active membranes, employing chromatophores and submitochondrial particles as models. These are vesicles isolated from the purple non-sulfur bacterium *Rhodobacter capsulatus* and from bovine heart-derived mitochondria, presenting all the functional elements of the respective electron transport chains in their native conformation, inserted in closed membrane vesicles.

The effect of ILs on chromatophores electrochemical potential was investigated through single-flash experiments by spectrophotometrically monitoring over time the variation of absorbance of the carotenoids associated to the light-harvesting complex II, since their visible spectrum of absorbance responds linearly to the intramembrane electric field generated by the charge separation occurring within the Reaction Center after its photoxidation, informing on the dissipation of the electrical component of the membrane electrochemical potential $(\Delta \Psi)$. A model derived from experiments regarding the interactions between ionophores and hydrophobic ions and artificial lipid bilayers was employed to better interpret the carotenoid shift experimental traces, yielding a deeper overall understanding of the physics that determine ILs-induced effects on the cell membrane. Subsequently, direct inhibition of the electron transfer reactions taking place within chromatophores cytochrome bc1 was investigated by spectrophotometrically monitoring cytochrome c2 oxidation and re-reduction and Heme b_h reduction, and the effect of ILs on chromatophores light-driven ATP synthesis under continuous illumination was tested using the quantitative ATP bioluminescence assay. Moreover, the study of ILs toxicity was extended to in vivo experiments, testing their ability to inhibit Rb. capsulatus photosynthetic growth.

Finally, three ILs previously studied on the chromatophore model were tested on submitochondrial particles. The effect of the three compounds on the electrochemical potential, whose formation is associated to the activity of the electron transport chain, was assessed through spectrophotometrical measurements of NADH consumption and production, respectively, in forward and reverse electron transfer reactions. ILs direct inhibition of complexes I, III and IV was also investigated.

3. Materials and Methods

3.1 Materials

The following Ionic liquids were purchased from IoLiTech Gmbh (Heilbronn, Germany): 1-Butyl-1-methylpyrrolidinium-bis(trifluoromethylsulfonyl)imide (BMPyrr-NTf₂); butyltriethylammonium-bis(trifluoromethylsulfonyl)imide Choline-(N2224-NTf2); bis(trifluoromethylsulfonyl)imide (Chol-NTf₂); 1-Ethyl-3-methylimidazoliumbis(trifluoromethylsulfonyl)imide (c1c2lm-NTf₂); 1-butyl-1-methylpyrrolidinium-chloride (BMPyrr-CI); 1-Ethyl-3-methylimidazolium chloride (c1c2 Im-CI); 1-Ethyl-3-methylimidazolium tetrafluoroborate (c1c2 Im-BF₄); 1-Ethyl-3-methylimidazolium-trifluoromethane- sulfonate (c1c2 Im-OTf); 1-Butyl-3-methylimidazolium chloride (C₄mim-Cl); 1-Butyl-3methylimidazolium dicyanamide (C₄mim-N(CN)₂).

Choline chloride (Chol-Cl) was purchased from Sigma-Aldrich. For *Rb. capsulatus* photosynthetic growth, yeast extract and meat Peptone were purchased, respectively, from Duchemie Farma B.V (Haarlem, Netherlands) and Millipore (Burlington, Massachusetts, USA). Bacterial growth was monitored by using a Multiskan™ FC plate reader (Thermo Fisher, Waltham, Massachusetts, USA), running the Skanlt 6.0.2 software. Liquid sterile paraffin was purchased from Scharlab (Barcellona, Spain). All the reagents for submitochondrial particle assays were purchased from Santa Cruz Biotechnology (Dallas, Texas, USA), with the exception of ADP, ATP and NAD⁺ (Sigma-Aldrich). These spectrophotometric assays were carried out with a Jasco V-550 spectrophotometer.

3.2 Bacterial growth and chromatophores isolation

Rhodobacter capsulatus cells (strain MT1131), from a stab generously gifted by F. Daldal, were streaked on solid MPYE medium (3 g/L Peptone, 3 g/L yeast extract, 1.6 mM MgCl₂, CaCl₂ 1mM, 15 g/L agar, pH 7) and grown aerobically in the dark at 30°C for 48 hours. A colony was then picked and additioned to 15 ml of liquid MPYE medium in a transparent tube full to the brim. Cells were left in the dark for 1h, in order for them to consume the oxygen dissolved in the solution, and then grown photosynthetically at 30°C for 48h. Subsequently, 5 ml of the suspension were additioned to 250 ml of medium in a transparent bottle full to the brim and placed under light for 48h. Next, 100 ml of the suspension were additioned to 5 L of liquid MPYE, equally distributed among 4 Roux bottles full to the brim and the culture was grown for 48h photosynthetically at 30°C. Cells were harvested in the late log phase by centrifugation at 26000g for 10' at 4°C and stored at -80°C.

To isolate chromatophore vesicles, cells were thawed and washed twice by resuspension in 200 ml of MOPS buffer, pH 7, followed by centrifugation at 26,000 g for 10'.

The cell pellet obtained from the second wash was resuspended to a final volume of 60-70 ml, homogenized with a Potter-Elvehjem glass homogenizer, and treated with a French Press operating at 1000 psi. Unbroken cells and debris were discarded by centrifugation at 27000*g* for 35' at 4°C, while chromatophores were collected by ultracentrifugation of the resulting supernatant at 200000*g* for 90' at 4°C. The chromatophores pellet was resuspended in 50mM MOPS buffer, pH 7.3, divided into 100 µl aliquots, forzen in liquid nitrogen and stored at -80°C. The bacteriochlorophyll (BChl) content was extimated by extracting 10 µl of vesicles suspension in 1 ml of an acetone:methanol 7:2 mixture, subsequently determining the Bchl concentration by evaluating the absorption at 772 nm using a molar extinction coefficient of 75 mM⁻¹ cm⁻¹ (Clayton, 1966).

3.3 Chromatophores visible absorption spectrum characterisation

The absorption spectrum profile of isolated chromatophores was analysed by measuring the absorbance of a sample containing 30 μ M BChl in the 400-900 nm range.

For the carotenoid shift spectra analysis, chromatophores were diluted in 10 mM MOPS buffer, pH 7.3 to a final concentration of 25 μ M BChl. These are Light-minus-dark absorption spectra acquired in the 425-550 nm range with a Jasco V-550 spectrophotometer. Continuous photoexcitation was obtained by illuminating the sample from above with an optical guide light connected to a tungsten halogen lamp (250 W, Oriel). Before entering the optical guide, the actinic light was collimated by an optical condenser and filtered through an 8 cm thick water layer and a long-pass colored glass filter (Oriel 51350, cut-on wavelength of 780nm).

3.4 Time-resolved evolution of the carotenoid shift and ILs titration

The time evolution of the carotenoid band shift following a single xenon flash of light was monitored at 503 nm employing a kinetic spectrophotometer of local design (Barz et al., 1995; Francia et al., 2008). The photoexciting flash, lasting less than 8 µs, radiated from a xenon lamp filtered through two Wratten 88 A gelatin filters, granting a light with wavelength longer than 700nm. The exciting light was directed onto the sample by an optical guide, placed perpendicularly to the direction of the measuring beam. A Corning 4-96 filter was used to protect the photomultiplier by the sample light scattering and data were acquired by a LeCroy 9361C digital oscilloscope connected to a computer.

For the carotenoid shift characterisation, chromatophores were suspended in 50mM MOPS, pH7.3 to a final concentration of 25 µM BChl, in the presence of 50 mM KCl. The redox

potential was tuned to the 100-150 mV range by adding 1mM Na-Ascorbate and the residual cytochrome c oxidase activity was inhibited with 1mM KCN. The absorbance was monitored over time for 200 ms after the flash.

For the ILs titration experiments, chromatophores were suspended in 50 mM MOPS, 1mM Na-Ascorbate, 1 mM KCN, pH 7.3 at a fixed BChl concentration of 70 μ M. 10 μ M Antimycin A was added in order to collapse the slow Phase III, while 10 μ M oligomycin was added to avoid any proton efflux through the ATPase F₀ subunit channel. A magnetic stirrer, housed by a conical flare on the bottom of the Hellma quartz cuvette (Hellma GmbH, Müllheim, Germany) employed for these measurements, granted both a maximal photoexcitation of chromatophores RC and the mixing of the suspension after each ILs addition.

The absorbance was monitored over time for 180 ms after the flash.

Stock solutions for ILs bearing the Ntf₂- anion were prepared by diluting the pure compounds in isopropanol, while the rest of the tested compounds were diluted in water.

The total concentration of RC photoxidized by the xenon flash in our experiments was estimated as reported in (Bowyer et al., 1981), by measuring the absorbance change induced at 542 nm using a $\Delta\epsilon$ of 10.3 mM⁻¹ cm⁻¹. Since there is a contribution by the carotenoid electrochromic shift signal at this wavelength, the membrane electrical potential was collapsed through the addition of 30 mM KCl and 10 μ M valinomycin, thus avoiding any spectral interference. With the addition of 0.5 mM ferro/ferricyanide, the redox potential was fixed at around 415 mV, leading to a total pre-oxidation of cytochrome c₂ (Meinhardt & Crofts, 1982), thus avoiding the fast unresolved re-reduction of the forming P⁺. By using the Nernst equation, and assuming a redox midpoint potential of 450 mV for the P/P⁺ couple, the concentration of P photoxidized by the single flash was corrected for the pre-oxidized fraction. The experimental traces were fitted using Origin 6.1 software.

3.5 Spectrophotometric assay of Cytochrome bc1 electron transfer reactions

For these measurements, the same spectrophotometrical apparatus used in the carotenoid shift experiments was employed.

Chromatophores were suspended in 25 mM MOPS, 1 mM KCN, pH 7.3 at a concentration of 40 μ M BChI, in the presence of 50mM KCI and 10 μ M valinomycin to avoid spectral interference from the carotenoid shift signal. A 2mM, 1:1 ratio succinate/fumarate buffer was added to obtain a partially reduced quinone pool, given the presence of KCN, as indicated in Klishin et al., 2002. 1,2-Naphthoquinone and 1,4-Naphthoquinone were added as redox mediators, both at a concentration of 8 μ M.

The kinetics of oxidation and re-reduction of both cytochrome c_1 and c_2 (cyt c) were measured by monitoring the sample absorbance at 550 nm over the 90 ms following the photoexcitation of RC, subtracting the signal acquired at 540 nm, where there is an isosbestic point for the cyt c_{red} /cyt c_{ox} couple. This was useful in canceling the RC absorbance signal contribution, which is constant at the two wavelengths (Bowyer et al., 1981).

For the measurements of the Heme b_h reduction kinetics, 10 μ M Animycin A in order to block the re-oxidation of the forming reduced Heme b_h . The sample absorbance was monitored for 90 ms at 560 nm, this time subtracting the signal acquired at 569 nm, for the same aforementioned reasons (Bowyer et al., 1981).

3.6 Quantitative bioluminescence assay of chromatophores ATP synthesis

For the quantification of chromatophores ATP production, particles were isolated following the same protocol reported in paragraph 3.2, with the sole exception being the buffer used, which in this case was 50 mM glycylglycine, 5 mM Mg-acetate, pH 7. This choice was driven by the widespread knowledge of the role of Mg²⁺ in stabilising the ATPase. The pellet resulting from the last step of ultracentrifugation, containing the isolated chromatophores, was resuspended in this same buffer, and 60% glycerol was added as a precaution, before storing them at -20°C, to better preserve ATPase and membrane integrity.

Light-driven ATP synthesis was carried out in a dark room. Chromatophores were suspended to a final concentration of 20 µM BChl in 50 mM glycylglycine, 5 mM Mg-acetate, 0.3 M sucrose, 10 mM NaH₂PO₄, pH 8.5 in a Hellma quartz cuvette. 0.5 mM Na-ascorbate and 10 µM diaminodurene were added, respectively, as a reducing agent and as a redox mediator, while 1mM KCN was added to inhibit cytochrome c oxidase acitivty. The suspension was incubated for 5' in the presence of growing concentration of ILs at a temperature of 30°C, kept constant by a water bath connected to the housing were the cuvette was located. 2 mM ADP was added to start the reaction, while simultaneously starting the sample exposure to continuous light, radiating from a tungsten halogen lamp (250 W, Oriel). The actinic light was collimated by an optical condenser, filtered through an 8 cm thick water layer and a long-pass colored glass filter (Oriel 51350, cut-on wavelength of 780nm), and directed on the sample by an optical guide. The exposure time was controlled by a shutter placed between the actinic light source and the optical guide. After 30 seconds, the stream of light was istantaneously interrupted by the shutter and trichloroacetic acid was added to a final concentration of 2% to stop the reaction. The sample was collected and centrifuged at 13000g for 5', causing the precipitation of membranes and non-soluble debris. In order to account for the background activity of adenylate kinase, which produces ATP and AMP from 2 molecules of ADP (Gubellini et al., 2007; Markland & Wadkins, 1966), control measurements were carried out as mentioned above, without exposing the sample to light.

The supernatant, containing the synthesised ATP was collected for ATP quantification, which was carried out through the bioluminescence assay as follows:

One vial of lyophilized powder containing luciferase, luciferin, MgSO₄, DTT, EDTA, BSA and tricine (ATP Bioluminescence Assay Kit, Sigma-Aldrich, product number: FL-AA) was dissolved in 5 ml of sterile water. For each sample, 10 µl of such solution were added to 200 ml of 100 mM glycylglycine, 10 mM Mg-acetate, BSA 1mg/ml, pH 7.5. Next, 10 µl of sample, diluted ten times, were added and the light emission was measured at 560nm with a Sirius L luminometer (Berthold Technologies Gmbh, Bad Wildbad, Germany). Finally, 5 µM ATP standard (provided by the supplier) were added, and the difference in bioluminescence was used to calculate the concentration of ATP in our sample.

3.7 Rb. Capsulatus photosynthetic growth

At first, *Rhodobacter capsulatus* cells (strain 1710, DSMZ) were grown in the following Rhodospirillaceae selective medium, as indicated by the supplier, in order to remove possible contaminants:

	g/L
Yeast extract	0,3
Na ₂ -succinate	1
(NH ₄)-acetate	0,5
FE(III) citrate	0,005
KH ₂ PO ₄	0,5
MgSO ₄ x 7 H ₂ O	0,4
NaCl	0,4
NH ₄ CI	0,4
CaCl ₂ x 2 H ₂ O	0,05
Vitamin B ₁₂	0,4
L-Cysteiniumchloride	0,3
ZnSO ₄ x 7 H ₂ O	1 · 10-4
MnCl ₂ x 4 H ₂ O	3 · 10 ⁻⁵
H ₃ BO ₃	3 · 10 ⁻⁴
CoCl ₂ x 6 H ₂ O	2 · 10-4
CuCl ₂ x 2 H ₂ O	1 · 10 ⁻⁵
NiCl ₂ x 6 H ₂ O	2 · 10 ⁻⁵
Na ₂ MoO ₄ x 2 H ₂ O	3 · 10 ⁻⁵

NaOH 5 M was used to adjust the pH to 6.8. A transparent tube full to the brim was placed 40 cm away from a tungsten lamp (100 W) and cells were allowed to grow for 48 h at 30°C.

Subsequently, cells were stored at -80°C in 1 ml aliquots in the presence of 25% sterile glycerol.

For each experiment, a pre-culture was prepared by additioning 150 µl of a thawed aliquot to 15 ml of liquid MPYE medium (3 g/L Peptone, 3 g/L yeast extract, 1.6 mM MgCl₂, CaCl₂ 1mM, pH 7) in a transparent tube full to the brim, which was placed in the dark for 1 hour and was then moved in front of a 100 W tungsten lamp, at a distance of 40 cm, where cells were allowed to grow for 48 h at 30°C.

From the pre-culture, a volume containing $2 \cdot 10^8$ CFU was used to start the photosynthetic growth in the presence of increasing concentrations of ILs. The cells were grown at 30°C in 96-well plates, with each well containing 300 μ l of MPYE covered with 100 μ l of liquid sterile paraffin, useful in mantaining an anaerobic enivironment. Optical density was monitored at 620nm (OD_{620nm}) once every 60 minutes for 48 hours. In between measurements, the microplate spectrophotometer was programmed to eject the plate, allowing the cells to grow under light conditions. Light radiated from a LED bulb (3000K, 15W) hanging 25cm over the exposed plate. For each concentration, the experiment was repeated over eight technical replicates and three biological replicates.

Ntf₂ containing ILs were diluted in isopropanol, in order to better carry the compound to the test medium, taking care of adding always the same volume regardless of the final IL concentration needed, with 1% being the final concentration of isopropanol in the wells. For control growths, 1% isopropanol was added as reference.

At the end of each experiment, samples from the wells were streaked on solid Rhodospirillaceae selective medium (15 g/L agar), to check for contaminations.

These experiments were carried out in collaboration with Renolab Srl (40016, San Giorgio di Piano, Bologna).

The mean growth rate constant *k* was determined by fitting, where possible, the growth curves exponential phase with the exponential equation:

$$y = y(0) \cdot e^{kx}$$

Where y(0) is the OD_{620nm} measured at time zero and x is time expressed in hours.

3.8 Isolation of submitochondrial particles from bovine heart tissue

Mitochondria were first isolated from bovine heart tissue essentially following the method described by Pallotti and Lenaz (2001), working consistently at 4°C. After fat and connective tissue were removed, the bovine heart was dissected into small slices and 1.5 volumes of

0.25 M sucrose, 0.01 M Tris HCl, 0.2 mM EDTA, pH 7.8 were added every 500 g of material, homogenizing with a blender in cycles of 30 seconds plus 30 seconds of pause, until a uniform suspension was obtained. The homogenate pH was adjusted to 7.8 with 1 M KOH. A second step of homogenization was carried out, this time using a glass Potter-Elvehjem homogenizer, again adjusting the pH with 1 M KOH. The homogenate was then centrifuged at 600*g* for 10' at 4°C. The resulting pellet was discarded and the supernatant was filtered through several layers of cheesecloth, homogenized with a glass Potter-Elvehjem homogenizer and centrifuged at 20000*g* for 20' at 4°C. The pellet was resuspended and washed in 0.25 M sucrose, 0.01 M Tris HCl, 0.2 mM EDTA, pH 7.8, homogenized and centrifuged again at 20000*g* for 20' at 4°C. The pellet was resuspended in 100 ml of the same buffer, homogenized and a small sample was employed to estimate the protein concentration using the Bradford protein assay. Finally, the suspension was fractioned into 10 aliquots with a protein concentration of around 60 mg/ml.

Phosphorylating electron transfer particles (ETPH) were isolated from the mitochondrial pellet, after a cycle of thawing and re-freezing, following the methods described by Hansen and Smith (1964), with minor modifications. One aliquot was thawed, diluted to a concentration of 20 mg/ml with 0.25 M sucrose, 0.01 M Tris HCl, pH 7.8, homogenized and centrifuged at 27000g for 10' at 4°C. The resulting pellet was resuspended in STAMS buffer (0.25 M sucrose, 0.01 M Tris HCl, 10 mM MnCl₂, 5 mM MgCl₂, 1 mM ATP, 1 mM potassium succinate, pH 7.8) and homogenized. Subsequently, the suspension was treated for 10' with gaseous nitrogen to induce cavitation. Next, the suspension was partitioned into 8 ml aliquots inside 10 ml glass tubes and each aliquot was treated with 10 cycles of sonication, alternating 10" of sonication to 60" of pause. A Branson SFX 150 Digital Sonifier was used, employing a 3.2 microtip and setting the amplitude to 50%, working in ice in order to avoid drammatic increases in sample temperature and placing the sonotrode slightly lower than the sample volume half. Afterwards, the sonified aliquots were united and centrifuged at 27000g for 20' at 4°C, and the resulting supernatant was ultracentrifuged at 200000g for 30' at 4°C. Finally, the resulting pellet was resuspended in a small volume of 0.25 M sucrose, 20 mM tricine, 5 mM MgCl₂, 2 mM ATP, 2 mM GSH, 2 mM potassium succinate, pH 7.6 and protein concentration was estimated through the Bradford protein assay. The suspension was aliquoted, frozen with liquid nitrogen and stored at -80°C.

3.9 Reverse electron transfer assay

The reduction of NAD⁺ to NADH at the level of CI was followed spectrophotometrically over time at 350 nm, using a molar extinction coefficient of 5.55 mM⁻¹ cm⁻¹, following a modified version of the method reported by Kotlyar and Vinogradov (1990). ETPH were diluted to a final concentration of 0.3 mg/ml in STMK buffer (0.125 mM sucrose, 50 mM tricine, 40 mM KCI, 2.5 mM MgCl₂, pH 8), with the addition of 1 mM NAD⁺. 10 µM antimycin and 1 mM KCN were added to inhibit, respectively, CIII and CIV activity, in order to avoid the oxidation of the reduced quinone pool formed once 5 mM potassium succinate was added, thanks to the CII activity. ETPH were left incubating for 5' in the presence of different ILs concentrations and the reaction was started with the addition of 1 mM ATP.

3.10 NADH:O₂ assay

The oxidation of NADH at the level of CI was monitored spectrophotometrically over time at 350 nm, using a molar extinction coefficient of 5.55 mM⁻¹ cm⁻¹, following a modified version of the method reported by Kotlyar and Vinogradov (1990). ETPH were diluted to a final concentration of 0.1 mg/ml in STMK buffer. Subsequently, 1 mM ADP and 2 mM K₂PO₄ were added in order to work in phosphorilating condition, softening the back pressure caused by respiratory control. ETPH were left incubating for 5' in the presence of different ILs concentration and the reaction was started by adding 150 µM NADH.

3.11 Complex I activity assay

CI ability to reduce NADH was monitored spectrophotometrically over time at 350 nm, using a molar extinction coefficient of 5.55 mM $^{-1}$ cm $^{-1}$, essentially following the method reported by (Estornell et al., 1993). ETPH were diluted to a final concentration of 0.1 mg/ml in hypotonic buffer (50 mM K₂PO₄, 2 mM EDTA, pH 7.8), in order for the particles to break, maximasing CI accessibility towards the substrate. 10 μ M antimycin and 1 mM KCN were added to avoid any possible flow of electrons towards CIII and CIV, and ETPH were incubated for 5' in the presence of different ILs concentrations and 50 μ M decylubiquinone, necessary as the electron acceptor, since endogenous quinone is lost in the particles burst. Finally, the reaction was started with the addition of 150 μ M NADH.

3.12 Complex III activity assay

The reduction of exogenous oxidized cyt *c* (*Equus caballus*) at the level of CIII was monitored spectrophotometrically over time at 550 nm, using a molar extinction coefficient of 19.1 mM⁻¹ cm⁻¹ (Fato et al., 1993). ETPH were diluted to a final concentration of 0.1 mg/ml in hypotonic

buffer (50 mM K₂PO₄, 2 mM EDTA, pH 7.8), to maximize substrate accessibility, in the presence of 5 mM cyt *c*. 1 mM KCN was added to inhibit CIV activity, avoiding any re-oxidation of the forming reduced cyt *c*. ETPH were left incubating for 5' in the presence of different concentrations of ILs and the reaction was started with the addition of 50 μM reduced decylubiquinone.

3.13 Complex IV activity assay

The oxidation of exogenous pre-reduced cyt c (E. caballus) at the level of CIV was followed spectrophotometrically over time at 550 nm, using a molar extinction coefficient of 19.1 mM⁻¹ cm⁻¹ (Fato et al., 1993). ETPH were diluted to a final concentration of 0.1 mg/ml in hypotonic buffer (50 mM K₂PO₄, 2 mM EDTA, pH 7.8), maximising substrate accessibility. 10 μ M antimycin was added to avoid the re-reduction of the forming oxidized cyt c caused by CIII activity. ETPH were left incubating 5' in the presence of different concentrations of ILs and the reaction was started by adding 20 μ M reduced cyt c.

4. Results

(The results presented in paragraphs 4.2 to 4.5 have been published in the following paper:

Bin T, Venturoli G, Ghelli AM, Francia F. *Use of bacterial photosynthetic vesicles to evaluate the effect of ionic liquids on the permeability of biological membranes*. Biochim Biophys Acta Biomembr. 2024 Mar;1866(3):184291.https://doi.org/10.1016/j.bbamem.2024.184291)

4.1 Isolated chormatophores characterisation

The absorption spectrum of chormatophores isolated from *Rb. Capsulatus* MT1131 cells was analysed in the 400-900 nm range (**Fig 4.1**).

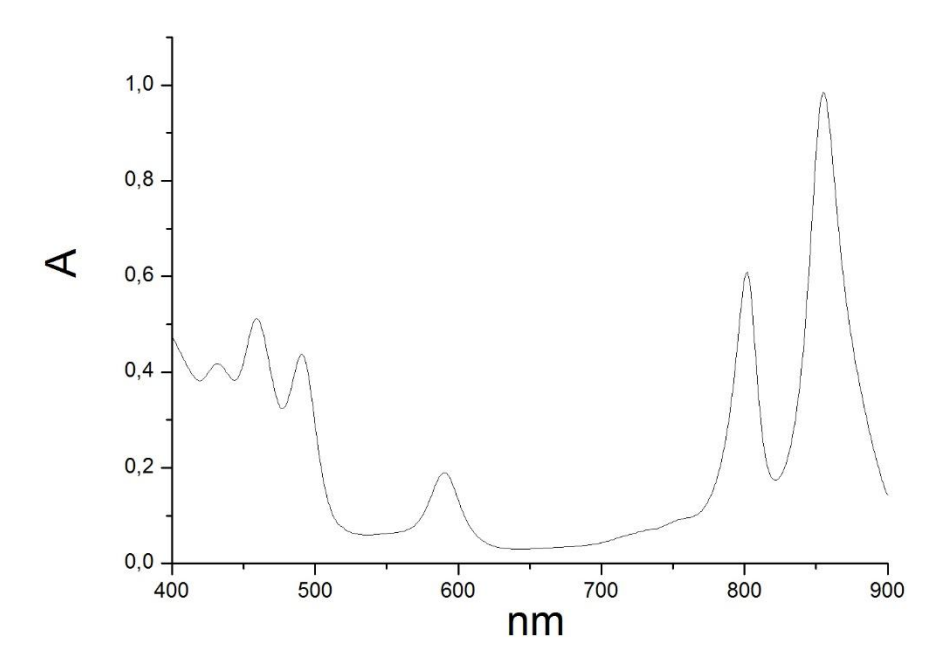


Figure 4.1. *Rb. Capsulatus* MT1131 chromatophores absorption spectrum in the 400-900 nm range (BChI = $30 \mu M$).

Chromatophores absorption spectrum showed the expected profile, with two bands in the infrared region, one at 855 nm and one at 804 nm, indicating the presence of BChl *a* incorporated into the protein-pigment complexes associated to the RC and into the RC itself, and three absorption bands in the region between 400 and 500nm, typical of the carotenoids. The absence of strong aspecific absorbance, expecially under 600 nm, indicates that superfluous cellular components were not present in our chromatophores preparation. Next, the carotenoids electrochromic shift was tested (**Fig. 4.2**). By acquiring the absorption

spectrum of our chromatophores preparation in the 425-550 nm range while illuminating with continuous light, and by subtracting to it the same sample absorption spectrum measured in

the dark. The light-dark spectrum shows two positive peaks at 475nm and 507 nm. From here on, we decided to work at 503 nm for the detection of the carotenoid shift signal, since it grants a good signal-to-noise ratio.

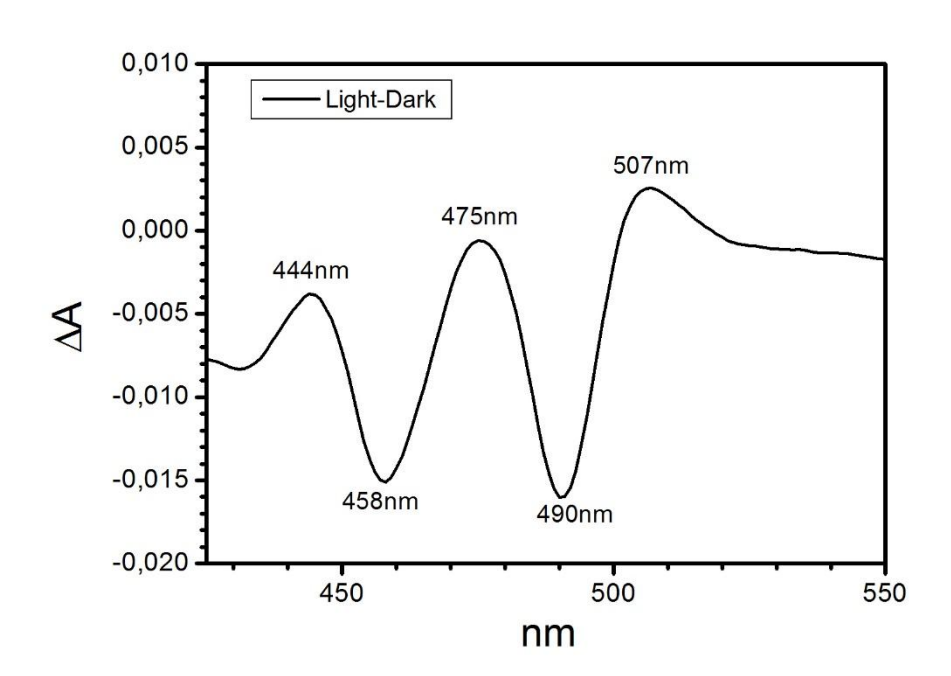


Figure 4.2. Light-minus-dark difference spectra of chromatophores (BChI = $25 \mu M$) in the 425-550 nm range.

The time evolution of the carotenoid shift band was measured at 503 nm over time for 200 ms after the RC photoexcitation, resulting in a fast increase in absorbance (Phase I and II), followed by the slower Phase III in the millisecond range (**Fig. 4.3a**).

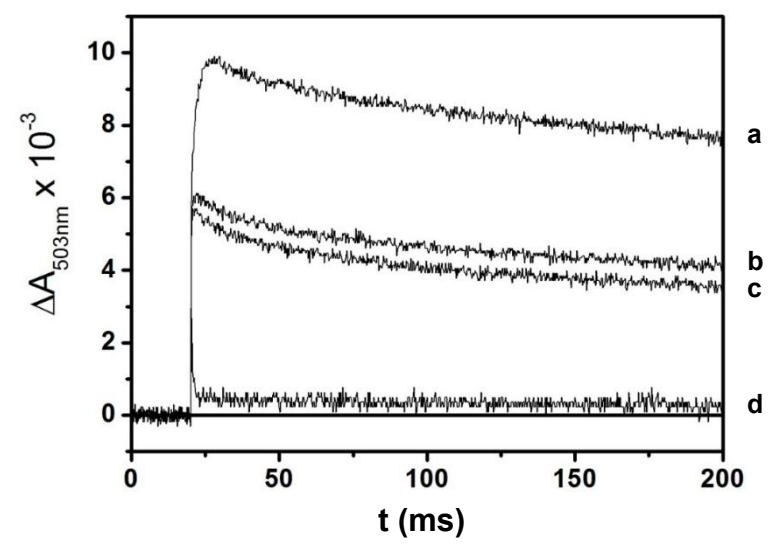


Figure 4.3. Time evolution of the carotenoid shift signal induced by a single turnover flash, monitored at 503 nm over time for 200 ms. (a) Control; (b) 10 μ M Antimycin A; (c) b + 2 μ M myxothiazol; (d) c + 50 mM KCl and 10 μ M valinomycin.

The signal then decayed slowly, as expected, since, in this condition, the only contributions for $\Delta\Psi$ dissipation are the passive flux of ions through the lipid bilayer and the passive efflux of H⁺ through the ATP synthase F₀ subunit (Saphon et al., 1975; Jackson, 1988). Phase III was completely canceled with the sequential addition of 10 μ M Antimycin A and 2 μ M myxothiazol (**Fig. 4.3b,c**), while the signal collapsed when chromatophores were uncoupled by the addition of 30 mM KCl and 10 μ M valinomycin, a specific ionophore for K⁺ ions.

Overall, these data confirmed that the isolated chromatophores retained the functional elements of Rb. Capsulatus photosynthetic electron transport chain, organised in closed vesicles able to form a $\Delta\Psi$ after photoexcitation of the RC. The slow kinetics of the signal decay indicated an intact phospholipid bilayer with a low background proton leakage.

4.2 Kinetics of the carotenoid shift decay in the presence of ILs

Chromatophores were suspended in the presence of growing ILs concentration and the carotenoid shift band signal was monitored spectrophotometrically at 503 nm for 180 ms after the short (µs) RC photoexcitation induced by a single xenon flash of light (**Fig. 4.4**). Antimycin A was added to better estimate the instantaneous decay of $\Delta\Psi$, since this inhibitor shuts down the electron transfer from Heme b_h to quinone at the level of the Qi site of cytochrome bc_1 complex, contributing to the electrochromic shift signal in the millisecond span (Glaser & Crofts, 1984). Oligomycin was added to inhibit H⁺ translocation through the F₀ subunit of damaged ATP synthases (Symersky et al., 2012). Under these conditions, the decay of the electrochromic shift signal in the untreated chromatophores suspension (lower-case **a** letter in each panel of Fig. 4.4) was essentially only due to ionic fluxes through the phospholipid bilayer, eventually informing quantitatively on the chromatophores membrane permeability. The experimental traces clearly show how Ntf2 containing ILs are able to accelerate the kinetics of carotenoid shift decay even at micromolar concentrations, with an almost complete collapse in the signal at around 100-200 µM. Interestingly, while c₁c₂lm Ntf₂ shows this effect at such concentrations, when the same cation is paired with a different anion, such as BF₄or OTf⁻, this occurs at much higher concentrations (c₁c₂lm BF₄⁻ and c₁c₂lm OTf⁻ panel, **Fig. 4.4**). In fact, both c₁c₂Im BF₄ and c₁c₂Im OTf start to increase the decay kinetics significantly at concentrations that are in the order of hundres of micromolar, eventually collapsing the carotenoid shift, respectively, at 90 mM and 180 mM. Chol Cl is shown as a negative control, since it is a non-permeant IL frequently used as a control in bioenergetic studies (Takamiya & Dutton, 1977).

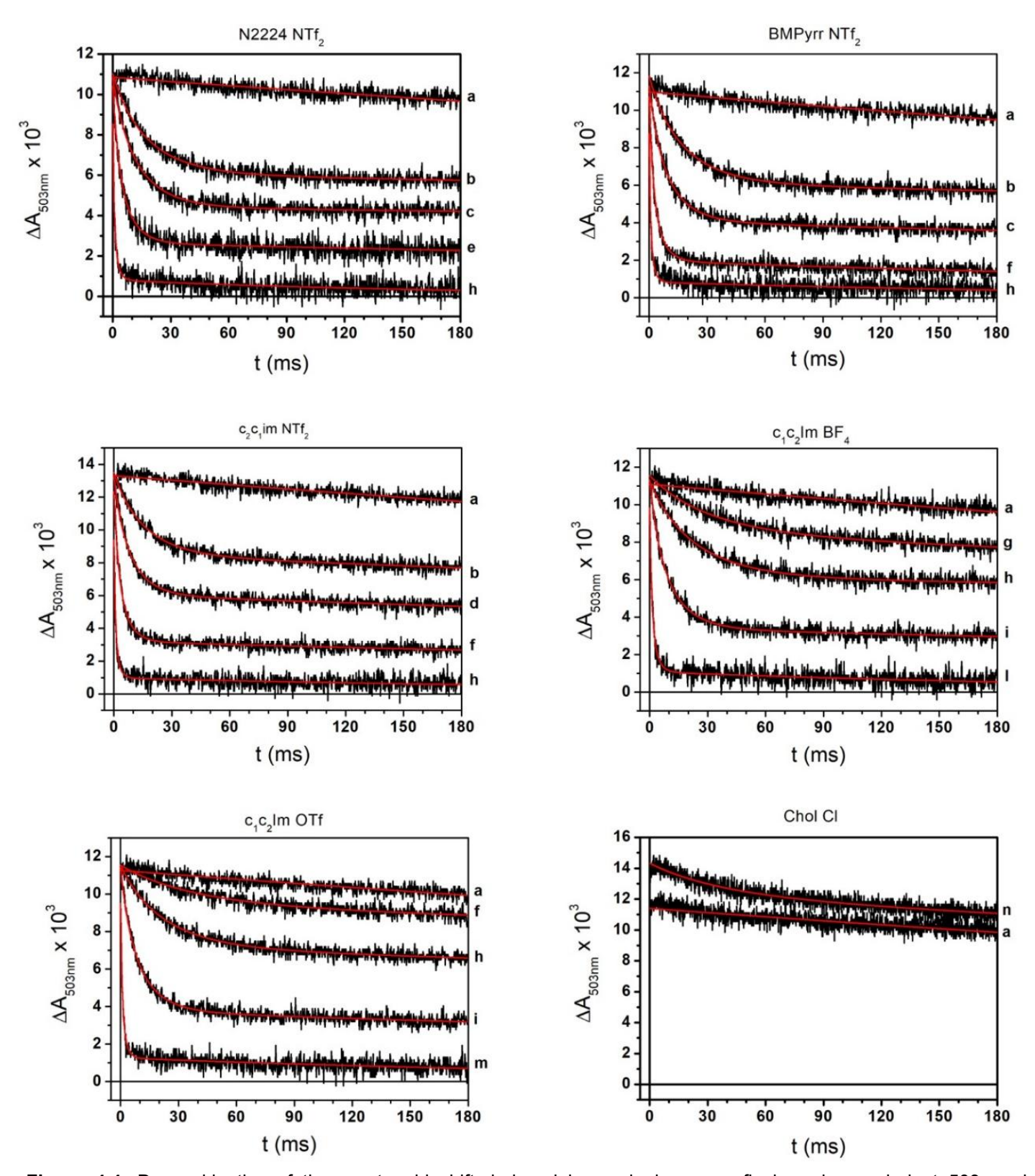


Figure 4.4. Decay kinetics of the carotenoid shift, induced by a single xenon flash and recorded at 503nm, in chromatophores suspended in the presence of increasing concentrations of ILs. Only the part of the experimental traces following the RC photoexcitation is shown. The lower-case letters correspond to the following ILs concentrations: a, 0 μM; b, 5 μM; c, 10 μM; d, 20 μM; e, 50 μM; f, 100 μM; g, 200 μM; h, 1mM; i, 5mM; I, 90 mM; m, 180 mM; n, 400 mM. Red lines represent best fit to eq. 2. Control traces (a) were fitted essentially to an exponential decay with eq. 1, by setting m=0. For Choline Chloride (Chol Cl panel), only the traced acquired at 0 and 400 mM concentrations are reported (respectively $\bf a$ and $\bf n$), to avoid the overlapping between the traces recorded at intermediate concentrations. The larger initial amplitude of trace $\bf n$ is due to a strong dilution of the sample that results in an enhanced penetration of the excitation light in the area of the sample interrogated by the measuring beam. Each trace represents the average of 16 individual signals.

4.3 Interpretation model and data analysis

For all the compounds tested on chromatophores suspension, the kinetics of decay of the carotenoid shift band are strongly biphasic (**Fig. 4.4**), with a first phase where the signal amplitude decreases rapidly and a second slower phase that shows a kinetic very similar to the one observed in control condition. Moreover, the steepness of the first phase increases with the increase in IL concentration, while the second phase seems constant and independent of the compound concentration.

At first, the experimental traces were interpreted with a model perviously employed in the study of imidazolium- and pyrrolidinium-based ILs effect on carotenoid shift in chromatophores suspension (Malferrari et al., 2015). In this study, where cations from the two aforementioned classes were paired with chloride and dicyanamide as counter anions, the experimental traces were interpreted satisfactorily by the statistical model developed by Schmid and Junge to analyse the behavior of ionophores interacting with tylakoid membranes (Schmid & Junge, 1975). The strong biphasicity of the curves was therefore explained by considering a Poisson distribution of the charges, where each chromatophore is considered as an independent unit whose conductivity is determined by the number of permeating ions, with each ion characterised by a specific individual conductance. In this sense, the slow kinetic phase would arise from the fraction of the chromatophores population not being permeated. Malferrari et al. described the non-homogenous decay of the electrochromic shift with eq. (1):

$$\Delta A(t) = \Delta A(0) \cdot e^{-m - k_l \cdot t} \cdot e^{m \cdot e^{-k \cdot t}} \tag{1}$$

Where ΔA is the maximum amplitude of the carotenoid shift band following the RC photoexcitation, m is the average number of permeating ions per chromatophore, k_l is a rate constant accounting for the membrane background leakage and k is the conductance constant of the single ion of the tested permeant species.

When interpreting our data with this model, while eq. (1) was able to provide an accurate fit of our traces (**Fig. 4.4**, red lines), some inconsistencies arose from the best fitting parameters, reported in **Table 1**. In fact, apart from Chol Cl, a proper fit of the carotenoid shift was yielded only when the value of the rate constant k was allowed to vary with the growth of IL concentration, increasing by up to one order of magnitude along the titration, when, in principle, according to the statistical model, k should be concentration-independent.

IL	с (µМ)	т	k₁ (s ⁻¹)	k (s ⁻¹)
	0	-	$(6.4 \pm 0.2) \cdot 10^{-1}$	-
	5	0.60 ± 0.01	$(3.2 \pm 0.6) \cdot 10^{-1}$	47 ± 1
	10	0.90 ± 0.01	$(2.6 \pm 0.7) \cdot 10^{-1}$	62 ± 2
N2224 Ntf ₂	20	1.08 ± 0.01	$(6.8 \pm 0.7) \cdot 10^{-1}$	86 ± 2
	50	1.37 ± 0.02	$(8.4 \pm 1.2) \cdot 10^{-1}$	123 ± 4
	100	1.80 ± 0.02	1.4 ± 0.2	182 ± 7
	200	2.07 ± 0.03	2.0 ± 0.2	235 ± 9
	500	2.20 ± 0.04	4.0 ± 0.4	366 ± 20
	1000	2.35 ± 0.05	5.6 ± 0.5	425 ± 20
	0		$(8.1 \pm 0.2) \cdot 10^{-1}$	-
	5	0.66 ± 0.01	$(3.8 \pm 0.7) \cdot 10^{-1}$	47 ± 1
BMPyrr Ntf ₂	10	0.84 ± 0.01	$(6.6 \pm 0.5) \cdot 10^{-1}$	64 ± 2
	20	1.02 ± 0.01	$(7.1 \pm 0.7) \cdot 10^{-1}$	78 ± 2
	100	1.69 ± 0.01	1.9 ± 0.1	176 ± 4
	200	2.04 ± 0.01	2.3 ± 0.2	210 ± 8
	500	2.24 ± 0.01	4.3 ± 0.3	363 ± 17
	1000	2.34 ± 0.01	3.9 ± 0.4	458 ± 28
	0	-	$(7.0 \pm 0.1) \cdot 10^{-1}$	-
	5	0.46 ± 0.01	$(5.6 \pm 0.4) \cdot 10^{-1}$	60 ± 2
	10	0.63 ± 0.01	$(5.5 \pm 0.4) \cdot 10^{-1}$	71 ± 2
C ₁ C ₂ Im Ntf ₂	20	0.78 ± 0.01	$(6.8 \pm 0.4) \cdot 10^{-1}$	94 ± 2
	50	0.99 ± 0.01	$(8.5 \pm 0.5) \cdot 10^{-1}$	126 ± 3
	100	1.35 ± 0.01	$(9.9 \pm 0.7) \cdot 10^{-1}$	173 ± 4
	200	1.86 ± 0.02	1.2 ± 0.2	244 ± 9
	500	2.16 ± 0.03	2.9 ± 0.2	383 ± 16
-	1000	2.26 ± 0.04	3.0 ± 0.3	450 ± 25
	0	-	$(8.0 \pm 0.2) \cdot 10^{-1}$	-
	100	0.20 ± 0.01	$(5.3 \pm 1.0) \cdot 10^{-1}$	29 ± 3
	200	0.30 ± 0.01	$(5.4 \pm 1.0) \cdot 10^{-1}$	29 ± 2
	400	0.43 ± 0.01	$(2.6 \pm 1.0) \cdot 10^{-1}$	28 ± 2
C ₁ C ₂ Im BF ₄	$1 \cdot 10^{3}$	0.61 ± 0.01	$(2.6 \pm 1.0) \cdot 10^{-1}$	35 ± 1
	$2 \cdot 10^{3}$	0.85 ± 0.01	$(6.2 \pm 1.0) \cdot 10^{-1}$	54 ± 1
	$5 \cdot 10^{3}$	1.20 ± 0.01	$(7.7 \pm 1.0) \cdot 10^{-1}$	74 ± 2
	$1 \cdot 10^4$	1.53 ± 0.01	1.2 ± 0.1	99 ± 2
	$2 \cdot 10^4$	1.81 ± 0.02	2.0 ± 0.2	133 ± 3
	$5 \cdot 10^4$	2.18 ± 0.04	3.7 ± 0.4	199 ± 9
	9 · 10 ⁴	2.20 ± 0.04	3.8 ± 0.3	312 ± 15
	18 · 104	2.02 ± 0.04	3.2 ± 0.3	374 ± 20
	0	-	$(7.0 \pm 0.1) \cdot 10^{-1}$	
	5	0.16 ± 0.06	$(1.2 \pm 2.6) \cdot 10^{-1}$	13 ± 5
	20	0.17 ± 0.01	$(3.6 \pm 0.9) \cdot 10^{-1}$	24 ± 3
C₁C₂Im Otf	100	0.20 ± 0.01	$(3.6 \pm 1.0) \cdot 10^{-1}$	24 ± 3
	$1 \cdot 10^3$	0.47 ± 0.01	$(4.8 \pm 0.6) \cdot 10^{-1}$	38 ± 1
	$5 \cdot 10^3$	1.10 ± 0.01	$(9.4 \pm 0.7) \cdot 10^{-1}$	78 ± 2
	$2 \cdot 10^4$	1.74 ± 0.02	1.97 ± 0.18	142 ± 5
	$5 \cdot 10^4$	2.12 ± 0.03	4.03 ± 0.32	223 ± 9
	$9 \cdot 10^4$	2.09 ± 0.03	4.26 ± 0.30	304 ± 14
-	18 · 104	2.02 ± 0.03	3.23 ± 0.24	444 ± 21
	0	- 0.12 - 0.05	$(8.0 \pm 0.2) \cdot 10^{-1}$	- 14 - 5
	$1 \cdot 10^3$	0.13 ± 0.05	$(2.3 \pm 2.2) \cdot 10^{-1}$	14 ± 5
	5· 10 ³	0.21 ± 0.03	$(0.5 \pm 1.4) \cdot 10^{-1}$	18 ± 3
OL 15:	1. 104	0.21 ± 0.01	$(3.6 \pm 0.8) \cdot 10^{-1}$	27 ± 2
Chol Cl	2· 10 ⁴	0.23 ± 0.01	$(3.5 \pm 0.7) \cdot 10^{-1}$	28 ± 2
	5· 10 ⁴	0.25 ± 0.01	$(2.5 \pm 0.9) \cdot 10^{-1}$	24 ± 2
	9· 10 ⁴	0.19 ± 0.01	$(5.2 \pm 0.7) \cdot 10^{-1}$	26 ± 2
	$18 \cdot 10^4$ $40 \cdot 10^4$	0.16 ± 0.01	$(5.4 \pm 0.6) \cdot 10^{-1}$	28 ± 3
		0.15 ± 0.01	$(5.9 \pm 0.7) \cdot 10^{-1}$	25 ± 3

Table 1. Values of the parameters m, k_l and k obtained by fitting the carotenoid shift experimental traces with eq. 1. ILs concentrations are expressed in the micromolar scale. For control traces (c=0), m was set to a value of 0, resulting in an exponential decay.

It must be pointed out that, instead, in Malferrari et al. eq. (1) yielded an accurate fit of the experimental traces without any variation of k, which remained fixed at its compound-specific value along the single titrations. This is coherent with their findings on how the polarity of alkyl side chains of cations increases membrane permeability. In our case, then, the increase of the rate constant k would be explainable only by a concentration-dependant effect of destabilisation of the chromatophore lipid bilayer by the compounds, causing an enhancement in the membrane conductivity, a possibility that strongly contrast with what we observed in paragraph 4.5.

A second oddity concerns the parameter m, whose value allows for an estimation of the average number of ions permeating each vesicle. As better shown in **Figure 4.5**, excluding Chol CI, for each compound tested, the m parameter tends to saturate at an extremely low value of around 2.

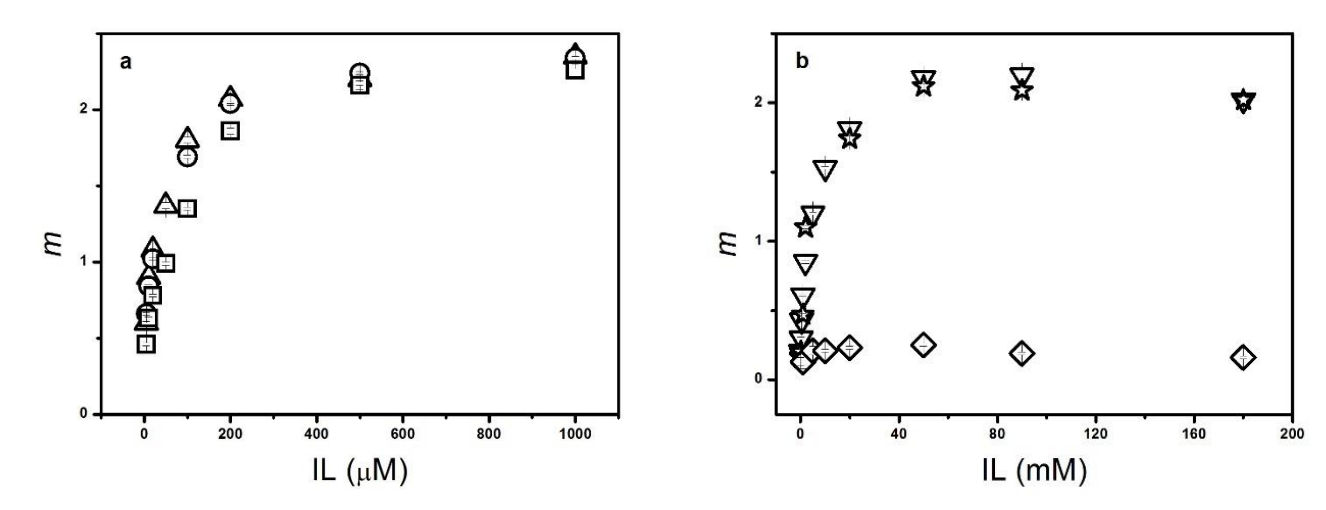


Figure 4.5. Average number of m permeating ions per chromatophore, expressed as a function of IL concentration. (a) Triangles, N2224-NTf₂; circles, BMPyrr-NTf₂; squares, c_1c_2 Im-NTf₂. (b) Inverted triangles, c_1c_2 Im-BF₄; stars, c_1c_2 Im-OTf; diamonds, Chol-Cl.

It is important to examine this value in light of the most recent chromatophore model, based on atom force microscopy data and molecular dynamics simulations (Singharoy et al., 2019). Given an average number of around 17200 lipids in the chromatophore membrane, the *m* parameter would indicate that, at saturating concentrations, only one ion per 8600 lipid is permeating the vesicle. While the chromatophore membrane is very rich in proteins, this is estimation remains extremely difficult to believe. In fact, with an average chromatophore surface of around 34000 nm², assuming a mean of 0.64 nm² occupied by a single phospholipid head and considering 8600 lipids for each side of the membrane (half of the total 17200 previously mentioned), the portion of the chromatophore area occupied by lipids

is approximately 5500 nm², i.e. 16% of the whole vesicle surface. Hence, given the large portion of membrane surface available, it is unlikely that such a low number of ions permeate the lipid bilayer.

Because of the aforementioned inconsistencies, a different model of interpretation was employed for the analysis of our data. Emerging from charge-pulse relaxation experiments on the behaviour of ionophores and hydrophobic ions permeating artificial lipid bilayers (Benz et al., 1976; Benz & McLaughlin, 1983), this model explains the resulting biphasic decay of membrane potential by considering the ion mechanism of permeation, which occurs in three steps: initially, the permeating ion locates at the membrane-solution interface, in a deep potential energy minimum; subsequently, the ion translocates across the membrane, overcoming the high central energy barrier, and reaches a new low energy pocket at the interface on the other side of the membrane; finally, the desorption into the aqueous phase occurs.

Assuming that the membrane electrical potential formed following the single flash photoexcitation is sufficiently small ($\Delta\Psi$ << RT/F, where R is the gas constant, T is the absolute temperature and F is the Faraday constant) and that the chromatophore membrane is symmetrically characterised by deep potential energy minima at the membrane-solution interfaces, and by a high central energy barrier, the dissipation of the $\Delta\Psi$ can be described by eq. (2):

$$\Delta_{\Psi}(t) = \Delta_{\Psi}(0) \left(a_1 e^{-t/\tau_1} + a_2 e^{-t/\tau_2} \right)$$
 (2)

Where τ_1 and τ_2 are the relaxation times, a_1 accounts for the relaxation amplitude and $\Delta\Psi$ (0) is the initial transmembrane potential, which, in our condition, is measured by the ΔA (0).

As shown in **Fig. 4.6**, eq. (2) provides an accurate fitting of the carotenoid shift decay for each compound tested. Moreover, from the values of the τ_1 , τ_2 and a_1 parameters, reported in **Table 2**, some calculation can be done to better interprete the data.

According to the work of Benz et al., 1976, where this model was originally developed, the three parameters can be expressed in terms of the kinetic rate constants k_i and k_{ma} , respectively accounting for the translocation of the ion across the central energy barrier and its absorption and desorption into the aqueous phase, while considering also the total concentration of ions interfacing with the lipid bilayer, namely N_t , expressed as picomoles of ions per membrane area (pmol · cm²). For $k_{ma} << k_i$, which is generally true when τ_1 and τ_2 are distinctly separated, the above-mentioned relationships can be expressed by eq. (3)-(5):

$$\tau_1 \approx \frac{1}{2 k_i (1 + \alpha^2 b N_t)} \tag{3}$$

$$\tau_2 \approx \frac{1 + \alpha^2 b N t}{k_{ma} b N_t} \tag{4}$$

$$a_1 \approx \frac{\alpha^2 b N_t}{1 + \alpha^2 b N_t} \tag{5}$$

Where α is the fraction of the $\Delta\Psi$ dropping across the membrane (the high central energy barrier) and b is related to the permeating ion valency (z) and to the membrane capacity (C_m), as expressed in eq. (6):

$$b = \frac{z^2 \cdot F^2}{4RTC_m} \tag{6}$$

From eq. (4) we know $\alpha^2 = k_{ma} \cdot \tau_2 - 1 / bN_t$, which can be replaced in eq. (3) and (5), resulting in eq. (7) and (8):

$$\tau_1 \approx \frac{1}{(2 k_i k_{ma} \tau_2 b N_t)} \tag{7}$$

$$a_1 \approx 1 - \frac{1}{(k_{ma}\tau_2 b N_t)} \tag{8}$$

From eq. (7) we have $bN_t = 1 / (2 k_i k_{ma} \tau_2 \tau_1)$, which, when replaced in eq. (8), gives use eq. (9):

$$k_i \approx \frac{1 - a_1}{2\tau_1} \tag{9}$$

Eq. (9) makes two things clear: one is that k_i , the rate constant accounting for the ion translocation across the high central energy barrier (the membrane), can be determined directly by the experimental value of a_1 and r_1 , i.e. the relaxation amplitude and time of the fast phase of the carotenoid shift curve; secondly, that the fast phase is essentially defined by the ions translocation across the membrane.

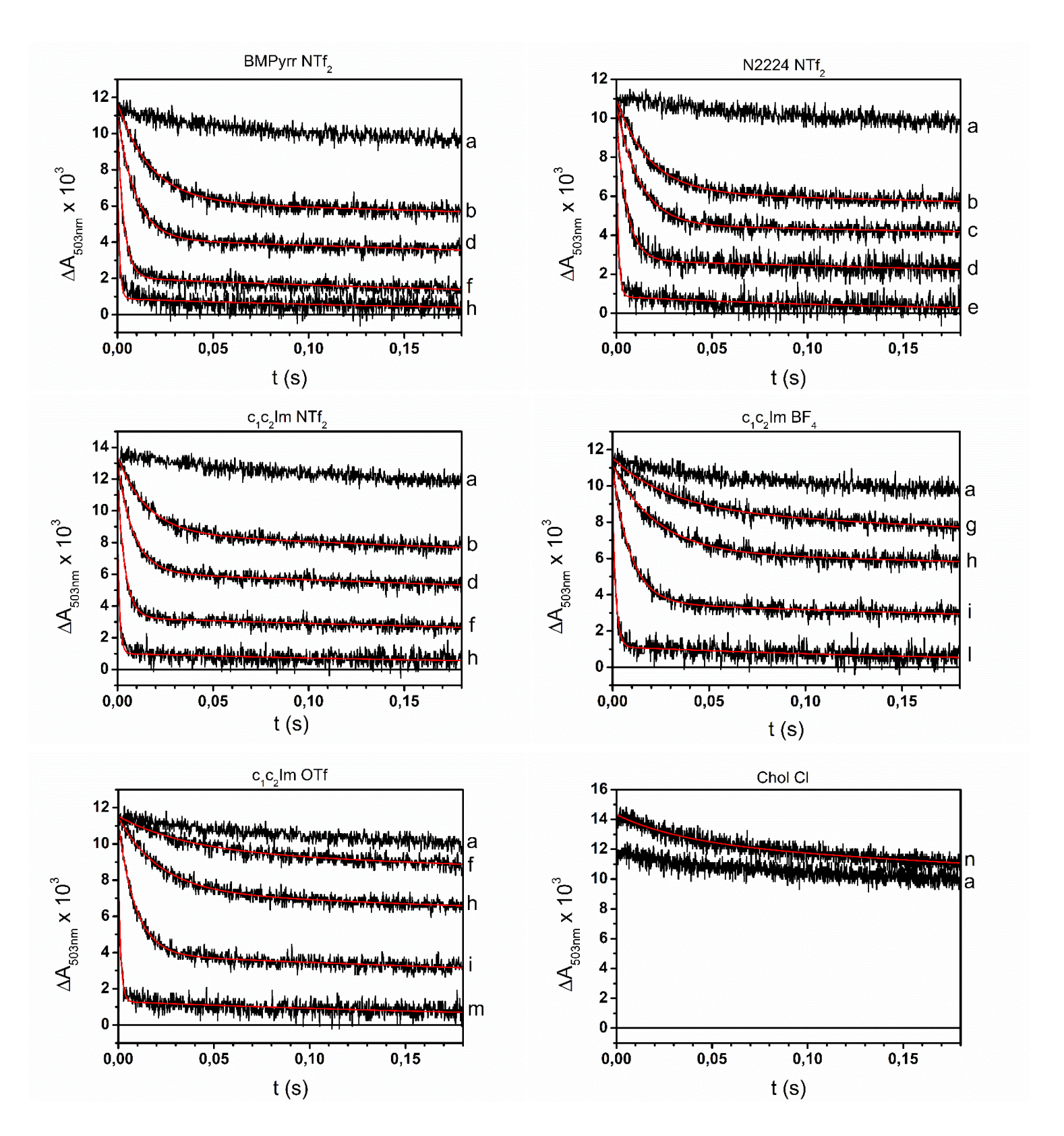


Figure 4.6. Decay kinetics of the carotenoid shift, induced by a single xenon flash and recorded at 503nm, in chromatophores suspended in the presence of increasing concentrations of ILs. Only the part of the experimental traces following the RC photoexcitation is shown. The lower-case letters correspond to the following ILs concentrations: a, 0 μ M; b, 5 μ M; c, 10 μ M; d, 20 μ M; e, 50 μ M; f, 100 μ M; g, 200 μ M; h, 1mM; i, 5mM; l, 90 mM; m, 180 mM; n, 400 mM. Red lines represent best fit to eq. 2. Each trace represents the average of 16 individual signals.

IL	с (µМ)	r_1 (s) · 10 ³	τ ₂ (s)	a ₁	<i>k_i</i> (s ⁻¹)	N_t (pmol · cm ²)
	5	17.25 ±0.47	2.33 ±0.30	0.4344 ±0.0040	16.39 ±0.46	0.449 ±0.007
	10	12.18 ±0.27	2.31 ±0.33	0.5736 ±0.0036	17.50 ±0.41	0.787 ±0.011
	20	8.42 ±0.17	1.17 ±0.09	0.6433 ±0.0032	21.18 ±0.47	1.055 ±0.015
N2224 Ntf ₂	50	5.46 ±0.16	0.96 ±0.11	0.7302 ±0.0044	24.71 ±0.83	1.583 ±0.036
	100	3.30 ±0.11	0.62 ±0.06	0.8146 ±0.0041	28.09 ±1.12	2.571 ±0.069
	200	2.29 ±0.08	0.41 ±0.04	0.8621 ±0.0038	30.11 ±1.35	3.657 ±0.118
	500	1.41 ±0.07	0.23 ±0.02	0.8802 ±0.0045	42.48 ±2.65	4.298 ±0.184
	1000	1.11 ±0.06	0.16 ±0.01	0.8963 ±0.0048	46.29 ±3.28	5.057 ±0.263
	5	17.13 ±0.43	1.96 ±0.22	0.4669 ±0.0039	15.56 ±0.41	0.512 ±0.008
BMPyrrNtf ₂	10	11.96 ±0.25	1.26 ±0.09	0.5529 ±0.0034	18.69 ±0.42	0.724 ±0.010
	20	9.38 ±0.18	1.14 ±0.08	0.6220 ±0.0031	20.15 ±0.42	0.963 ±0.013
	100	3.43 ±0.08	0.48 ±0.02	0.8030 ±0.0029	28.71 ±0.79	2.385 ±0.044
	200	2.56 ±0.09	0.37 ±0.03	0.8585 ±0.0040	27.64 ±1.25	3.549 ±0.116
	500	1.40 ±0.06	0.21 ±0.02	0.8847 ±0.0041	41.19 ±2.29	4.487 ±0.180
	1000	1.03 ±0.06	0.23 ±0.02	0.8957 ±0.0048	50.65 ±3.77	5.022 ±0.259
	5	15.55 ±0.43	1.64 ±0.11	0.3616 ±0.0036	20.53 ±0.58	0.331 ±0.005
	10	11.65 ±0.25	1.61 ±0.10	0.4587 ±0.0032	23.23 ±0.52	0.496 ±0.006
	20	8.47 ±0.17	1.32 ±0.07	0.5306 ±0.0031	27.71 ±0.59	0.661 ±0.008
C ₁ C ₂ Im Ntf ₂	50	5.98 ±0.12	1.06 ±0.05	0.6150 ±0.0031	32.19 ±0.69	0.934 ±0.012
	100	3.93 ±0.08	0.89 ±0.05	0.7276 ±0.0029	34.65 ±0.79	1.563 ±0.023
	200	2.36 ±0.08	0.70 ±0.08	0.8332 ±0.0037	35.34 ±1.43	2.922 ±0.078
	500	1.36 ±0.05	0.32 ±0.02	0.8764 ±0.0037	45.46 ±2.15	4.146 ±0.140
	1000	1.10 ±0.06	0.30 ±0.03	0.8885 ±0.0045	50.70 ±3.43	4.660 ±0.210
C ₁ C ₂ Im BF ₄	100	31.30 ±2.86	1.78 ±0.23	0.1747 ±0.0084	13.19 ±1.21	0.124 ±0.007
	200	30.28 ±1.90	1.68 ±0.23	0.2537 ±0.0081	12.32 ±0.78	0.199 ±0.009
	400	30.01 ±1.40	2.66 ±0.60	0.3309 ±0.0077	11.14 ±0.54	0.289 ±0.010
	$1 \cdot 10^3$	22.56 ±0.70	2.28 ±0.38	0.4352 ±0.0053	12.51 ±0.41	0.451 ±0.010
	$2 \cdot 10^3$	14.15 ±0.30	1.24 ±0.10	0.5535 ±0.0036	15.77 ±0.36	0.725 ±0.010
	$5 \cdot 10^3$	9.34 ±0.17	0.98 ±0.07	0.6796 ±0.0031	17.13 ±0.35	1.241 ±0.017
	$1\cdot 10^4$	6.32 ±0.12	0.65 ±0.04	0.7658 ±0.0029	18.53 ±0.42	1.913 ±0.031
	$2\cdot 10^4$	4.38 ±0.10	0.41 ±0.02	0.8215 ±0.0029	20.38 ±0.57	2.692 ±0.054
	$5 \cdot 10^4$	2.64 ±0.10	0.24 ±0.02	0.8751 ±0.0041	23.66 ±1.19	4.098 ±0.155
	$9 \cdot 10^4$	1.67 ±0.07	0.24 ±0.02	0.8801 ±0.0043	35.89 ±1.98	4.294 ±0.175
	18 · 10 ⁴	1.47 ±0.07	0.29 ±0.02	0.8572 ±0.0050	48.56 ±2.87	3.512 ±0.144
	5	73.98 ±24.18	17.82 ±2.85	0.1569 ±0.0543	5.70 ±1.90	0.109 ±0.045
C₁C₂lm Otf	20	47.48 ±6.11	5.71 ±1.20	0.1805 ±0.0176	8.63 ±1.13	0.129 ±0.015
	100	36.65 ±3.67	2.55 ±0.57	0.1754 ±0.0106	11.25 ±1.14	0.124 ±0.009
	1 · 10 ³	21.79 ±0.69	1.75 ±0.17	0.3642 ±0.0046	14.59 ±0.47	0.335 ±0.007
	5 · 10 ³	9.11 ±0.17	0.88 ±0.05	0.6518 ±0.0030	19.11 ±0.39	1.095 ±0.014
	2 · 10 ⁴	4.19 ±0.12	0.43 ±0.03	0.8091 ±0.0038	22.78 ±0.79	2.480 ±0.061
	5 · 10 ⁴	2.34 ±0.08	0.22 ±0.01	0.8690 ±0.0040	27.99 ±1.29	3.881 ±0.137
	9 · 10 ⁴	1.75 ±0.07	0.22 ±0.01	0.8668 ±0.0042	38.06 ±1.94	3.807 ±0.139
	18 · 10 ⁴	1.22 ±0.06	0.29 ±0.02	0.8590 ±0.0044	57.80 ±3.36	3.563 ±0.129
	1 · 10 ³	63.39 ±19.28	3.82 ±2.80	0.1199 ±0.0354	6.94 ±2.13	0.080 ±0.027
	5 · 10 ³	48.06 ±5.94	9.95 ±1,49	0.1804 ±0.0168	8.53 ±1.07	0.129 ±0.015
Chol Cl	1 · 10 ⁴	33.68 ±2.78	2.57 ±0.47	0.1826 ±0.0082	12.13 ±1.01	0.123 ±0.013 0.131 ±0.007
	2 · 10 ⁴	32.12 ±2.22	2.56 ±0.43	0.2007 ±0.0073	12.44 ±0.87	0.131 ±0.007 0.147 ±0.007
	5 · 10 ⁴	36.52 ±2.75	3.26 ±0.43	0.2137 ±0.0075	10.77 ±0.82	0.159 ±0.009
	9 · 10 ⁴	33.84 ±2.80	1.81 ±0.22	0.2137 ±0.0093 0.1708 ±0.0079	10.77 ±0.82 12.25 ±1.02	0.139 ±0.009 0.120 ±0.007
	9 · 10 18 · 10⁴	33.08 ±2.95	1.78 ±0.22	0.1708 ±0.0079 0.1446 ±0.0070	12.23 ±1.02 12.93 ±1.16	0.120 ±0.007 0.100 ±0.006
	40 · 10 ⁴	36.68 ±3.78	1.64 ±0.18	0.1381 ±0.0087	11.72 ±1.21	0.094 ±0.007

Table 2. Values of the parameters τ_1 , τ_2 and a_1 obtained by fitting the carotenoid shift experimental traces with eq. 2. ILs concentrations are expressed in the micromolar scale. For control traces (c=0), m was set to a value of 0, resulting in an exponential decay.

Also, from eq. (5) we can obtain the following relationship:

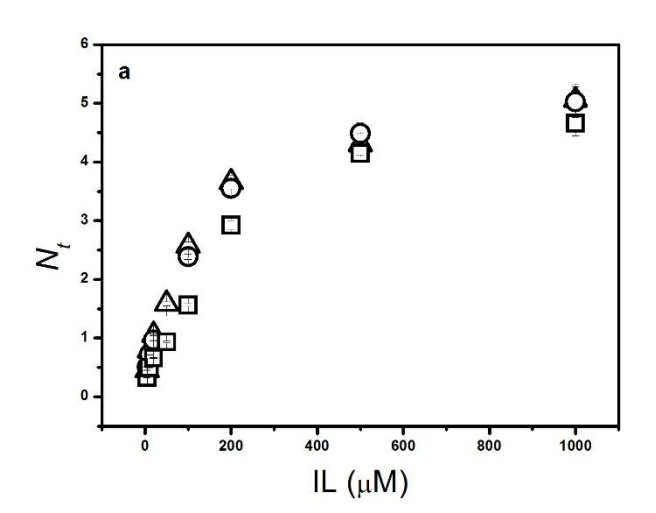
$$N_t \approx \frac{a_1}{\alpha^2 b(1 - a_1)} \tag{10}$$

where *b* is defined by eq. (6), with a chromatophore membrane capacitance of $C_m = 5.5 \cdot 10^3$ Fm² (Casadio et al., 1988) and $\alpha \approx 1$. Eq. (10) allows for an estimation of N_t , informing on the membrane partition of the ion from the experimentally determined a_1 .

The values of k_i and N_t extracted through eq. (9) and (10) from the experimental traces are reported in **Table 2**. According to the model, the kinetic rate constant k_i for each compound should be concentration-independent, since the ion adsorption from the aqueous phase is not supposed to destabilise the membrane structure. At variance, for each compond tested, k_i value increases with the increase in concentration. However, this occurs on a much more limited scale when compared to the increase in the k constant of the first model employed (Table 1), whose range of variation was approximately three times larger. Most importantly, the N_t values for the total adsorbed surface concentration appear to be much more reasonable that the ones calculated for the *m* average number of permeating ions of the first model (**Table** 1). In fact, even if N_t also tends to saturate, this occurs at around 5 pmoles \cdot cm⁻² (**Fig. 4.7**), which corresponds to a density of approximately 3.011 · 10¹² ions per cm², or 0.0311 ions per nm². This, taken with the aforementioned estimated total chromatophore surface of 34000 nm², 16% of which is occupied by 0.64 nm²-wide phospholipid, results in a maximum surface density of ions of approximately one every 8 lipids. This is a much more meaningful value than the one calculated with the Poissonian statistical model, and, overall, allows for a better interpretation of the phenomenon. Moreover, it is important to point out how this estimation is not taking into consideration the fact that, in such a protein-rich membrane, the substantial portion of lipids interacting with protein complexes is significantly rigid (Dezi et al., 2007; Nagatsuma et al., 2019; Swainsbury et al., 2023), while a high mobility of lipids composing a membrane is known to be an important property for ion permeation (Fathizadeh & Elber, 2019; Vorobyov et al., 2014). This shrinks even more the portion of the chromatophore surface able to interact with the ions, resulting in an even higher ion:lipid ratio.

When examining the N_t parameter (**Fig. 4.7**), comparing Ntf₂ containg ILs to the others, it is noticeable how C₁C₂Im BF₄ and C₁C₂Im Otf reach saturation at concentrations one order of magnitude higher, suggesting that the Ntf₂ containing ILs partition much more easily in the membrane. Finally, **Table 2** also show a similar trend regarding k_i , suggesting that the high central energy barrier for translocating across the membrane encounterd by Ntf₂ containg ILs

is much lower. Hence, what observed for the N_t and k_i parameters could explain the higher effectiveness of Ntf₂ containing ILs in collapsing the ΔΨ.



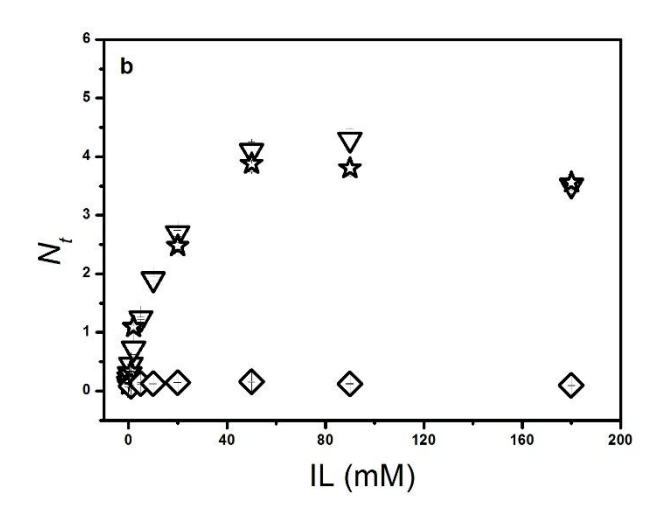


Figure 4.7. Total number of ions adsorbed at the water-membrane interface (N_t , pmol·cm²), as a function of IL concentration. (**a**) Triangles, N2224-NTf₂; circles, BMPyrr-NTf₂; squares, c₁c₂Im-NTf₂. (**b**) Inverted triangles, c₁c₂Im-BF₄; stars, c₁c₂Im-OTf; diamonds, Chol-Cl.

4.4 ILs effect on membrane ionic current

Since, as previously mentioned, the amplitude of the carotenoid shift (ΔA) linearly correlates to $\Delta \Psi$ and the $\Delta \Psi$ dissipation depends on ionic fluxes across the membrane, it is possible to measure the ionic current of the membrane by monitoring the ΔA overtime. Given a constant membrane capacitance C_m , $\Delta \Psi$ relates to the amount of separated charge Q as shown in eq. (11):

$$\Delta \Psi = \frac{Q}{C_m}$$

Therefore, if the overall ionic current j, dissipating the $\Delta\Psi$, is given by j = dQ / dt, then, by substituting to eq. (11), we have the relation $j = C_m d \Delta\Psi / dt$, which in terms of carotenoid shift signal can be described by eq. (12):

$$j \approx \frac{d\Delta A}{dt} \tag{12}$$

By considering the first derivative of eq. (2) and changing its sign, we obtain information on the inital (at time = 0) slope of the carotenoid shift signal decay, r(0):

$$r(0) = \Delta A(0) \cdot \left(\frac{a_1}{\tau_1} + \frac{a_2}{\tau_2}\right) \tag{13}$$

For each compound, the values for r(0), calculated by substituting the parameters extracted from eq. (2) reported in **Table 2**, can be converted to the istantaneous ionic current variation across the chromatophore membrane j_0 , expressed as electrons translocated across the membrane per bacteriochlorophyll per second (e · BChl⁻¹ · s⁻¹), and defined by eq. (14):

$$j_0 = \frac{r(0) \cdot [P^+]}{\Delta A(0) \cdot [BChl]} \tag{14}$$

Where [BChl] is the concentration of bacteriochlorophyll of the chromatophores samples, kept constant at a value of 70 μ M, and [P⁺] is the concentration of the primary donor P (210 nM) photoxidized at the level of RC by a single flash. In fact, in our conditions, the sole contribution to the carotenoid shift comes from the charge separation occurring within the RC. Therefore, the Δ A(0) measures the Δ Ψ generated by the translocation of a single electron per RC.

The effect of the tested compounds on the membrane ionic current is shown in Fig. 4.8.

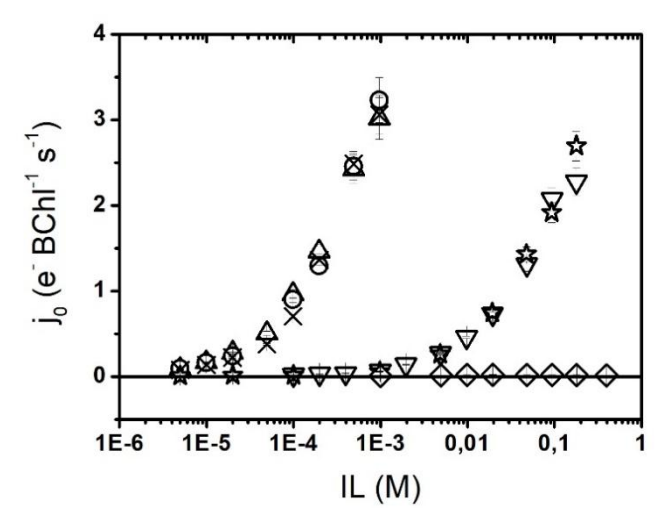


Figure 4.8. Dependence of the ionic current j_0 on the molar concentration of ILs. Triangles, N2224-NTf₂; circles, BMPyrr-NTf₂; crosses, c_1c_2 Im-NTf₂; inverted triangles, c_1c_2 Im-BF₄; stars, c_1c_2 Im-OTf; diamonds, Chol-Cl.

All the tested compound, with the exception of Chol CI (**Fig. 4.8**, diamonds), show the ability to increase the ionic current across, clustering into two clearly distinct groups. A first group, comprising the three Ntf₂ containing ILs, where j_0 is consistently enhanced at micromolar concentrations, and a second group showing how c_1c_2 Im BF₄ and c_1c_2 Im Otf are also able to increase j_0 , though this occurs at concentrations three orders of magnitude higher than the ones registered for the first group.

Since these results strongly suggest that it is the Ntf₂⁻ anion causing such an effective dissipation of $\Delta\Psi$, BMPyrr Cl and c₁c₂Im Cl were tested on chromatophore to investigate the outcome of the replacement of such moiety with the Cl⁻ anion (**Fig. 4.9**).

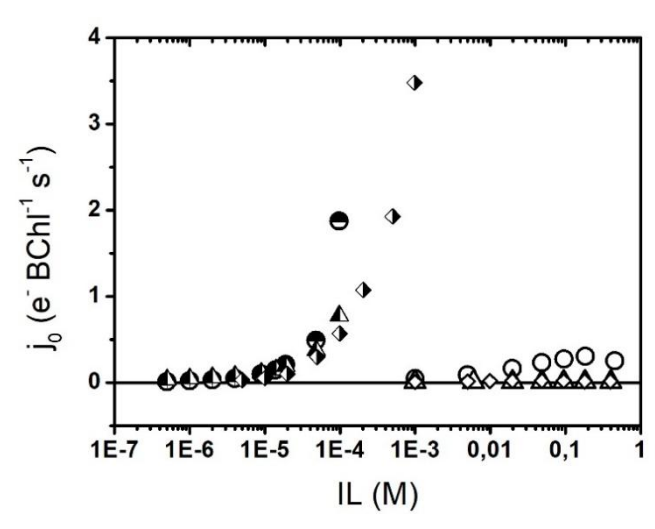


Figure 4.9. The dependence of the ionic current j_0 on the molar concentration of BMPyrr NTf₂ and BMPyrr CI (circles), c_1c_2 Im NTf₂ and c_1c_2 Im CI (triangles), Chol NTf₂ and Chol CI (diamonds). Half-filled and empty symbols refer to the ILs with NTf₂⁻ or chloride anion, respectively.

For both BMPyrr⁺ and $c_1c_2lm^+$, the strong effect of enhancement of j_0 observed at micromolar concentration when Ntf₂ is present as the counter anion is completely removed by its substitution with the chloride anion, with a slight increase in j_0 for BMPyrr Cl, possibly due to the cation alkyl chain (Kumar et al., 2019; Sharma & Mukhopadhyay, 2018). Moreover, it is particularly striking to notice how Chol Ntf₂ is also able to carry out such effect (**Fig. 4.9**, half-filled diamonds), since, as already mentioned, Chol Cl is a typical negative control.

Overall, these results indicate that the Ntf₂⁻ anion is able to augment the ionic current across the chromatophore membrane (j_0), resulting in a faster dissipation of the transmembrane electrical potential ($\Delta\Psi$), and that this behaviour is essentially independent from the cationic component for all the ILs tested.

Finally, it must be highlighted that, while all three Ntf₂ containing ILs showed consistency as far as reproducibility is concerned, $c_1c_2\text{Im BF}_4$ and $c_1c_2\text{Im Otf}$ ability to increase ionic currents across the membrane and collapse the $\Delta\Psi$ seemingly decreased over time after the purchase of the pure compounds. In figure **Fig. 4.10**, it is shown the effect on j_0 of the compounds tested on chromatophores over the month following the opening of the sealed vials. As stated by the manufacturer, the BF₄⁻ anion has a tendency to decompose over time, when exposed to ambient humidity. This seems to have happend in our case. Moreover, the same could have

happened to c₁c₂lm Otf and, to our knowledge, this is the first time such case has been reported.

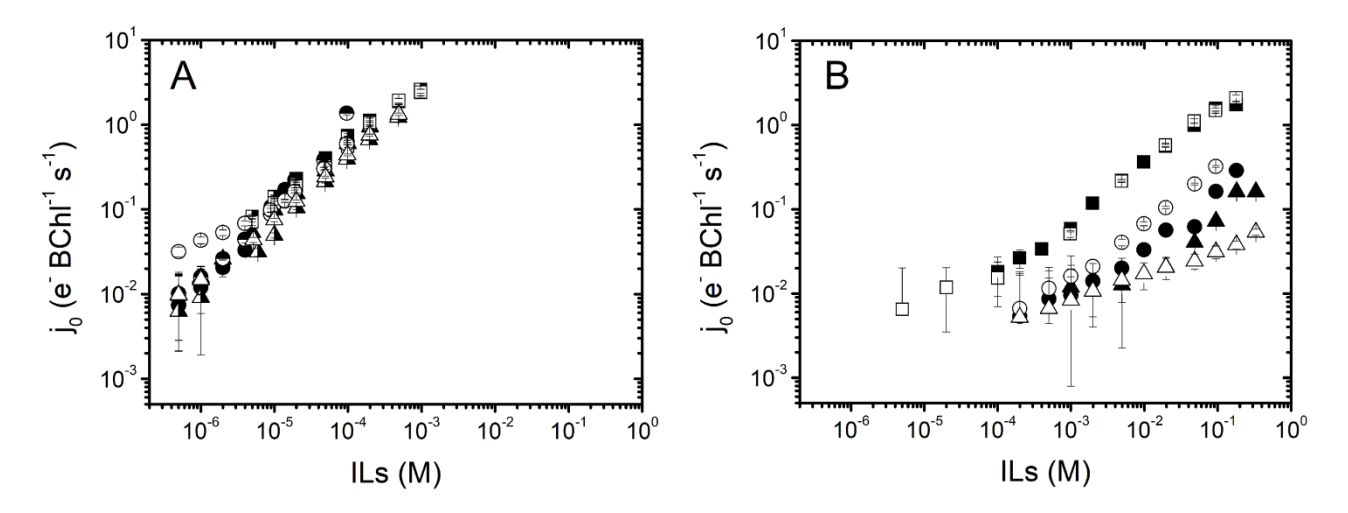


Figure 4.10. Dependence of the ionic current j_0 on the molar concentration of the ILs examined. For each IL the figure shows the results of three set of measurements performed at different times elapsed after opening the sealed container received from the supplier, i.e. immediately after the opening (squares), two weeks after opening (circles), one month after opening (triangles). Panel A: N2224-NTf₂, filled symbols; BMPyrr-NTf₂, half-filled symbols; c₁c₂Im-NTf₂, open symbols. Panel B: c₁c₂Im-BF₄ (filled simbols); c₁c₂Im-OTf (open simbols).

4.5 Reversibility of the Ntf₂ anion effect on carotenoid shift

To test whether the Ntf₂-induced acceleration of the decay kinetic of the carotenoid shift signal is reversible, two different chromatophores suspensions (50 mM MOPS, pH 7.3, 2 ml each) were kept in the dark for 30 minutes. One of such suspensions contained 1 mM N2224 Ntf₂, a concentration that ensures a total collapse of $\Delta\Psi$ (**Fig. 4.6**). Next, both samples were placed in cellulose membrane dialysis tubings with a cut-off molecular weight of 14000 (Sigma-Aldrich) and abundantly dialyzed against 500 ml of fresh medium every 8 hours for three times. Finally, the carotenoid shift band of both samples was acquired, following the same procedure of the previous experiments (**Fig. 4.11**).

The removal through dialysis of the IL from the suspension results in a clear reversal of the electrochromic band shift kinetic to the control signal, implying that the interaction between Ntf_2 and the chromatophore is completely reversible. This confirms that the collapse in $\Delta\Psi$ caused by the anion does not depend on a permanent destabilisation of the lipid bilayer, strongly supporting what suggested by the interpretation model employed to fit the experimental traces (paragraph 4.3).

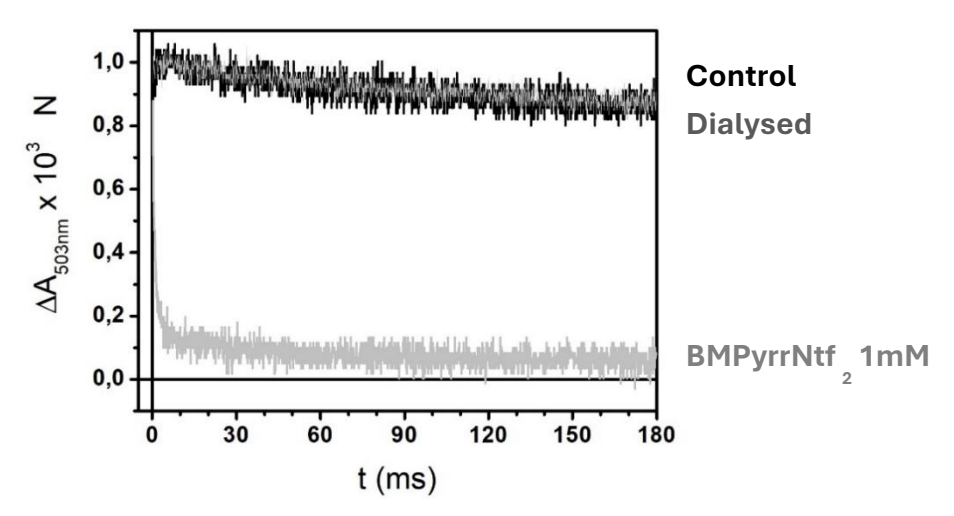


Figure 4.11. Kinetics of the carotenoid shift decay of samples from chromatophores suspended in the absence or presence of 1 mM BMPyrr Ntf₂ after dialysis (respectively, *control* and *dialysed*). The pre-dialysis carotenoid shift signal of the suspension containing the IL is reported as *BMPyrr Ntf*₂ 1 mM. The experimental traces have been normalized to the ΔA amplitude immediatly following the single flash excitation. Each trace represents the average of 8 individual signals.

4.6 Ntf2 anion effect on cytochrome bc1

To test whether there was any impairment caused by the Ntf_2^- anion in the electron transfer reactions occurring at the level of chromatophores cytochrome bc_1 , the oxidation and rereduction of cytochromes $(c_1 + c_2)$ (cyts c) and the reduction of Heme b_h were monitored spectrophotometrically over time at 550 nm and 560 nm respectively. ILs were present at a concentration of 1 mM, a concentration sufficient to exert a strong effect on the carotenoid shift (**Fig. 4.12**), and at 5 mM.

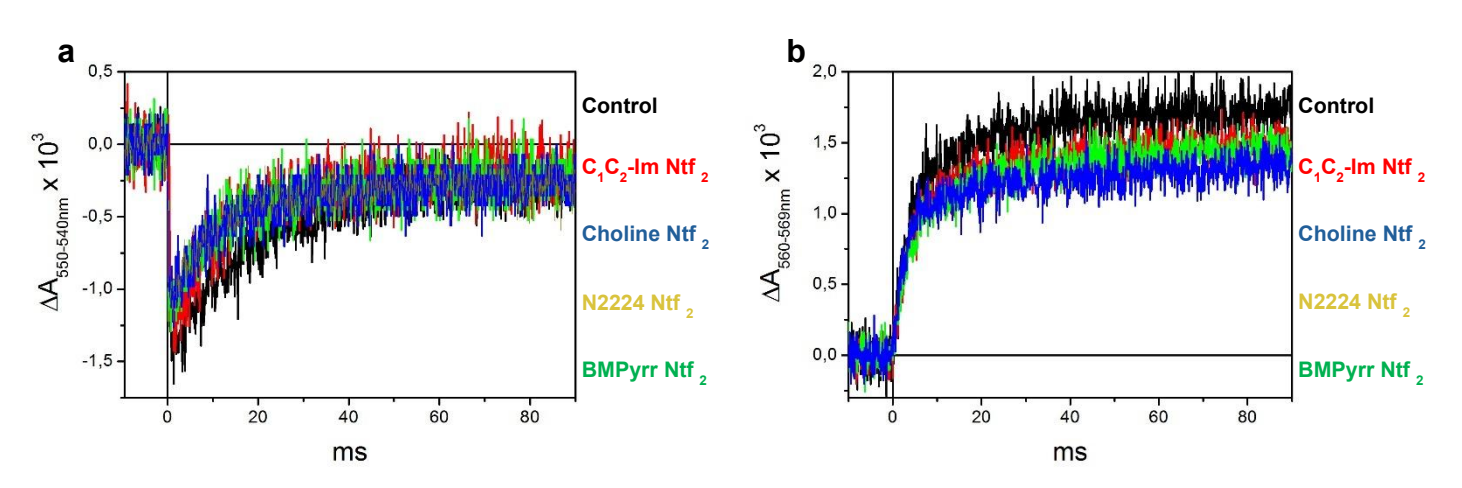


Figure 4.12. Effect of Ntf₂ containing ILs on the electron transfer reaction of cytochrome bc_1 . (a) Kinetics of oxidation and re-reduction of cyts c in the presence of 1 mM ILs. (b) Heme b_h reduction kinetics on antimycin-inhibited chromatophores in the presence of 1 mM ILs. Each trace represents the average of 32 individual signals.

No significant effect of inhibition of the electron flow towards cyt c or Heme b_h was observed. For cyts c, neither the amplitude of the absorbance signal measuring its oxidation nor the kinetics of re-reduction appear to differ (**Fig. 4.12a**), while a slighty smaller amplitude is observed for Heme b_h reduction. In this case, the half times of the reaction kinetics were directly evaluated from the experimental traces to better understand whether there was any impairment in the electron transfer. Half-time values were determined by considering, on the x-axis, the time corresponding to half the maximum absorbance value measured. As reported in **Table 3**, no significant discrepancies were observed between the control and the treated samples, with fluctuations that can be attributed to the impossibility of totally control the state of pre-oxidation of the system.

	ht 1mM (ms)	ht 5 mM (ms)
Control	3.23 ± 0.07	3.23 ± 0.12
C ₁ C ₂ Im Ntf ₂	3.61 ± 0.11	2.9 ± 0,05
N2224 Ntf ₂	3.72 ± 0.09	2.62 ± 0.07
Chol Ntf ₂	4.06 ± 0.09	3.29 ± 0.04
BMPyrr Ntf ₂	2.91 ± 0.06	3.16 ± 0.12

Table 3. Half time of the reduction kinetics of Heme b_h , expressed in milliseconds (ht), in chromatophores suspended in the presence of 1 mM and 5 mM Ntf₂ containing ILs. Error was evaluated from the background noise in the experimental traces.

4.7 ILs effect on chromatophores light-driven ATP synthesis

Chromatophores bear all the functional elements of *Rb. Capsulatus* photosynthetic transport chain. Under continuous illumination, the photoxidation of P within the RC sets the cyclic electron transport flow in constant motion, with the formation of a proton gradient which is steadily dissipated by the ATPase, when sufficient ADP and inorganic phosphate are provided, producing ATP. Since the proton motive force is composed of an electrical ($\Delta\Psi$) and a pH (Δ pH) component, undermining one of these elements would lead to a decrease in the system performance.

Given the solid evidence on the Ntf_2 ability to increase the ionic current across chromatophores membrane, consequently collapsing $\Delta\Psi$, the chromatophores light-driven ATP synthesis was tested in the presence of growing concentrations of BMPyrr Ntf_2 . The

samples were illuminated for a period of 30 seconds, after which 2% trichloric acid was added to stop the reaction and precipitate the sample. After centrifugation to remove membrane debris, the ATP present in the supernatant was quantified with a bioluminescence assay based on the activity of luciferase, a firefly-derived enzyme which, in the presence of oxygen, oxidizes luciferin through the following two-step reaction:

$$ATP + Luciferin \rightleftharpoons Adenyl - luciferin + PP_i$$

 $Adenyl - luciferin + O_2 \rightleftharpoons Oxyluciferin + AMP + CO_2 + light$

The light emitted in the second step, which is proportional to the ATP when ATP is the limiting reagent, was measured with a luminometer.

In control condition, 30 seconds of illumination produced $1.62 \pm 0.066 \,\mu\text{molATP} \cdot \mu\text{molBChl}^{-1}$ on average. The data on BMPyrr Ntf₂ titration, expressed as a percentage of control, are reported in **Figure 4.13**.

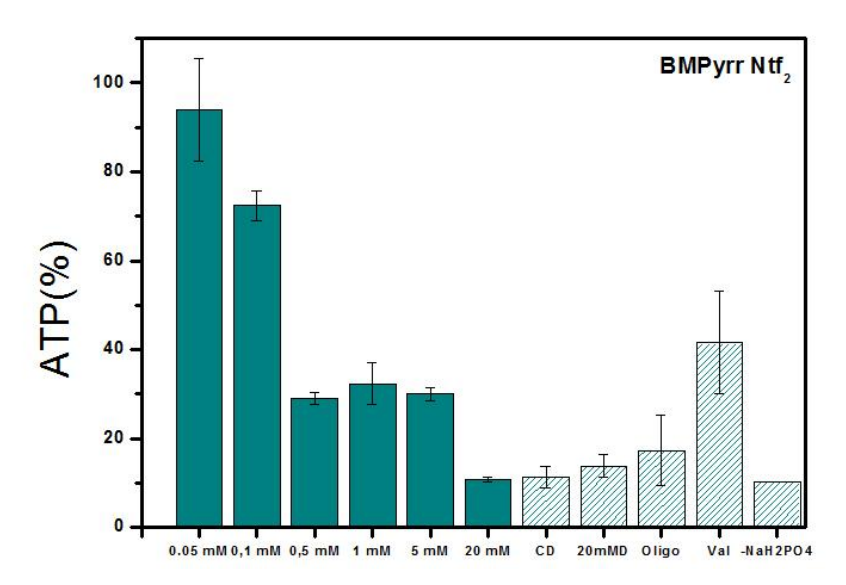


Figure 4.13. BMPyrr Ntf₂ effect on chromatophores light-driven ATP synthesis. The ATP content is expressed as a percentage of the ATP produced in control condition. Full bars represent the ATP content of samples treated with increasing concentrations of the compound, expressed in millimolar (mM). Striped bars represent the following negative controls: CD, control dark; 20 mM D, 20 mM BMPyrr Ntf₂ dark; Oligo, 10 μ M oligomycin; Val, 20 μ M valinomycin + 30 mM KCI; - NaH₂PO₄, absence of inorganic phosphate in the reaction buffer.

BMPyrr Ntf₂ was able to undermine chromatophores light-driven ATP synthesis drammatically already at a concentration of 0.5 mM, with a decrease in the ATP content of around 70%. This effect seems to remain constant up to 5 mM, a concentration ten times higher, suggesting a possible saturation. At 20 mM, the ATP production decreases even more, reaching values comparable to the ones of negative controls such as non-illuminated samples (CD and 20

mM D), chromatophores pre-incubated with 10 µM oligomycin (Oligo) and chromatophores suspended in a reaction buffer lacking inorganic phosphate, necessary for the ATP synthesis (-NaH₂PO₄), whose low percentages of ATP are ascribable to the sole background activity of adenylate kinase (Gubellini et al., 2007; Markland & Wadkins, 1966). This additional reduction in ATP production might be due to a destabilisation of the membrane caused by BMPyrr⁺ alkyl chain, as BMPyrr CI was observed exerting a slight enhancement of ionic current at similar concentrations (Fig. 4.9). Interestingly, treatment with 30 mM KCl and 20 µM valinomycin (Val), a concetration of valinomycin more than sufficient for completely collapsing $\Delta\Psi$ in single flash experiments (Fig. 4.3), only reduces the ATP content by some 55%, showing how, in the stady state achieved under continuous illumination, a stronger effort is required to collapse the $\Delta\Psi$. In this regard, the concentrations at which BMPyrr Ntf₂ is able to impair ATP synthesis are surprisingly close to the ones able to collapse the carotenoid shift signal in single-flash experiments. To further investigate Ntf₂⁻ effect, BMPyrr⁺ was paired with Cl⁻ as a counter anion, and BMPyrrCl was tested on chromatophores following the same aforementioned procedure (Figure 4.14). As expected, BMPyrr CI effect was found to be drastically different, with a maximal reduction of ATP synthesis of only 10% at a concentration of 20 mM (cyan bars).

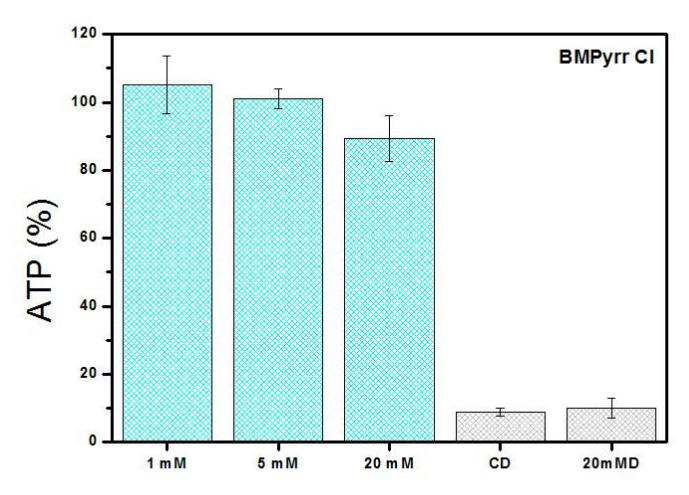


Figure 4.14. BMPyrr CI effect on chromatophores light-driven ATP synthesis. The ATP content is expressed as a percentage of the ATP produced in control condition. Cyan bars represent the ATP content of samples treated with increasing concentrations of the compound, expressed in millimolar (mM). Grey bars represent the following negative controls: CD, control dark; 20 mM D, 20 mM BMPyrr CI dark.

4.8 Ionic liquids effect on Rb. Capsulatus photosynthetic growth

Given the results obtained on chromatophores, we decided to test the effect of ILs *in vivo*. *Rb. Capsulatus* cells were grown photosynthetically at 30°C in the presence of increasing concentrations of Ntf₂ containing ILs (**Fig. 4.15**).

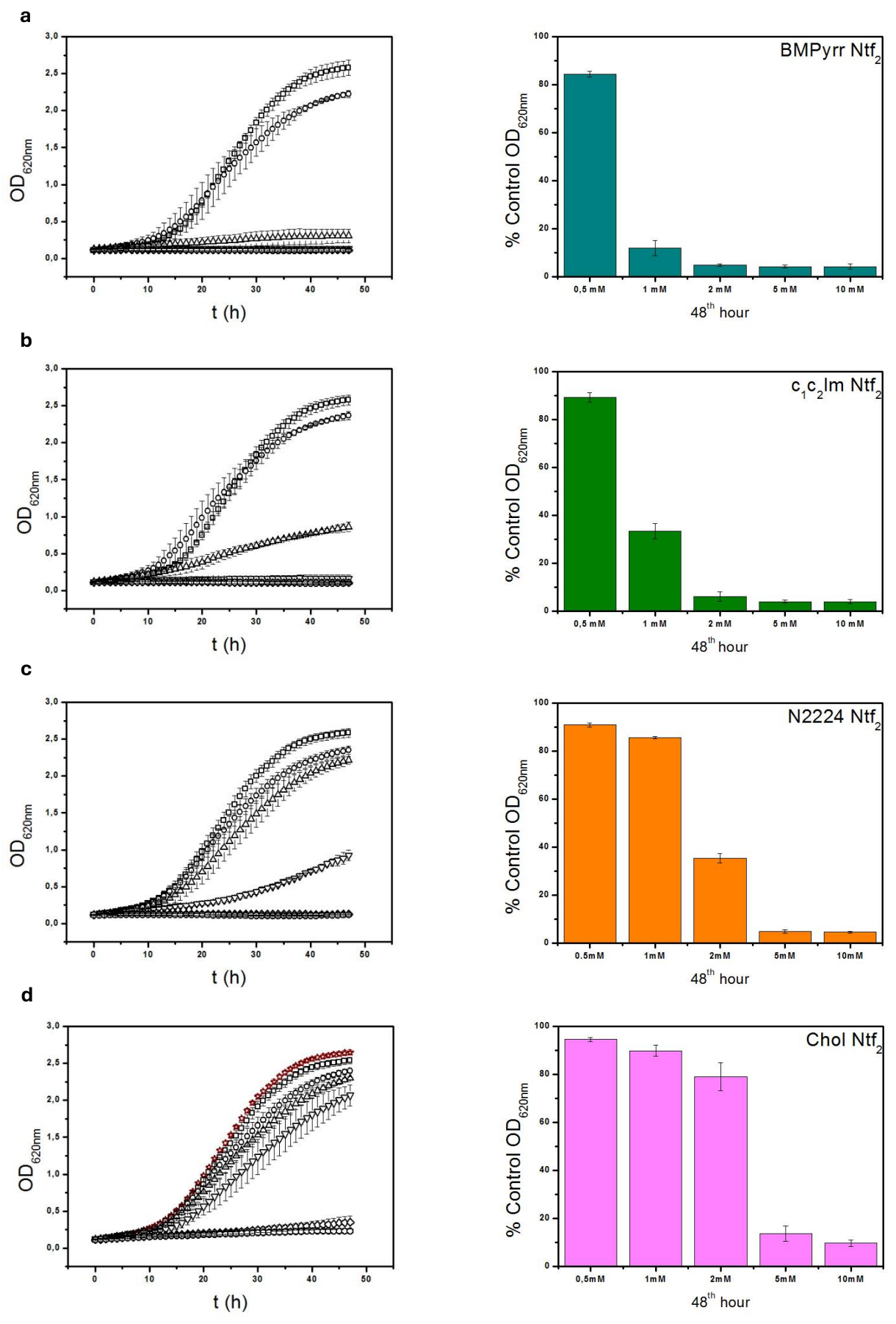


Figure 4.15. Effect of Ntf₂ containing ILs on *Rb. capsulatus* photosynthetic growth. Left panels show the growth curves registered by monitoring the OD_{620nm} once every hour for 48 h in the presence of increasing ILs concentrations, represented by the following symbols: squares, 0 mM; circles, 0.5 mM; triangles, 1 mM; inverted triangles, 2 mM; diamonds, 5 mM; hexagons, 10 mM. Red stars in panel **d** represent the growth curve registered in the presence of 80 mM Chol Cl. Traces represent the average of three biological replicates, each consisting of eight technical replicates. Right panels show the OD_{620nm} register at the last point in time, expressed as a percentage of control.

All Ntf₂ containing ILs appear to be able to inhibit *Rb. Capsulatus* growth, exerting such effect in a range of concentrations that spans from 1 to 5 mM, as also shown by the mean growth rate constant (k) values reported in **Figure 4.16**. The order of toxicity for the tested compounds appears to be: BMPyrr Ntf₂ > c₁c₂Im Ntf₂ > N2224 Ntf₂ > Chol Ntf₂. For BMPyrr Ntf₂, there was a drammatic difference in growth between cells exposed to 0.5 mM and 1 mM BMPyrr Ntf₂, with a drop in k value from 87% of control to 28%. A slightly milder effect was observed for c₁c₂Im Ntf₂, where passing from 0.5 mM to 1 mM reduced k from 93% to 44%.

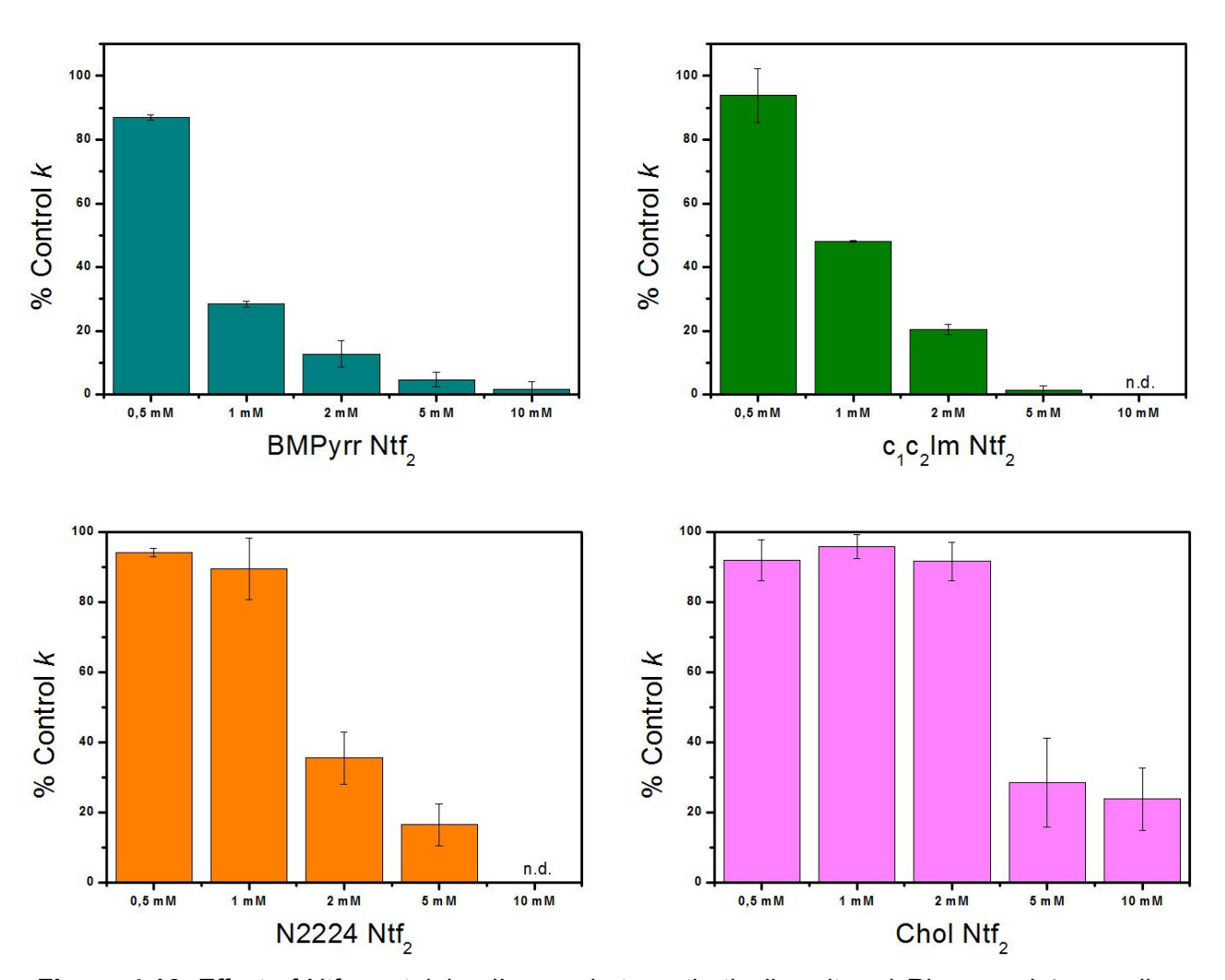


Figure 4.16. Effect of Ntf₂ containing ILs on photosynthetically cultured *Rb. capsulatus* medium growth rate constant (k). For each concentration (mM), k is reported as a percentage of control k. N.d.= non determinable.

For N2224 Ntf₂, a similar behaviour was observed when shifting from 1 mM to 2 mM, while for Chol Ntf₂ a comparable decrease was observed between 2 mM and 5 mM. Although the differences observed between the compounds are relatively significant, the range of efficacy remains small, suggesting a close similarity among the tested Ntf₂ containing ILs.

Subsequently, the chloride containing ILs BMPyrr CI, c_1c_2 Im CI and Chol CI were tested on *Rb. capsulatus* photosynthetic growth, once again to investigate the effect of Ntf_2 - anion by combining the different cations with CI-, which is known to be harmless. The experiments followed the same protocol employed for the growth curves in the presence of Ntf_2 - containing ILs. OD_{620nm} values measured at the last point in time (48th hour) and k values for BMPyrr CI and c_1c_2 Im CI are reported in **Figure 4.17**, expressed as a percentage of control values.

Both BMPyrr Cl and c₁c₂Im Cl show an inhibition of the bacterial growth at concentrations up to 10 to 20 times higher than those of Ntf₂ containing ILs, with a complete inhibition of bacterial growth occurring at 40 mM. While c₁c₂Im Cl seemed slightly more effective than BMPyrr Cl in exerting such effect, the two compounds show extremely similar behaviour. At variance, Chol Cl did not inhibit bacterial growth, as reported in **Figure 4.15d** (red stars).

Overall, Ntf₂ containing ILs showed a more aggressive effect also in *in vivo* experiments, even if the toxicity observed was not worrying from an ecotoxicological point of view, since this concentrations are above the limit of 100 mg/L set by OECD 201.

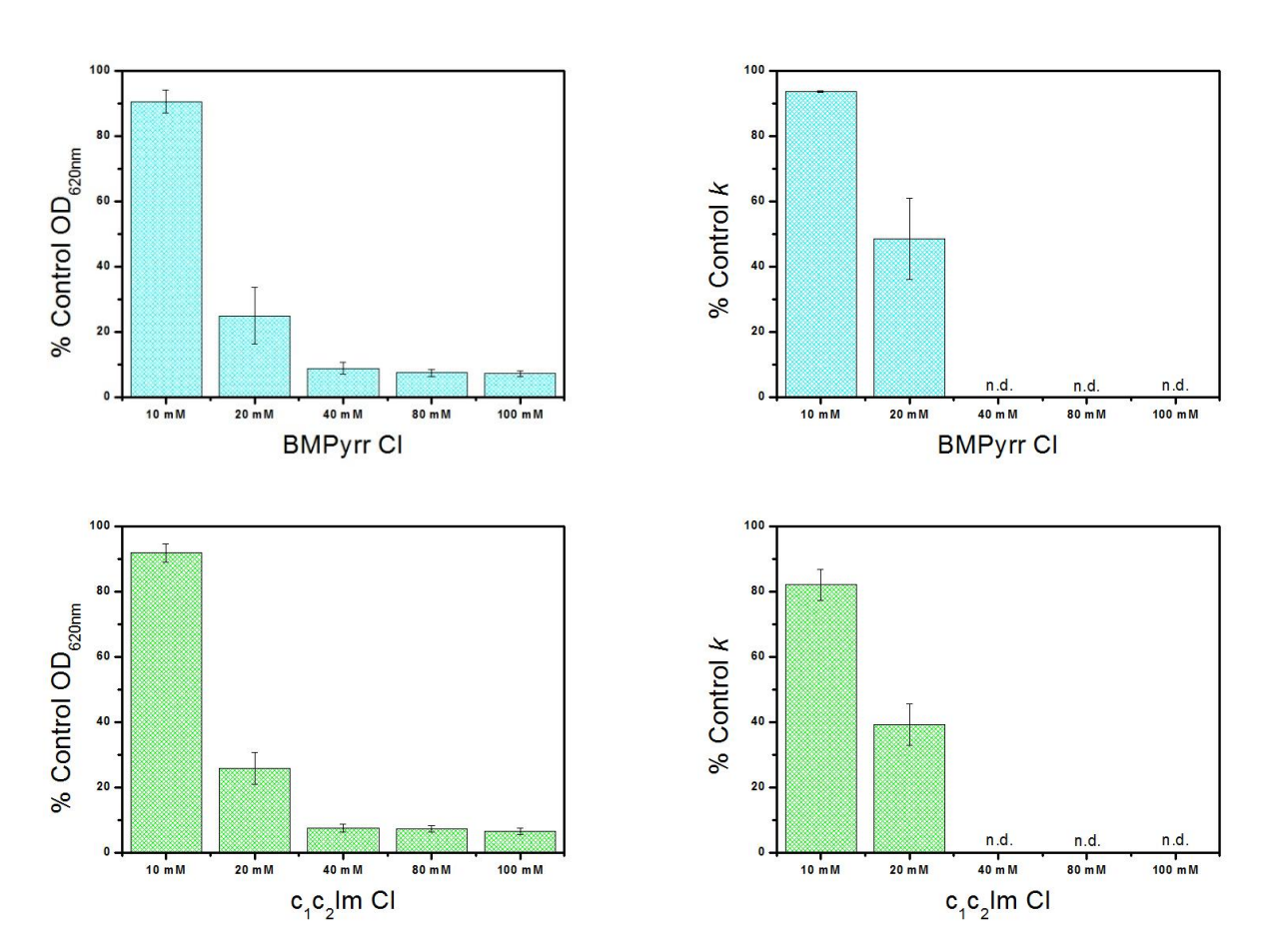


Figure 4.17. Effect of BMPyrr Cl (cyan) and c_1c_2 Im Cl (light green) on *Rb. capsulatus* photosynthetic growth. Left panels show the OD_{620nm} values measured at the 48th hour and expressed as a percentage of control values. Right panels show the medium growth rate constant (k) values expressed as a percentage of control. ILs concentrations are expressed in millimolar (mM).

The realisation of the experiments reported in this paragraph was made possible thanks to the collaboration with Renolab Srl (40016, San Giorgio di Piano, Bologna).

4.9 Effect of ionic liquids on mitochondrial reverse electron transfer

To investigate the effect of BMPyrr CI, C₄mim CI and C₄mim N(CN)₂ (**Fig. 1.9**) on the mitochondrial $\Delta\mu_{H^+}$, ETPH ability to perform RET in the presence of the compounds was tested. Here, as shown in **Figure 4.18**, the addition of an uncoupler such as carbonyl-cyanide-4-(trifluoromethoxy)phenylhydrazone (FCCP, 4 μ M) results in the dissipation of the protonmotive force that drives the electron flow from the quinone pool, reduced by the activity of CII, to NAD⁺, eventually stopping its reduction to NADH at the level of CI.

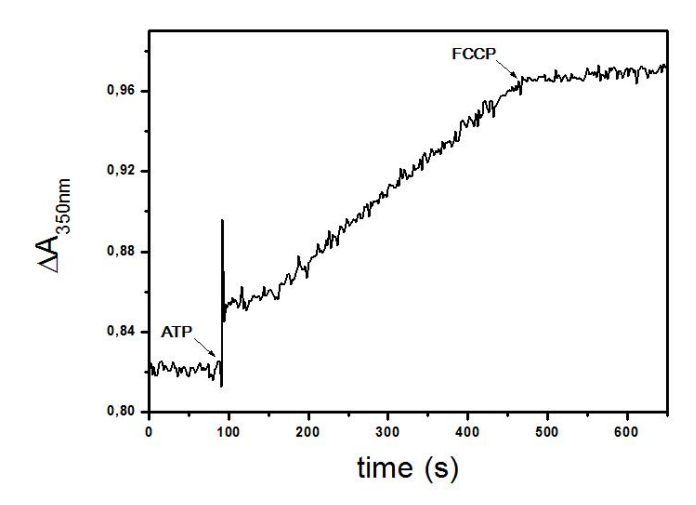


Figure 4.18. ETPH NAD⁺ reduction through RET. The reaction is started with the addition of ATP, and the formation of NADH is monitored spectrophotometrically at 350nm over time. The addition of FCCP immediately stops the reaction.

ETPH were suspended to a final concentration of 0.3 mg/ml in the presence of growing ILs concentrations, and the RET activity was compared to those measured in control condition, which, depending on the preparation, yielded an average NADH production that spanned from 15 to 25 nmol·mg⁻¹·min⁻¹.

As reported in **Figure 4.19**, while all three compounds were able to undermine RET, C₄mim N(CN)₂ appeared to be particularly effective, causing a decrease in NADH production of 50% at 5 mM and up to 70% at 10 mM, therefore showing a more aggressive behaviour. Moreover, BMPyrr Cl and C₄mim Cl exerted a comparable effect only at concentrations three to four times higher.

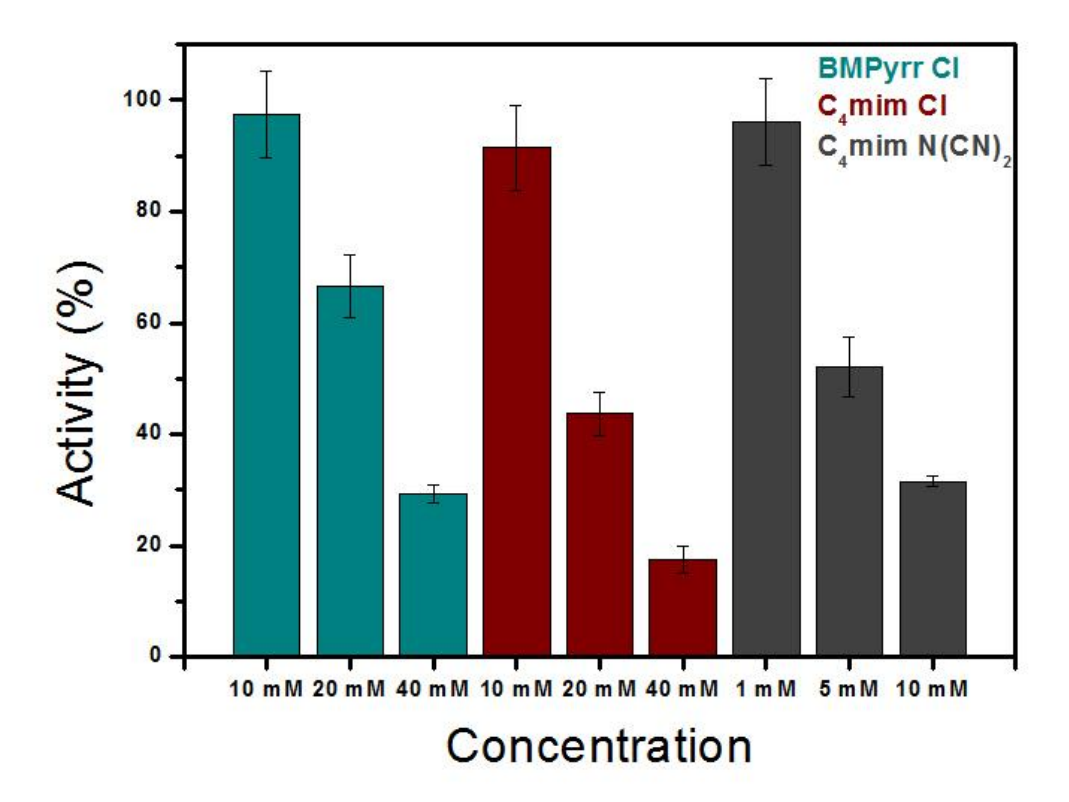


Figure 4.19. ILs effect on ETPH RET. The activity of NAD $^+$ reduction in the presence of BMPyrr Cl (dark cyan), C₄mim Cl (red) and C₄mim N(CN)₂ (dark grey) is reported as a percentage of control activity. Concentrations are expressed in millimolar (mM).

4.10 ILs effect on ETPH NADH consumption in phosphorylating conditions

Contrary to RET, during NADH oxidation in the forward electron transfer, a dissipation of $\Delta\mu_{h+}$ results in a relaxation of the respiratory control, eventually leading to a faster rate of NADH oxidation (**Fig. 4.20**, FCCP). Conversely, an inhibition of CI activity results in a decreased NADH consumption.

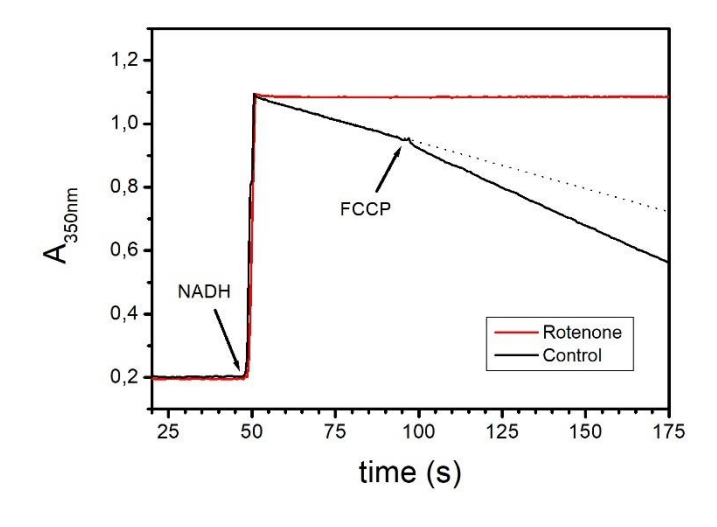


Figure 4.20. ETPH oxidation of NADH. The reaction is started with the addition of NADH, whose consumption is monitored over time spectrophotometrically at 350 nm. The addition of the protonophore FCCP causes an increase in NADH oxidation rate, while rotenone exert the opposite effect, inhibiting CI activity.

To further investigate the interaction between ILs and the mitochondrial electron transport chain, and since we could not exclude that the effect observed on RET was due to a direct inhibition of CI, the ETPH ability to oxidize NADH was tested, treating 0.1 mg/ml particles with growing ILs concentrations (**Fig. 4.21**).

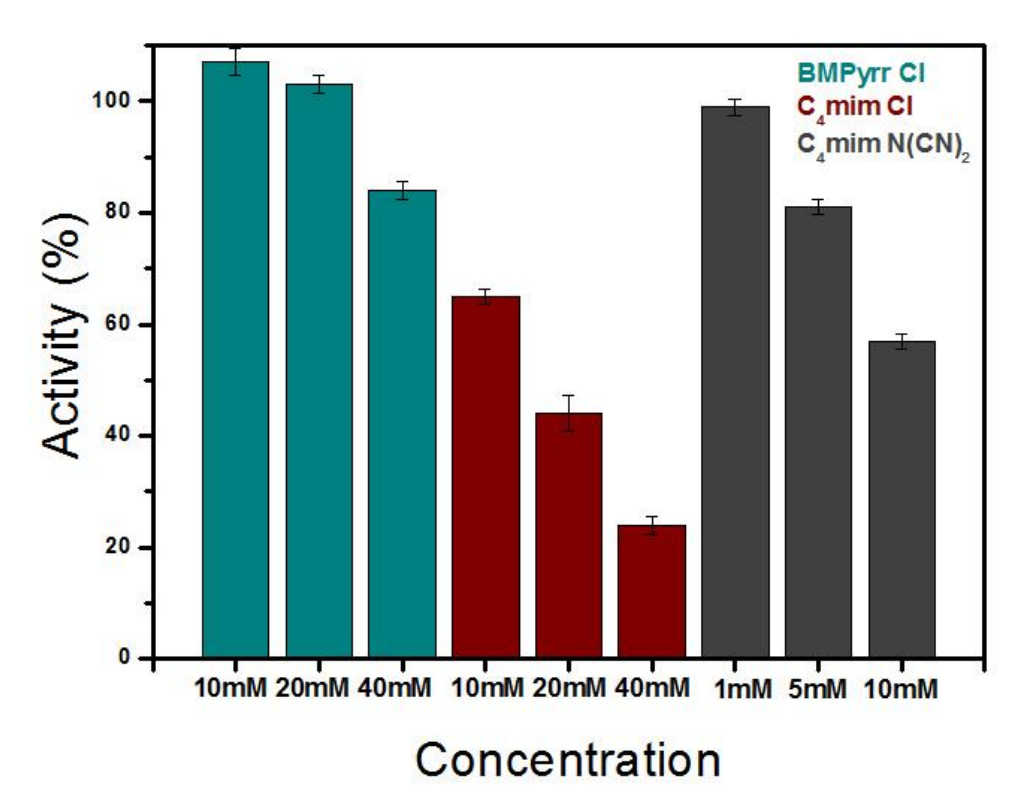


Figure 4.21. ILs effect on ETPH oxidation of NADH. The activity of NADH reduction in the presence of BMPyrr CI (dark cyan), C_4 mim CI (red) and C_4 mim $N(CN)_2$ (dark grey) is reported as a percentage of control activity. Concentrations are expressed in millimolar (mM).

Surprisingly, all three tested compounds showed an inhibition of NADH oxidation, suggesting a direct effect on CI and, possibly, on other complexes of the electron transport chain. The inhibitory behaviour observed was milder for BMPyrr CI when compared to C_4 mim CI and C_4 mim $N(CN)_2$, with the latter two exerting a similar effect at 10 mM, resulting in a reduction in NADH consumption of around 40%. It must be noted that, since, as already mentioned, a relaxation of the respiratory control, caused by the dissipation of one or both components of the $\Delta\mu_{h+}$, would lead to a faster rate of NADH oxidation, the joint presence of such effect and of an inhibitory effect on one or more complexes would lead to these two phenomena masking each other in this reaction. At variance, the two would add up in the case of RET, directly impairing CI catalysis while at the same time dissipating the proton motive force that drives the electron flow towards NAD+. Hence, to better understand the forces at play, direct inhibition of CI was assessed.

4.11 Effect of ILs on Complex I activity

To test the effect of ILs on CI activity, ETPH were diluted to a final concentration of 0.1 mg/ml in an hypotonic buffer, useful in breaking the membranes, maximizing the quantity of CI accessible to substrates, while eliminating the respiratory control. The NADH oxidation activity, expressed as a percentage of control, in the presence of growing ILs concentrations is reported in **Figure 4.22**.

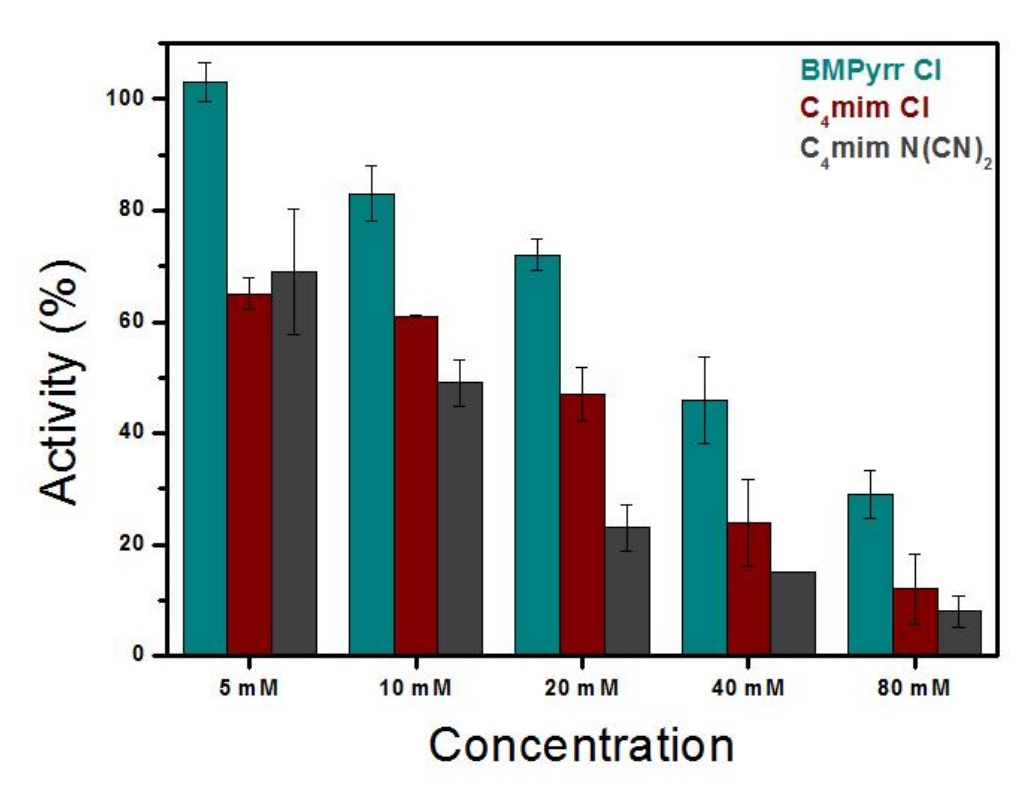


Figure 4.22. ILs effect on CI oxidation of NADH. The activity of NADH reduction in the presence of BMPyrr CI (dark cyan), C_4 mim CI (red) and C_4 mim $N(CN)_2$ (dark grey) is reported as a percentage of control activity. Concentrations are expressed in millimolar (mM).

All three compounds were able to inhibit CI activity, with C₄mim N(CN)₂ showing the strongest effect, decreasing CI performance of around 50% at 10 mM. C₄mim CI exerted a milder effect, suggesting that the N(CN)₂- anion might play a part in this phenomenon, while BMPyrr CI exhibited the least aggressive behaviour, reaching 50% of inhibition at 40 mM, a concentration four times higher than the one register for C₄mim N(CN)₂. Yet, this data become more relevant in the context of the previous two experiments. For each IL, a comparison of complex I (CI) activity, NADH oxidation in sealed particles (NADH:O₂) and RET is reported in **Figure 4.23**.

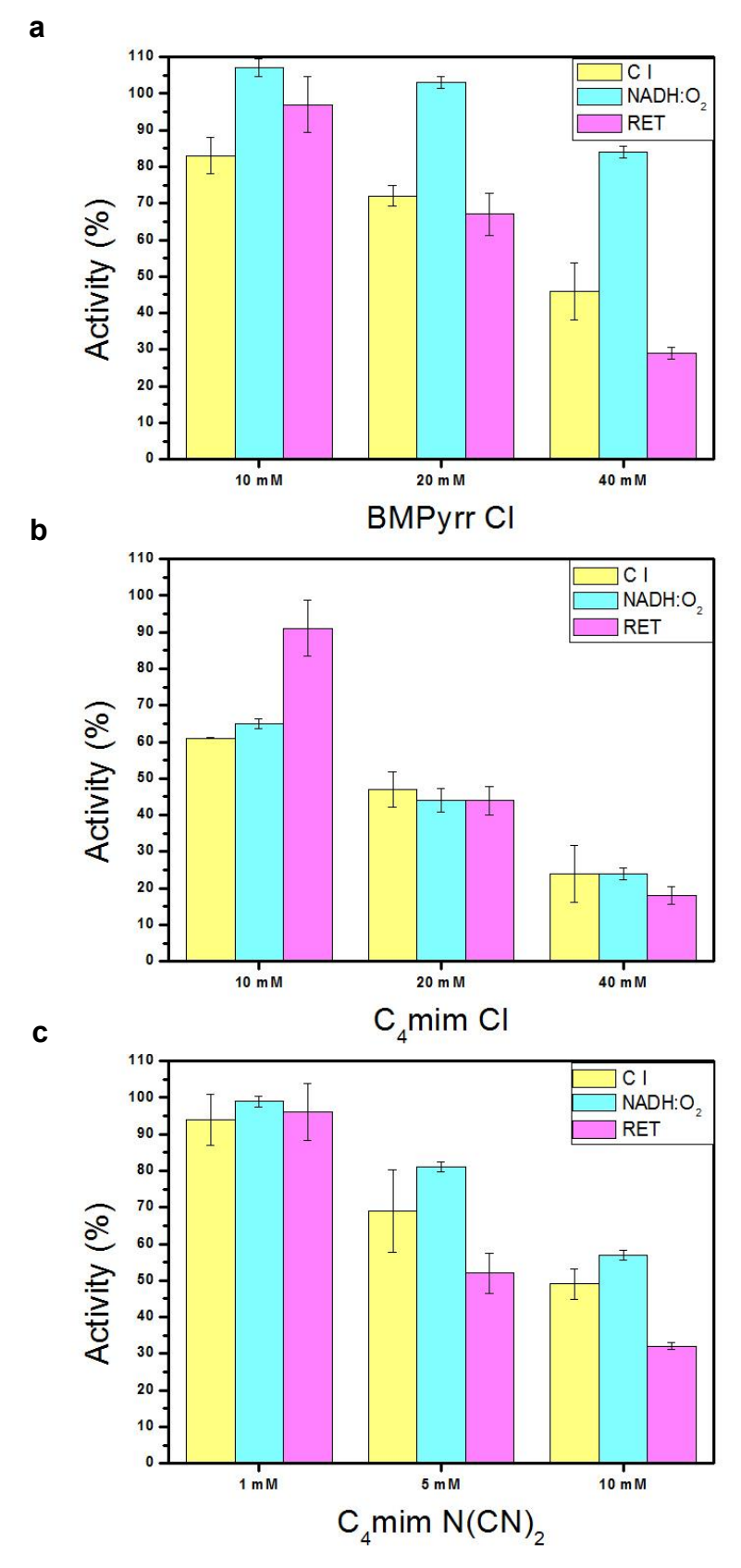
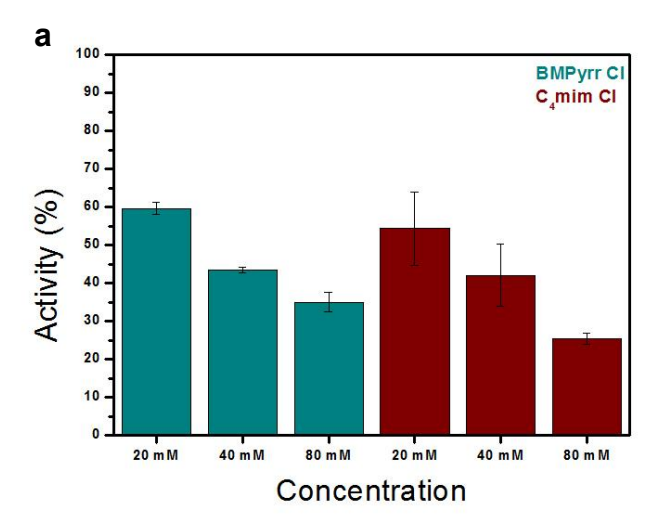


Figure 4.23. ILs effect on ETPH. For each compound, CI activity (yellow), NADH consumption in sealed particles (NADH:O₂, cyan) and RET (magenta) are reported as a percentage of control. Concentrations are expressed in millimolar (mM).

While for C₄mim Cl (**Fig. 4.23b**) the three activities show a comparable degree of inhibition (except for RET values at 10 mM), for BMPyrr Cl and C₄mim N(CN)₂ (respectively **a** and **c**) some discrepancies are observed, with both compounds exhibiting a higher rate of NADH oxidation in sealed particles and a lower RET activity when compared to the CI activity. This could be explained by the coexistence of both a direct inhibition of CI acitivity and a dissipation of the membrane electrochemical potential. In this sense, during NADH oxidation, the portion of CI still active might be working in a condition of decreased respiratory control, with an overall higher perfromance than the one observed for Cl. At the same time, as already mentioned, the dissipation of the membrane potential would add up to the inhibitory effect on CI in RET measurements, explaining the lower residual activity when compared to CI activity. Finally, for BMPyrr Cl, although the fact that the surplus in NADH:O₂ activity did not exactly match the surplus in RET inhibition could be explained by simply acknowledging that it is generally difficult to make a precise comparison between such complex and different acitivities, a possible explanation could be attributed to an overestimation of CI inhibition, meaning that, in osmotically burst ETPH, the compound might be able to interfere with a portion of CI which is normally not exposed, resulting in the detection of a higher CI inhibition.

4.12 ILs effect on CIII and CIV activities

To ultimate the characterisation of the three compounds interaction with the mitochondrial electron transport chain, CIII and CIV activities were tested in the presence of growing ILs concentration (**Fig. 4.24**).



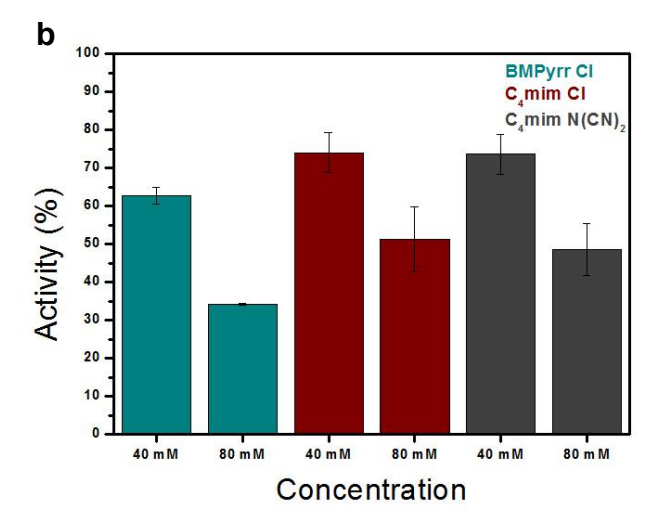


Figure 4.24. ILs effect on CIII (**a**) and CIV (**b**) activity. For each compound, CI activity (yellow), NADH consumption in sealed particles (NADH:O₂, cyan) and RET (magenta) are reported as a percentage of control. Concentrations are expressed in millimolar (mM).

CIII activity appeared to be inhibited similarly by both BMPyrr CI and C₄mim CI, with values that are comparable to the one registered for CI. These data must be integrated with data on C₄mim N(CN)₂ in the future. For CIV, inhibition of the enzymatic activity seemed way milder for all three compounds, with BMPyrr CI exerting a preeminent effect.

Overall, these data suggest that all three compounds are able to affect the mitochondrial electron transport chain, primarily through an effect of inhibition at the level of the complexes, which, for BMPyrr Cl and C₄mim N(CN)₂, could possibly be aggravated by an effect on the membrane electrochemical potential.

5. Discussion

All the ionic liquids tested on chromatophores, except choline chloride, were able to accelerate the carotenoid shift decay kinetics in single-flash experiments. This is due to an ILs concentration-dependent increase of the membrane ionic currents, which ultimately dissipates the electrical component $\Delta\Psi$ of the membrane electrochemical potential. Ntf2 containing ILs were particularly efficient in exerting such effect, collapsing the electrochromic shift signal at concentrations in the order of hundreds of micromolar, a range at least two orders of magnitude lower than that observed for the other ILs tested. The results obtained strongly suggest that this behaviour can be entirely attributed to the action of the Ntf2 $^{-}$ anion alone, since the same cations paired with the chloride anion showed little to no effect on the $\Delta\Psi$. Regarding BF4 $^{-}$ and Otf $^{-}$, both ILs containing these anions were able to increase ionic currents across the chromatophores membrane, though at concentrations in the order of tens of millimolar. Moreover, both compounds showed a visible decrease in their effect over the first few weeks following their arrival and opening, suggesting a tendency to decompose when in contact with air. For this reason, both compounds might be viewed as close to harmless when considering their release into the environment.

BMPyrr Ntf₂ was able to impair cromatophores light-driven ATP synthesis under continuous illumination, drammatically reducing ATP production by up to 70% already at a concentration of 500 μ M. Interestingly, this same effect was registered for concentration ten times higher, before a complete inhibition of ATP synthesis was observed at 20 mM. Once again, this effect seems to be attributed entirely to the anionic component, given that its replacement with Clalmost completely cancels it. Since no significant direct effect of inhibition was observed when testing the electron transfer reactions occuring at the level of cytochrome bc_1 in the presence of Ntf₂ containing ILs (i.e. the flash-induced cyts c re-reduction kinetics and heme b_H reduction kinetics, see paragraph 4.6), the impairment in ATP production is most likely to be attributed to the dissipation of $\Delta\Psi$, although the possibility of a direct inhibition of ATP synthase cannot be entirely discarded. In this sense, while data on chromatophores ATP synthesis in the presence of the other Ntf₂ containing ILs, bearing different cations, must be collected in the future, it is expected that such compounds would show a very similar behaviour to the one observed for BMPyrr NTf₂, knowing that they share the same ability to collapse the $\Delta\Psi$.

When testing the effect of these ILs *in vivo* on the photosynthetic growth of *Rb. capsulatus*, it was observed that Ntf₂ containing ILs were able to inhibit growth in the 2-5 mM range. This is coherent with what reported in literature for Ntf₂ containing short-chained imidazolium- and pyrrolidinium-based ILs toxicity to *Aliivibrio fischeri*, another Gram-negative bacteria (Ventura

et al., 2013). Most importantly, the ATP synthesis impairment observed on chromatophores takes place in this same range of concentrations, suggesting that the $\Delta\Psi$ dissipation caused by the Ntf₂ anion, which most likely causes a decrease in ATP production, might be the mechanism through which these ILs exert their toxic effect on Rb. capsulatus photosynthetic growth and, possibly, on the growth of other Gram-negative bacteria. In this sense, the BMPyrr Ntf₂ impairment of ATP synthesis observed in chromatophores under continuous light stimulation and the inhibition of Rb. capsulatus cell growth takes place at very similar concentrations, although growth inhibition reaches considerable values at 1 mM BMPyrr Ntf₂, when ATP synthesis is already significantly inhibited at 0.5 mM. This could be due to the fact that the compound might need to reach a certain concentration in the culture medium before being able to reach the cell membrane, possibly having to overcome the barrier presented by the bacterial cell wall. Overall, on an important side note, the system employed for monitoring Rb. capsulatus photosynthetic growth in the presence of ILs in 96-well plates proved to be a practical, cost-effective and accurate method for testing ILs toxicity, able to yield consistent data on relatively short amounts of time and based on a simple setup that can be easily assembled in any biological laboratory. On these premises, we would like to propose this system as a fast screening tool for examining the toxicity of ILs and other contaminants of ecotoxicological interest, joining Liu and coworkers proposal for the employment of purple bacteria as model systems to evaluate ecotoxicity of various effectors (X. Liu et al., 2023). In addition, the relative ease with which chromatophores can be isolated allows for their utilisation in analyses aimed at clarifying whether the toxic effect detected in growth tests is to be attributed to detrimental interactions ath the level of the cell membrane.

ETPH were employed to test BMPyrr CI, C₄mim CI and C₄mim N(CN)₂ effect on a different model for native bioenergetically active membranes. To our knowledge, this is the first time the effect of ILs has been tested on submitochondrial particles. Surprisingly, the tested compounds primarily showed an effect of direct inhibition of the electron transport chain complexes, especially towards complex I. While this behaviour seems to be the sole effect exerted by C₄mim CI, both BMPyrr CI and C₄mim N(CN)₂ also showed a secondary effect on the membrane electrochemical potential, seemingly producing a relaxation of the respiratory control in NADH:O₂ measurements, and a decrease in NADH production rate in RET measurements. The latter effect is higher than what would be justified by the sole impairment of the CI activity, suggesting that also a dissipation of the proton-motive force, needed to direct the electron flow towards NAD⁺, can be responsible for the observed inhibition. Although it is hard to compare qualitatively the two systems, these data resemble what

Malferrari and colleagues reported about this compounds effect on chromatophores carotenoid shift, where the more hydrophobic C₄mim N(CN)₂ showed a more aggressive behaviour than the chlorinated ones, substantially affecting the membrane potential at concentration around 10-20 mM (Malferrari et al., 2015). Albeit the hydrophobicity of a compound does not always correlate to its lipophilicity (Dołżonek et al., 2017; Ventura et al., 2013), C₄mim N(CN)₂ is likely more capable of inserting into a biological membrane than the chlorinated compounds, and this is probably the most decisive force driving its detrimental effect towards both the chromatophore and the submitochondrial particle.

Overall, taking together the data obtained on both cromatophores and submitochondrial particles, our results strongly reinforce the already existent idea that the ability of ILs anions to intercalate into a native biological membrane is the determining factor in their toxicity. This is also supported by the values extracted from the equation used to fit the carotenoid shift experimental traces for the parameters N_t and k_i which, respectively, tell us that the Ntf₂ anion is characterised by a larger partition in the membrane phase and that it encounters a lower energy barrier for intramembrane translocation. Our data call for a comprehensive study of ILs lipophilicity. In this regard, ILs lipophilicity has been often studied by determining their octanol-water partition, a technique that is commonly employed to estimate a compound possible impact on organisms inhabiting water environment, based on the dielectric properties of 1-octanol, which mimics a generalized lipid phase (Choua et al., 2003; Domańska et al., 2003; Domańska & Bogel-Łukasik, 2005; S. H. Lee & Lee, 2009; Ropel et al., 2005; Sangster, 1997). However, doubts have been raised about this method, since it fails to consider that charged species, such as ionic liquids, interact differently with the polar and charged phospholipids of the membrane system (Dołżonek et al., 2017; Klamt et al., 2008; Ventura et al., 2011). In their 2017 paper, Dołżonek and colleagues estimated the membrane partitioning of some ILs using a system based on commercially available solid-supported lipid membranes, which better represents the cell membrane system (Dołżonek et al., 2017). In this regard, we believe that chromatophores might also be employed as a system to better understand how ILs partition into a native biological membrane. This kind of information can be extremely useful in predicting ILs toxicity and bioaccumulation into living organisms membrane, through the use of the ever improving computational modeling methods such as the quantitative structure-activity relationships (QSAR), an in silico method for assessing compounds hazard based on their structure (Roy et al., 2015). Moreover, in the future we would also like to test the combined effect of different lipophilic anions on chromatophores.

For some time now, a part of the scientific community has put an effort in designing more hydrophobic ILs, capable of isolating themselves in an aqueous environment, with a lower lipophilicity (Ventura et al., 2013). In our opinion, the study of the interaction with native biological membranes is a fundamental prerequisite for synthesising more ecologically friendly, less toxic ionic liquids.

6. Bibliography

- Abu Talip, R. A., Yahya, W. Z., & Bustam, M. A. (2020). Ionic Liquids Roles and Perspectives in Electrolyte for Dye-Sensitized Solar Cells. In *Sustainability* (Vol. 12, Issue 18). https://doi.org/10.3390/su12187598
- Abushammala, H., & Mao, J. (2020). A Review on the Partial and Complete Dissolution and Fractionation of Wood and Lignocelluloses Using Imidazolium Ionic Liquids. In *Polymers* (Vol. 12, Issue 1). https://doi.org/10.3390/polym12010195
- Allen, J. P., Feher, G., Yeates, T. O., Komiya, H., & Rees, D. C. (1987). Structure of the reaction center from Rhodobacter sphaeroides R-26: the protein subunits. *Proceedings of the National Academy of Sciences of the United States of America*, *84*(17), 6162–6166. https://doi.org/10.1073/pnas.84.17.6162
- Amsel, A.-K., Olsson, O., & Kümmerer, K. (2022). Inventory of biodegradation data of ionic liquids. *Chemosphere*, 299, 134385. https://doi.org/https://doi.org/10.1016/j.chemosphere.2022.134385
- Angell, C. A., Byrne, N., & Belieres, J.-P. (2007). Parallel Developments in Aprotic and Protic Ionic Liquids: Physical Chemistry and Applications. *Accounts of Chemical Research*, *40*(11), 1228–1236. https://doi.org/10.1021/ar7001842
- Angell, M., Zhu, G., Lin, M.-C., Rong, Y., & Dai, H. (2020). Ionic Liquid Analogs of AlCl3 with Urea Derivatives as Electrolytes for Aluminum Batteries. *Advanced Functional Materials*, *30*(4). https://doi.org/10.1002/adfm.201901928
- Anthony, J. L., Maginn, E. J., & Brennecke, J. F. (2001). Solution Thermodynamics of Imidazolium-Based Ionic Liquids and Water. *The Journal of Physical Chemistry B*, 105(44), 10942–10949. https://doi.org/10.1021/jp0112368
- Argese, E., Bettiol, C., Miana, P., Luzzolino, L., & Giurin, G. (1996). Submitochondrial particles as in vitro biosensors of heavy metal toxicity. *Journal of Aquatic Ecosystem Stress and Recovery*, *5*(2), 125–134. https://doi.org/10.1007/bf00662801
- Armand, M., Endres, F., MacFarlane, D. R., Ohno, H., & Scrosati, B. (2009). Ionic-liquid materials for the electrochemical challenges of the future. *Nature Materials*, *8*(8), 621–629. https://doi.org/10.1038/nmat2448
- Aschenbrenner, O., Supasitmongkol, S., Taylor, M., & Styring, P. (2009). Measurement of vapour pressures of ionic liquids and other low vapour pressure solvents. *Green Chemistry*, *11*(8), 1217–1221. https://doi.org/10.1039/B904407H
- Baccarini-Melandri, A., & Melandri, B. A. B. T.-M. in E. (1971). [50] Partial resolution of the photophosphorylating system of Rhodopseudomonas capsulata. In *Photosynthesis and*

- Nitrogen Part A (Vol. 23, pp. 556–561). Academic Press. https://doi.org/https://doi.org/10.1016/S0076-6879(71)23126-8
- Baracca, A., Barogi, S., Carelli, V., Lenaz, G., & Solaini, G. (2000). Catalytic activities of mitochondrial ATP synthase in patients with mitochondrial DNA T8993G mutation in the ATPase 6 gene encoding subunit a. *The Journal of Biological Chemistry*, 275(6), 4177–4182. https://doi.org/10.1074/jbc.275.6.4177
- Barz, W. P., Francia, F., Venturoli, G., Melandri, B. A., Verméglio, A., & Oesterhelt, D. (1995). Role of PufX Protein in Photosynthetic Growth of Rhodobacter sphaeroides. 1. PufX Is Required for Efficient Light-Driven Electron Transfer and Photophosphorylation under Anaerobic Conditions. *Biochemistry*, 34(46), 15235–15247. https://doi.org/10.1021/bi00046a032
- Belesov, A. V, Ladesov, A. V, Pikovskoi, I. I., Faleva, A. V, & Kosyakov, D. S. (2020).
 Characterization of Ionic Liquid Lignins Isolated from Spruce Wood with 1-Butyl-3-methylimidazolium Acetate and Methyl Sulfate and Their Binary Mixtures with DMSO.
 In Molecules (Vol. 25, Issue 11). https://doi.org/10.3390/molecules25112479
- Bender, C. R., Kuhn, B. L., Farias, C. A. A., Ziembowicz, F. I., Beck, T. S., & Frizzo, C. P. (2019). Thermal stability and kinetic of decomposition of mono- And dicationic imidazolium-based ionic liquids. *Journal of the Brazilian Chemical Society*, 30(10), 2199–2209. https://doi.org/10.21577/0103-5053.20190114
- Benz, R., Läuger, P., & Janko, K. (1976). Transport kinetics of hydrophobic ions in lipid bilayer membranes Charge-pulse relaxation studies. *Biochimica et Biophysica Acta* (BBA) - Biomembranes, 455(3), 701–720. https://doi.org/https://doi.org/10.1016/0005-2736(76)90042-0
- Benz, R., & McLaughlin, S. (1983). The molecular mechanism of action of the proton ionophore FCCP (carbonylcyanide p-trifluoromethoxyphenylhydrazone). *Biophysical Journal*, *41*(3), 381–398. https://doi.org/10.1016/S0006-3495(83)84449-X
- Beyer, R. E. B. T.-M. in E. (1967). [34] Preparation, properties, and conditions for assay of phosphorylating electron transport particles (ETPH) and its variations. In *Oxidation and Phosphorylation* (Vol. 10, pp. 186–194). Academic Press. https://doi.org/https://doi.org/10.1016/0076-6879(67)10037-2
- Bhattacharjee, A., Lopes-da-Silva, J. A., Freire, M. G., Coutinho, J. A. P., & Carvalho, P. J. (2015). Thermophysical properties of phosphonium-based ionic liquids. *Fluid Phase Equilibria*, *400*, 103–113. https://doi.org/https://doi.org/10.1016/j.fluid.2015.05.009
- Bhongale, P. V, Joshi, S. S., & Mali, N. A. (2020). Selective monoalkylation of hydroquinone

- in the presence of SO3H-functionalized ionic liquids as catalysts. *Chemical Papers*, 74(12), 4461–4471. https://doi.org/10.1007/s11696-020-01230-1
- Biczak, R., Śnioszek, M., Telesiński, A., & Pawłowska, B. (2017). Growth inhibition and efficiency of the antioxidant system in spring barley and common radish grown on soil polluted ionic liquids with iodide anions. *Ecotoxicology and Environmental Safety*, 139, 463–471. https://doi.org/10.1016/j.ecoenv.2017.02.016
- Bin T, Venturoli G, Ghelli AM, Francia F. Use of bacterial photosynthetic vesicles to evaluate the effect of ionic liquids on the permeability of biological membranes. Biochim Biophys Acta Biomembr. 2024 Mar;1866(3):184291. doi: 10.1016/j.bbamem.2024.184291. Epub 2024 Jan 30. PMID: 38296218.
- Blankenship, R.E. (2014). Molecular mechanisms of photosynthesis, 2nd edn. Wiley, Indianapolis
- Bowyer, J. R., Meinhardt, S. W., Tierney, G. V, & Crofts, A. R. (1981). Resolved difference spectra of redox centers involved in photosynthetic electron flow in Rhodopseudomonas capsulata and Rhodopseudomonas sphaeroides. *Biochimica et Biophysica Acta*, *635*(1), 167–186. https://doi.org/10.1016/0005-2728(81)90016-5
- Bracun, L., Yamagata, A., Christianson, B. M., Shirouzu, M., & Liu, L.-N. (2023). Cryo-EM structure of a monomeric RC-LH1-PufX supercomplex with high-carotenoid content from Rhodobacter capsulatus. *Structure (London, England : 1993)*, *31*(3), 318-328.e3. https://doi.org/10.1016/j.str.2023.01.006
- Bragadin, M., Moret, I., Piazza, R., Grasso, M., & Manente, S. (2002). The interactions of cetyltrimethylammonium with mitochondria: an uncoupler or a detergent?

 Chemosphere, 46(2), 219–223. https://doi.org/https://doi.org/10.1016/S0045-6535(01)00095-9
- Brand, M. D., & Nicholls, D. G. (2011). Assessing mitochondrial dysfunction in cells. *Biochemical Journal*, 435(2), 297–312. https://doi.org/10.1042/BJ20110162
- Butt, H. S., Lethesh, K. C., & Fiksdahl, A. (2020). Fuel oil desulfurization with dual functionalized imidazolium based ionic liquids. *Separation and Purification Technology*, 248, 116959. https://doi.org/https://doi.org/10.1016/j.seppur.2020.116959
- Carroll, J., Fearnley, I. M., Skehel, J. M., Shannon, R. J., Hirst, J., & Walker, J. E. (2006). Bovine complex I is a complex of 45 different subunits. *The Journal of Biological Chemistry*, *281*(43), 32724–32727. https://doi.org/10.1074/jbc.M607135200
- Cartron, M. L., Olsen, J. D., Sener, M., Jackson, P. J., Brindley, A. A., Qian, P., Dickman, M. J., Leggett, G. J., Schulten, K., & Neil Hunter, C. (2014). Integration of energy and

- electron transfer processes in the photosynthetic membrane of Rhodobacter sphaeroides. *Biochimica et Biophysica Acta (BBA) Bioenergetics*, *1837*(10), 1769–1780. https://doi.org/https://doi.org/10.1016/j.bbabio.2014.02.003
- Carvalho, P. J., Álvarez, V. H., Marrucho, I. M., Aznar, M., & Coutinho, J. A. P. (2009). High pressure phase behavior of carbon dioxide in 1-butyl-3-methylimidazolium bis(trifluoromethylsulfonyl)imide and 1-butyl-3-methylimidazolium dicyanamide ionic liquids. *The Journal of Supercritical Fluids*, *50*(2), 105–111. https://doi.org/https://doi.org/10.1016/j.supflu.2009.05.008
- Casadio, R., Venturoli, G., & Melandri, B. A. (1988). Evaluation of the electrical capacitance in biological membranes at different phospholipid to protein ratios. *European Biophysics Journal*, *16*(4), 243–253. https://doi.org/10.1007/BF00261266
- Cecchini, G. (2003). Function and structure of complex II of the respiratory chain. *Annual Review of Biochemistry*, 72, 77–109. https://doi.org/10.1146/annurev.biochem.72.121801.161700
- Chatel, G., & Macfarlane, D. R. (2014). Ionic liquids and ultrasound in combination: Synergies and challenges. *Chemical Society Reviews*, *43*(23), 8132–8149. https://doi.org/10.1039/c4cs00193a
- Cho, C.-W., Phuong Thuy Pham, T., Jeon, Y.-C., & Yun, Y.-S. (2008). Influence of anions on the toxic effects of ionic liquids to a phytoplankton Selenastrum capricornutum.

 *Green Chemistry, 10(1), 67–72. https://doi.org/10.1039/B705520J
- Cho, C.-W., & Yun, Y.-S. (2016). Correlating toxicological effects of ionic liquids on Daphnia magna with in silico calculated linear free energy relationship descriptors.
 Chemosphere, 152, 207–213.
 https://doi.org/https://doi.org/10.1016/j.chemosphere.2016.02.108
- Choua, C.-H., Perng, F.-S., Wong, D. S. H., & Su, W. C. (2003). 1-Octanol/water partition coefficient of ionic liquids. *Proc. 15th Symp. on Thermophysical Properties, Boulder, CO, USA*.
- Clayton, R. K. (1966). SPECTROSCOPIC ANALYSIS OF BACTERIOCHLOROPHYLLS IN VITRO AND IN VIVO. *Photochemistry and Photobiology*, *5*(8), 669–677. https://doi.org/https://doi.org/10.1111/j.1751-1097.1966.tb05813.x
- Cogdell, R. J., Isaacs, N. W., Freer, A. A., Arrelano, J., Howard, T. D., Papiz, M. Z., Hawthornthwaite-Lawless, A. M., & Prince, S. (1997). The structure and function of the LH2 (B800–850) complex from the purple photosynthetic bacterium Rhodopseudomonas acidophila strain 10050. *Progress in Biophysics and Molecular*

- Biology, 68(1), 1–27. https://doi.org/https://doi.org/10.1016/S0079-6107(97)00010-2
- Crinnion, W. J. (2010). The CDC fourth national report on human exposure to environmental chemicals: What it tells us about our toxic burden and how it assists environmental medicine physicians. *Alternative Medicine Review*, *15*(2), 101–108. https://www.scopus.com/inward/record.uri?eid=2-s2.0-77954634254&partnerID=40&md5=ee36537f7abc02f98b88e0296770a307
- Crofts, A. R. (2021). The modified Q-cycle: A look back at its development and forward to a functional model. *Biochimica et Biophysica Acta. Bioenergetics*, *1862*(8), 148417. https://doi.org/10.1016/j.bbabio.2021.148417
- Cui, Y., He, B., Liu, X., & Sun, J. (2020). Ionic Liquids-Promoted Electrocatalytic Reduction of Carbon Dioxide. *Industrial & Engineering Chemistry Research*, *59*(46), 20235–20252. https://doi.org/10.1021/acs.iecr.0c04037
- Degli Esposti, M., Carelli, V., Ghelli, A., Ratta, M., Crimi, M., Sangiorgi, S., Montagna, P., Lenaz, G., Lugaresi, E., & Cortelli, P. (1994). Functional alterations of the mitochondrially encoded ND4 subunit associated with Leber's hereditary optic neuropathy. *FEBS Letters*, *352*(3), 375–379. https://doi.org/10.1016/0014-5793(94)00971-6
- Degli Esposti, M., & Lenaz, G. (1982). Kinetics of ubiquinol-1-cytochrome c reductase in bovine heart mitochondria and submitochondrial particles. *Biochimica et Biophysica Acta*, *682*(2), 189–200. https://doi.org/10.1016/0005-2728(82)90098-6
- Deisenhofer, J., Epp, O., Miki, K., Huber, R., & Michel, H. (1984). X-ray structure analysis of a membrane protein complex. Electron density map at 3 A resolution and a model of the chromophores of the photosynthetic reaction center from Rhodopseudomonas viridis. *Journal of Molecular Biology*, *180*(2), 385–398. https://doi.org/10.1016/s0022-2836(84)80011-x
- Deyab, M. A. (2019). Sulfonium-based ionic liquid as an anticorrosive agent for thermal desalination units. *Journal of Molecular Liquids*, 296, 111742. https://doi.org/https://doi.org/10.1016/j.molliq.2019.111742
- Deyab, M. A. (2020). Understanding the anti-corrosion mechanism and performance of ionic liquids in desalination, petroleum, pickling, de-scaling, and acid cleaning applications. *Journal of Molecular Liquids*, 309, 113107. https://doi.org/https://doi.org/10.1016/j.molliq.2020.113107
- Dezi, M., Francia, F., Mallardi, A., Colafemmina, G., Palazzo, G., & Venturoli, G. (2007). Stabilization of charge separation and cardiolipin confinement in antenna–reaction

- center complexes purified from Rhodobacter sphaeroides. *Biochimica et Biophysica Acta (BBA) Bioenergetics*, *1767*(8), 1041–1056. https://doi.org/https://doi.org/10.1016/j.bbabio.2007.05.006
- Dołżonek, J., Cho, C. W., Stepnowski, P., Markiewicz, M., Thöming, J., & Stolte, S. (2017). Membrane partitioning of ionic liquid cations, anions and ion pairs Estimating the bioconcentration potential of organic ions. *Environmental Pollution*, 228, 378–389. https://doi.org/10.1016/j.envpol.2017.04.079
- Domańska, U., Bogel-Łukasik, E., & Bogel-Łukasik, R. (2003). 1-Octanol/Water Partition Coefficients of 1Alkyl-3-methylimidazolium Chloride. *Chemistry A European Journal*, 9(13), 3033–3041. https://doi.org/https://doi.org/10.1002/chem.200204516
- Domańska, U., & Bogel-Łukasik, R. (2005). Physicochemical Properties and Solubility of Alkyl-(2-hydroxyethyl)-dimethylammonium Bromide. *The Journal of Physical Chemistry B*, 109(24), 12124–12132. https://doi.org/10.1021/jp058015c
- Drachev, L. A., Mamedov, M. D., Mulkidjanian, A. Y., Semenov, A. Y., Shinkarev, V. P., & Verkhovsky, M. I. (1988). Phase II of carotenoid bandshift is mainly due to the electrogenic protonation of the secondary quinone acceptor. *FEBS Letters*, *233*(2), 315–318. https://doi.org/https://doi.org/10.1016/0014-5793(88)80450-2
- Efremov, R. G., & Sazanov, L. A. (2011). Structure of the membrane domain of respiratory complex I. *Nature*, 476(7361), 414–420. https://doi.org/10.1038/nature10330
- Egorova, K. S., & Ananikov, V. P. (2014). Toxicity of ionic liquids: Eco(cyto)activity as complicated, but unavoidable parameter for task-specific optimization. *ChemSusChem*, 7(2), 336–360. https://doi.org/10.1002/cssc.201300459
- El Seoud, O. A., Keppeler, N., Malek, N. I., & Galgano, P. D. (2021). Ionic Liquid-Based Surfactants: Recent Advances in Their Syntheses, Solution Properties, and Applications. In *Polymers* (Vol. 13, Issue 7). https://doi.org/10.3390/polym13071100
- Ermler, U., Fritzsch, G., Buchanan, S. K., & Michel, H. (1994). Structure of the photosynthetic reaction centre from Rhodobacter sphaeroides at 2.65 å resolution: cofactors and protein-cofactor interactions. *Structure*, *2*(10), 925–936. https://doi.org/https://doi.org/10.1016/S0969-2126(94)00094-8
- Escher, B. I., Snozzi, M., Häberli, K., & Schwarzenbach, R. P. (1997). A new method for simultaneous quantification of uncoupling and inhibitory activity of organic pollutants in energy-transducing membranes. *Environmental Toxicology and Chemistry*, *16*(3), 405–414. https://doi.org/10.1002/etc.5620160303
- Esser, L., Elberry, M., Zhou, F., Yu, C.-A., Yu, L., & Xia, D. (2008). Inhibitor-complexed

- Structures of the Cytochrome bc1 from the Photosynthetic Bacterium Rhodobacter sphaeroides*. *Journal of Biological Chemistry*, 283(5), 2846–2857. https://doi.org/https://doi.org/10.1074/jbc.M708608200
- Esson, M. M., & Mecozzi, S. (2020). Preparation, Characterization, and Formulation Optimization of Ionic-Liquid-in-Water Nanoemulsions toward Systemic Delivery of Amphotericin B. *Molecular Pharmaceutics*, *17*(6), 2221–2226. https://doi.org/10.1021/acs.molpharmaceut.9b00809
- Estornell, E., Fato, R., Pallotti, F., & Lenaz, G. (1993). Assay conditions for the mitochondrial NADH:coenzyme Q oxidoreductase. *FEBS Letters*, *332*(1–2), 127–131. https://doi.org/https://doi.org/10.1016/0014-5793(93)80498-J
- Faisal Elmobarak, W., Almomani, F., Tawalbeh, M., Al-Othman, A., Martis, R., & Rasool, K. (2023). Current status of CO2 capture with ionic liquids: Development and progress. *Fuel*, 344, 128102. https://doi.org/https://doi.org/10.1016/j.fuel.2023.128102
- Fathizadeh, A., & Elber, R. (2019). Ion Permeation through a Phospholipid Membrane:

 Transition State, Path Splitting, and Calculation of Permeability. *Journal of Chemical Theory and Computation*, *15*(1), 720–730. https://doi.org/10.1021/acs.jctc.8b00882
- Fato, R., Cavazzoni, M., Castelluccio, C., Parenti Castelli, G., Palmer, G., Degli Esposti, M., & Lenaz, G. (1993). Steady-state kinetics of ubiquinol-cytochrome c reductase in bovine heart submitochondrial particles: diffusional effects. *The Biochemical Journal*, 290 (Pt 1)(Pt 1), 225–236. https://doi.org/10.1042/bj2900225
- Francia, F., Dezi, M., Mallardi, A., Palazzo, G., Cordone, L., & Venturoli, G. (2008).

 Protein-Matrix Coupling/Uncoupling in "Dry" Systems of Photosynthetic Reaction

 Center Embedded in Trehalose/Sucrose: The Origin of Trehalose Peculiarity. *Journal of the American Chemical Society*, *130*(31), 10240–10246.

 https://doi.org/10.1021/ja801801p
- Freire, M. G., Carvalho, P. J., Gardas, R. L., Marrucho, I. M., Santos, L. M. N. B. F., & Coutinho, J. A. P. (2008). Mutual Solubilities of Water and the [Cnmim][Tf2N]

 Hydrophobic Ionic Liquids. *The Journal of Physical Chemistry B*, *112*(6), 1604–1610. https://doi.org/10.1021/jp7097203
- Freire, M. G., Neves, C. M. S. S., Marrucho, I. M., Coutinho, J. A. P., & Fernandes, A. M. (2010). Hydrolysis of Tetrafluoroborate and Hexafluorophosphate Counter Ions in Imidazolium-Based Ionic Liquids. *The Journal of Physical Chemistry A*, *114*(11), 3744–3749. https://doi.org/10.1021/jp903292n
- Galletti, P., Malferrari, D., Samorì, C., Sartor, G., & Tagliavini, E. (2015). Effects of ionic

- liquids on membrane fusion and lipid aggregation of egg-PC liposomes. *Colloids and Surfaces B: Biointerfaces*, *125*, 142–150.
- https://doi.org/https://doi.org/10.1016/j.colsurfb.2014.11.021
- Gan, C., Liang, T., Li, W., Fan, X., Li, X., Li, D., & Zhu, M. (2020). Hydroxyl-terminated ionic liquids functionalized graphene oxide with good dispersion and lubrication function. *Tribology International*, *148*, 106350. https://doi.org/https://doi.org/10.1016/j.triboint.2020.106350
- Gao, X., Wen, X., Esser, L., Quinn, B., Yu, L., Yu, C.-A., & Xia, D. (2003). Structural basis for the quinone reduction in the bc1 complex: a comparative analysis of crystal structures of mitochondrial cytochrome bc1 with bound substrate and inhibitors at the Qi site. *Biochemistry*, *42*(30), 9067–9080. https://doi.org/10.1021/bi0341814
- García-Lorenzo, A., Tojo, E., Tojo, J., Teijeira, M., Rodríguez-Berrocal, F. J., González, M. P., & Martínez-Zorzano, V. S. (2008). Cytotoxicity of selected imidazolium-derived ionic liquids in the human Caco-2 cell line. Sub-structural toxicological interpretation through a QSAR study. *Green Chemistry*, 10(5), 508–516. https://doi.org/10.1039/B718860A
- Giernoth, R. (2010). Task-Specific Ionic Liquids. *Angewandte Chemie International Edition*, 49(16), 2834–2839. https://doi.org/https://doi.org/10.1002/anie.200905981
- Glaser, E. G., & Crofts, A. R. (1984). A new electrogenic step in the ubiquinol: Cytochrome c2 oxidoreductase complex of Rhodopseudomonas sphaeroides. *Biochimica et Biophysica Acta (BBA) Bioenergetics*, 766(2), 322–333. https://doi.org/https://doi.org/10.1016/0005-2728(84)90248-2
- Gonçalves, A. R. P., Paredes, X., Cristino, A. F., Santos, F. J. V., & Queirós, C. S. G. P. (2021). Ionic liquids—a review of their toxicity to living organisms. *International Journal of Molecular Sciences*, *22*(11). https://doi.org/10.3390/ijms22115612
- Gubellini, F., Francia, F., Turina, P., Lévy, D., Venturoli, G., & Melandri, B. A. (2007). Heterogeneity of photosynthetic membranes from Rhodobacter capsulatus: Size dispersion and ATP synthase distribution. *Biochimica et Biophysica Acta (BBA) Bioenergetics*, *1767*(11), 1340–1352. https://doi.org/https://doi.org/10.1016/j.bbabio.2007.08.007
- Gujjala, L. K. S., Kundu, D., Dutta, D., Kumar, A., Bal, M., Kumar, A., Singh, E., Mishra, R., Kumar, S., & Vo, D.-V. N. (2024). Advances in ionic liquids: Synthesis, environmental remediation and reusability. *Journal of Molecular Liquids*, 396, 123896. https://doi.org/https://doi.org/10.1016/j.molliq.2023.123896
- Hallenbeck, P. C. (2017). Modern Topics in the Phototrophic Prokaryotes: Metabolism,

- Bioenergetics, and Omics. In *Modern Topics in the Phototrophic Prokaryotes: Metabolism, Bioenergetics, and Omics.* https://doi.org/10.1007/978-3-319-51365-2
- Hansen, M., & Smith, A. L. (1964). Studies on the mechanism of oxidative phosphorylation: VII. Preparation of a submitochondrial particle (ETPH) which is capable of fully coupled oxidative phosphorylation. *Biochimica et Biophysica Acta (BBA) - Specialized Section* on Enzymological Subjects, 81(2), 214–222. https://doi.org/https://doi.org/10.1016/0926-6569(64)90036-7
- Hayes, R., Warr, G. G., & Atkin, R. (2015). Structure and Nanostructure in Ionic Liquids. *Chemical Reviews*, *115*(13), 6357–6426. https://doi.org/10.1021/cr500411q
- Hinchliffe, A. B., & Porter, K. E. (2000). A comparison of membrane separation and distillation. *Chemical Engineering Research and Design*, *78*(2), 255–268. https://doi.org/10.1205/026387600527121
- Hinkle, P. C., Butow, R. A., Racker, E., & Chance, B. (1967). Partial resolution of the enzymes catalyzing oxidative phosphorylation. XV. Reverse electron transfer in the flavin-cytochrome beta region of the respiratory chain of beef heart submitochondrial particles. *The Journal of Biological Chemistry*, 242(22), 5169–5173.
- Holmes, N. G., Hunter, C. N., Niederman, R. A., & Crofts, A. R. (1980). Identification of the pigment pool responsible for the flash-induced carotenoid band shift in Rhodopseudomonas sphaeroides chromatophores. *FEBS Letters*, *115*(1), 43–48. https://doi.org/https://doi.org/10.1016/0014-5793(80)80723-X
- Hommes, F. A. (1963). The succinate-linked nicotinamide-adenine dinucleotide reduction in submitochondrial particles II. Studies with inhibitors. *Biochimica et Biophysica Acta*, 77, 183–190. https://doi.org/https://doi.org/10.1016/0006-3002(63)90491-8
- Hossain, M. M., Rawal, A., & Aldous, L. (2019). Aprotic vs protic ionic liquids for lignocellulosic biomass pretreatment: Anion effects, enzymatic hydrolysis, solid-state NMR, distillation, and recycle. ACS Sustainable Chemistry and Engineering, 7(14), 11928–11936. https://doi.org/10.1021/acssuschemeng.8b05987
- Hu, Y., & Peng, X. (2014). Effect of the Structures of Ionic Liquids on Their Physical
 Chemical Properties BT Structures and Interactions of Ionic Liquids (S. Zhang, J. Wang, X. Lu, & Q. Zhou (eds.); pp. 141–174). Springer Berlin Heidelberg.
 https://doi.org/10.1007/978-3-642-38619-0_5
- Huang, X., Yamasaki, K., Kudo, S., Sperry, J., & Hayashi, J. (2020). Influence of ionic liquid type on porous carbon formation during the ionothermal pyrolysis of cellulose. *Journal of Analytical and Applied Pyrolysis*, *145*, 104728.

- https://doi.org/https://doi.org/10.1016/j.jaap.2019.104728
- Isikli, S., & Ryan, K. M. (2020). Recent advances in solid-state polymer electrolytes and innovative ionic liquids based polymer electrolyte systems. *Current Opinion in Electrochemistry*, *21*, 188–191. https://doi.org/10.1016/j.coelec.2020.01.015
- Iverson, T. M. (2013). Catalytic mechanisms of complex II enzymes: A structural perspective. *Biochimica et Biophysica Acta (BBA) Bioenergetics*, *1827*(5), 648–657. https://doi.org/https://doi.org/10.1016/j.bbabio.2012.09.008
- Jackson, J. B., & Crofts, A. R. (1969). The high energy state in chromatophores from Rhodopseudomonas spheroides. *FEBS Letters*, *4*(3), 185–189. https://doi.org/https://doi.org/10.1016/0014-5793(69)80230-9
- Jackson, J. B., & Dutton, P. L. (1973). The kinetic and redox potentiometric resolution of the carotenoid shifts in Rhodopseudomonas spheroides chromatophores: Their relationship to electric field alterations in electron transport and energy coupling. *Biochimica et Biophysica Acta (BBA) - Bioenergetics*, 325(1), 102–113. https://doi.org/https://doi.org/10.1016/0005-2728(73)90155-2
- Jackson, J.B., Bacterial Photosynthesis, in: C, Bacterial Energy Transduction, Academic Press, London, Anthony, 1988 317–375.
- Jones, A. J. Y., Blaza, J. N., Varghese, F., & Hirst, J. (2017). Respiratory Complex I in Bos taurus and Paracoccus denitrificans Pumps Four Protons across the Membrane for Every NADH Oxidized. *The Journal of Biological Chemistry*, 292(12), 4987–4995. https://doi.org/10.1074/jbc.M116.771899
- Kampjut, D., & Sazanov, L. A. (2022). Structure of respiratory complex I An emerging blueprint for the mechanism. *Current Opinion in Structural Biology*, 74, 102350. https://doi.org/https://doi.org/10.1016/j.sbi.2022.102350
- Katre, N. V, & Wilson, D. F. (1978). Interaction of uncouplers with the mitochondrial membrane: Identification of the high affinity binding site. *Archives of Biochemistry and Biophysics*, 191(2), 647–656. https://doi.org/https://doi.org/10.1016/0003-9861(78)90403-4
- Kaur, G., Kumar, H., & Singla, M. (2022). Diverse applications of ionic liquids: A comprehensive review. *Journal of Molecular Liquids*, 351, 118556. https://doi.org/https://doi.org/10.1016/j.molliq.2022.118556
- Kaur, N., Kumar, S., Shiksha, Gahlay, G. K., & Mithu, V. S. (2021). Cytotoxicity and Membrane Permeability of Double-Chained 1,3-Dialkylimidazolium Cations in Ionic Liquids. *The Journal of Physical Chemistry B*, 125(14), 3613–3621.

- https://doi.org/10.1021/acs.jpcb.1c00592
- Kaur, N., Mithu, V. S., & Kumar, S. (2024). A review on (eco)toxicity of ionic liquids and their interaction with phospholipid membranes. *Journal of Molecular Liquids*, 397, 124095. https://doi.org/https://doi.org/10.1016/j.molliq.2024.124095
- Kawada, S., Okubo, H., Watanabe, S., Tadokoro, C., Tsuboi, R., Sasaki, S., & Miyatake, M. (2020). Lubricating Properties of Cyano-Based Ionic Liquids against Tetrahedral Amorphous Carbon Film. In *Coatings* (Vol. 10, Issue 2). https://doi.org/10.3390/coatings10020153
- Khoo, Y. S., Tjong, T. C., Chew, J. W., & Hu, X. (2024). Techniques for recovery and recycling of ionic liquids: A review. *Science of The Total Environment*, 922, 171238. https://doi.org/https://doi.org/10.1016/j.scitotenv.2024.171238
- King, A. W. T., Asikkala, J., Mutikainen, I., Järvi, P., & Kilpeläinen, I. (2011). Distillable acid-base conjugate ionic liquids for cellulose dissolution and processing. *Angewandte Chemie (International Ed. in English)*, 50(28), 6301–6305. https://doi.org/10.1002/anie.201100274
- Klamt, A., Huniar, U., Spycher, S., & Keldenich, J. (2008). COSMOmic: A Mechanistic Approach to the Calculation of Membrane–Water Partition Coefficients and Internal Distributions within Membranes and Micelles. *The Journal of Physical Chemistry B*, 112(38), 12148–12157. https://doi.org/10.1021/jp801736k
- KLINGENBERG, M., & SLENCZKA, W. (1959). [Pyridine nucleotide in liver mitochondria. An analysis of their redox relationships]. *Biochemische Zeitschrift*, 331, 486–517.
- Klishin, S., Junge, W., & Mulkidjanian, A. Y. (2002). cytochrome bc 1 complex in chromatophores of Rhodobacter capsulatus: binding of Zn 2+ decelerates likewise the oxidation of cytochrome b, the reduction of. *Biochimica et Biophysica Acta (BBA ...*, 1553, 177–182. http://www.sciencedirect.com/science/article/pii/S000527280100250X
- Kontro, I., Svedström, K., Duša, F., Ahvenainen, P., Ruokonen, S.-K., Witos, J., & Wiedmer, S. K. (2016). Effects of phosphonium-based ionic liquids on phospholipid membranes studied by small-angle X-ray scattering. *Chemistry and Physics of Lipids*, 201, 59–66. https://doi.org/10.1016/j.chemphyslip.2016.11.003
- Kore, R., Uppara, P. V., & Rogers, R. D. (2020). Replacing HF or AlCl3 in the Acylation of Isobutylbenzene with Chloroaluminate Ionic Liquids. ACS Sustainable Chemistry & Engineering, 8(28), 10330–10334. https://doi.org/10.1021/acssuschemeng.0c03951
- Kotlyar, A. B., & Vinogradov, A. D. (1990). Slow active/inactive transition of the mitochondrial NADH-ubiquinone reductase. *BBA Bioenergetics*, *1019*(2), 151–158.

- https://doi.org/10.1016/0005-2728(90)90137-S
- Kumar, S., Scheidt, H. A., Kaur, N., Kang, T. S., Gahlay, G. K., Huster, D., & Mithu, V. S. (2019). Effect of the Alkyl Chain Length of Amphiphilic Ionic Liquids on the Structure and Dynamics of Model Lipid Membranes. *Langmuir*, 35(37), 12215–12223. https://doi.org/10.1021/acs.langmuir.9b02128
- Kumarasinghe, K. D. M. S. P. K., de Silva, L. A., Perera, A. G. U., Tennakone, K., Dehipawala, S., & Kumara, G. R. A. (2020). Usage of Ionic Liquid Electrolyte in Tin and Zinc Oxide Composite Dye-sensitized Solar Cells. *Chemistry Letters*, 49(12), 1470– 1472. https://doi.org/10.1246/cl.200535
- Kuzmina, O. (2016). Chapter 5 Methods of IL Recovery and Destruction (O. Kuzmina & J. P. B. T.-A. Hallett Purification, and Recovery of Ionic Liquids (eds.); pp. 205–248).
 Elsevier. https://doi.org/https://doi.org/10.1016/B978-0-444-63713-0.00005-5
- Lazzús, J. A., & Pulgar-Villarroel, G. (2015). A group contribution method to estimate the viscosity of ionic liquids at different temperatures. *Journal of Molecular Liquids*, 209, 161–168. https://doi.org/https://doi.org/10.1016/j.molliq.2015.05.030
- Lee, S. H., & Lee, S. B. (2009). Octanol/water partition coefficients of ionic liquids. *Journal of Chemical Technology & Biotechnology*, *84*(2), 202–207. https://doi.org/https://doi.org/10.1002/jctb.2025
- Lee, Y.-Y., Edgehouse, K., Klemm, A., Mao, H., Pentzer, E., & Gurkan, B. (2020). Capsules of Reactive Ionic Liquids for Selective Capture of Carbon Dioxide at Low Concentrations. *ACS Applied Materials & Interfaces*, *12*(16), 19184–19193. https://doi.org/10.1021/acsami.0c01622
- Lemus, J., Palomar, J., Heras, F., Gilarranz, M. A., & Rodriguez, J. J. (2012). Developing criteria for the recovery of ionic liquids from aqueous phase by adsorption with activated carbon. *Separation and Purification Technology*, 97, 11–19. https://doi.org/10.1016/j.seppur.2012.02.027
- Li, B., Asikkala, J., Filpponen, I., & Argyropoulos, D. S. (2010). Factors Affecting Wood Dissolution and Regeneration of Ionic Liquids. *Industrial & Engineering Chemistry Research*, *49*(5), 2477–2484. https://doi.org/10.1021/ie901560p
- Li, C., Han, J., Wang, Y., Yan, Y., Pan, J., Xu, X., & Zhang, Z. (2010). Phase behavior for the aqueous two-phase systems containing the ionic liquid 1-butyl-3-methylimidazolium tetrafluoroborate and kosmotropic salts. *Journal of Chemical and Engineering Data*, 55(3), 1087–1092. https://doi.org/10.1021/je900533h
- Li, H.-Y., & Chu, Y.-H. (2023). Expeditious Discovery of Small-Molecule Thermoresponsive

- Ionic Liquid Materials: A Review. *Molecules (Basel, Switzerland)*, 28(19). https://doi.org/10.3390/molecules28196817
- Li, Q., & Ardebili, H. (2016). Flexible thin-film battery based on solid-like ionic liquid-polymer electrolyte. *Journal of Power Sources*, *303*, 17–21. https://doi.org/https://doi.org/10.1016/j.jpowsour.2015.10.099
- Li, Y., Yang, M., Liu, L., Zhang, R., Cui, Y., Dang, P., Ge, X., & Chen, X. (2018). Effects of 1-butyl-3-methylimidazolium chloride on the photosynthetic system and metabolism of maize (Zea mays L.) seedlings. *Ecotoxicology and Environmental Safety*, *161*(April), 648–654. https://doi.org/10.1016/j.ecoenv.2018.06.037
- Liu, T., Guo, Y., Wang, J., Wang, J., Zhu, L., Zhang, J., & Zhang, C. (2016). Assessing toxic effects of [Omim]Cl and [Omim]BF4 in zebrafish adults using a biomarker approach. *Environmental Science and Pollution Research*, 23(8), 7360–7368. https://doi.org/10.1007/s11356-015-5887-3
- Liu, X., Chen, M., Jiang, Y., Gao, R., Wang, Z., & Wang, P. (2023). *Rhodobacter sphaeroides as a model to study the ecotoxicity of. January*, 1–9. https://doi.org/10.3389/fmolb.2023.1106832
- Liu, X. L., Chen, M. Q., Jiang, Y. L., Gao, R. Y., Wang, Z. J., & Wang, P. (2023).

 Rhodobacter sphaeroides as a model to study the ecotoxicity of 1-alkyl-3-methylimidazolium bromide. *Frontiers in Molecular Biosciences*, *10*(January), 1–9. https://doi.org/10.3389/fmolb.2023.1106832
- Liu, Y., Friesen, J. B., McAlpine, J. B., Lankin, D. C., Chen, S.-N., & Pauli, G. F. (2018).
 Natural Deep Eutectic Solvents: Properties, Applications, and Perspectives. *Journal of Natural Products*, 81(3), 679–690. https://doi.org/10.1021/acs.jnatprod.7b00945
- Magina, S., Barros-Timmons, A., Ventura, S. P. M., & Evtuguin, D. V. (2021). Evaluating the hazardous impact of ionic liquids Challenges and opportunities. *Journal of Hazardous Materials*, *412*, 125215. https://doi.org/https://doi.org/10.1016/j.jhazmat.2021.125215
- Mai, N. L., Ahn, K., & Koo, Y.-M. (2014). Methods for recovery of ionic liquids A review. *Process Biochemistry*, 49(5), 872–881. https://doi.org/10.1016/j.procbio.2014.01.016
- Malferrari, M., Malferrari, D., Francia, F., Galletti, P., Tagliavini, E., & Venturoli, G. (2015). Ionic liquids effects on the permeability of photosynthetic membranes probed by the electrochromic shift of endogenous carotenoids. *Biochimica et Biophysica Acta Biomembranes*, 1848(11), 2898–2909. https://doi.org/10.1016/j.bbamem.2015.09.006
- Malolan, R., Gopinath, K. P., Vo, D.-V. N., Jayaraman, R. S., Adithya, S., Ajay, P. S., & Arun, J. (2021). Green ionic liquids and deep eutectic solvents for desulphurization,

- denitrification, biomass, biodiesel, bioethanol and hydrogen fuels: a review. *Environmental Chemistry Letters*, *19*(2), 1001–1023. https://doi.org/10.1007/s10311-020-01113-7
- Maniam, K. K., & Paul, S. (2020). Progress in Electrodeposition of Zinc and Zinc Nickel Alloys Using Ionic Liquids. In *Applied Sciences* (Vol. 10, Issue 15). https://doi.org/10.3390/app10155321
- Markland, F. S., & Wadkins, C. L. (1966). Adenosine triphosphate-adenosine 5'monophosphate phosphotransferase of bovine liver mitochondria. II. General kinetic and structural properties. *Journal of Biological Chemistry*, 241(18), 4136–4145. https://www.scopus.com/inward/record.uri?eid=2-s2.0-0014027988&partnerID=40&md5=b64a4354dd8f706a8f90cd6da68bd798
- Martínez-Palou, R. (2010). Microwave-assisted synthesis using ionic liquids. *Molecular Diversity*, *14*(1), 3–25. https://doi.org/10.1007/s11030-009-9159-3
- Matczuk, M., Timerbaev, A. R., Keppler, B. K., & Ruzik, L. (2024). Ionic liquid-mediated drug delivery: A review on progress and challenges focused on poly(ionic liquid) nanoplatforms. *Journal of Molecular Liquids*, 399, 124403. https://doi.org/https://doi.org/10.1016/j.molliq.2024.124403
- Matzke, M., Stolte, S., Arning, J., Uebers, U., & Filser, J. (2008). Imidazolium based ionic liquids in soils: effects of the side chain length on wheat (Triticum aestivum) and cress (Lepidium sativum) as affected by different clays and organic matter. *Green Chemistry*, 10(5), 584–591. https://doi.org/10.1039/B717811E
- Matzke, M., Stolte, S., Thiele, K., Juffernholz, T., Arning, J., Ranke, J., Welz-Biermann, U., & Jastorff, B. (2007). The influence of anion species on the toxicity of 1-alkyl-3-methylimidazolium ionic liquids observed in an (eco)toxicological test battery. *Green Chemistry*, 9(11), 1198–1207. https://doi.org/10.1039/B705795D
- McLaughlin, M., Earle, M. J., Gîlea, M. A., Gilmore, B. F., Gorman, S. P., & Seddon, K. R. (2011). Cytotoxicity of 1-alkylquinolinium bromide ionic liquids in murine fibroblast NIH 3T3 cells. *Green Chemistry*, *13*(10), 2794–2800. https://doi.org/10.1039/C0GC00813C
- Meinhardt, S. W., & Crofts, A. R. (1982). The site and mechanism of action of myxothiazol as an inhibitor of electron transfer in Rhodopseudomonas sphaeroides. *FEBS Letters*, 149(2), 217–222. https://doi.org/https://doi.org/10.1016/0014-5793(82)81104-6
- MITCHELL, P. (1961). Coupling of phosphorylation to electron and hydrogen transfer by a chemi-osmotic type of mechanism. *Nature*, *191*, 144–148. https://doi.org/10.1038/191144a0

- Mitchell, P. (1972). Chemiosmotic coupling in energy transduction: a logical development of biochemical knowledge. *Journal of Bioenergetics*, *3*(1), 5–24. https://doi.org/10.1007/BF01515993
- Mitchell, P. (1976). Possible molecular mechanisms of the protonmotive function of cytochrome systems. *Journal of Theoretical Biology*, *62*(2), 327–367. https://doi.org/10.1016/0022-5193(76)90124-7
- Mitchell, P, & Moyle, J. (1967). Acid-base titration across the membrane system of rat-liver mitochondria. Catalysis by uncouplers. *The Biochemical Journal*, *104*(2), 588–600. https://doi.org/10.1042/bj1040588
- Mitchell, Peter. (2011). Chemiosmotic coupling in oxidative and photosynthetic phosphorylation. *Biochimica et Biophysica Acta (BBA) Bioenergetics*, *1807*(12), 1507–1538. https://doi.org/https://doi.org/10.1016/j.bbabio.2011.09.018
- Mitra, S., Sharma, V. K., & Ghosh, S. K. (2023). Effects of ionic liquids on biomembranes: A review on recent biophysical studies. *Chemistry and Physics of Lipids*, 256(August), 105336. https://doi.org/10.1016/j.chemphyslip.2023.105336
- Mohd Faridz Hilmy, N. I., Yahya, W. Z. N., & Kurnia, K. A. (2020). Eutectic ionic liquids as potential electrolytes in dye-sensitized solar cells: Physicochemical and conductivity studies. *Journal of Molecular Liquids*, *320*, 114381. https://doi.org/https://doi.org/10.1016/j.molliq.2020.114381
- Molodkina, E. B., Ehrenburg, M. R., Broekmann, P., & Rudnev, A. V. (2020).
 Electrodeposition of chromium on single-crystal electrodes from solutions of Cr(II) and Cr(III) salts in ionic liquids. *Journal of Electroanalytical Chemistry*, 860.
 https://doi.org/10.1016/j.jelechem.2020.113892
- Morales-Rios, E., Montgomery, M. G., Leslie, A. G. W., & Walker, J. E. (2015). Structure of ATP synthase from Paracoccus denitrificans determined by X-ray crystallography at 4.0 Å resolution. *Proceedings of the National Academy of Sciences*, *112*(43), 13231–13236. https://doi.org/10.1073/pnas.1517542112
- Morton, M. D., & Hamer, C. K. (2018). Ionic liquids The beginning of the end or the end of the beginning? – A look at the life of ionic liquids through patent claims. Separation and Purification Technology, 196, 3–9. https://doi.org/https://doi.org/10.1016/j.seppur.2017.11.023
- Mu, T., & Han, B. (2014). Structures and Thermodynamic Properties of Ionic Liquids BT -Structures and Interactions of Ionic Liquids (S. Zhang, J. Wang, X. Lu, & Q. Zhou (eds.); pp. 107–139). Springer Berlin Heidelberg. https://doi.org/10.1007/978-3-642-

- 38619-0 4
- Nagatsuma, S., Gotou, K., Yamashita, T., Yu, L.-J., Shen, J.-R., Madigan, M. T., Kimura, Y., & Wang-Otomo, Z.-Y. (2019). Phospholipid distributions in purple phototrophic bacteria and LH1-RC core complexes. *Biochimica et Biophysica Acta (BBA) Bioenergetics*, 1860(6), 461–468. https://doi.org/https://doi.org/10.1016/j.bbabio.2019.04.001
- Nancarrow, P., Al-Othman, A., Mital, D. K., & Döpking, S. (2021). Comprehensive analysis and correlation of ionic liquid conductivity data for energy applications. *Energy*, 220, 119761. https://doi.org/https://doi.org/10.1016/j.energy.2021.119761
- Ngo, H. L., LeCompte, K., Hargens, L., & McEwen, A. B. (2000). Thermal properties of imidazolium ionic liquids. *Thermochimica Acta*, *357–358*, 97–102. https://doi.org/https://doi.org/10.1016/S0040-6031(00)00373-7
- Nicholls, D.G, Ferguson, S.J., Bioenergetics, fourth ed., Academic Press, 2013
- OECD (2011), *Test No. 201: Freshwater Alga and Cyanobacteria, Growth Inhibition Test*, OECD Guidelines for the Testing of Chemicals, Section 2, OECD Publishing, Paris, https://doi.org/10.1787/9789264069923-en.
- Okoturo, O. O., & VanderNoot, T. J. (2004). Temperature dependence of viscosity for room temperature ionic liquids. *Journal of Electroanalytical Chemistry*, *568*, 167–181. https://doi.org/https://doi.org/10.1016/j.jelechem.2003.12.050
- Ortiz-Martínez, V. M., Gómez-Coma, L., Pérez, G., Ortiz, A., & Ortiz, I. (2020). The roles of ionic liquids as new electrolytes in redox flow batteries. Separation and Purification Technology, 252. https://doi.org/10.1016/j.seppur.2020.117436
- Paduszyński, K. (2019). Extensive Databases and Group Contribution QSPRs of Ionic Liquids Properties. 2. Viscosity. *Industrial & Engineering Chemistry Research*, *58*(36), 17049–17066. https://doi.org/10.1021/acs.iecr.9b03150
- Paduszyński, K., & Domańska, U. (2012). A New Group Contribution Method For Prediction of Density of Pure Ionic Liquids over a Wide Range of Temperature and Pressure.
 Industrial & Engineering Chemistry Research, 51(1), 591–604.
 https://doi.org/10.1021/ie202134z
- Pal, A., & Punia, R. (2019). Mixed micellization behaviour of tri-substituted surface active ionic liquid and cationic surfactant in aqueous medium and salt solution: Experimental and theoretical study. *Journal of Molecular Liquids*, 296, 111831. https://doi.org/https://doi.org/10.1016/j.molliq.2019.111831
- Pallotti, F., & Lenaz, G. B. T.-M. in C. B. (2001). Chapter 1 Isolation and subfractionation of mitochondria from animal cells and tissue culture lines. In *Mitochondria* (Vol. 65, pp. 1–

- 35). Academic Press. https://doi.org/https://doi.org/10.1016/S0091-679X(01)65002-7
- Pan, S., Yao, M., Zhang, J., Li, B., Xing, C., Song, X., Su, P., & Zhang, H. (2020).
 Recognition of Ionic Liquids as High-Voltage Electrolytes for Supercapacitors. *Frontiers in Chemistry*, 8, 261. https://doi.org/10.3389/fchem.2020.00261
- Parajó, J. J., Villanueva, M., & Salgado, J. (n.d.). Ionic Liquids. In R. Fehrmann & C. Santini (Eds.), *Synthesis, Properties, Technologies and Applications* (pp. 1–16). De Gruyter. https://doi.org/doi:10.1515/9783110583632-001
- Plechkova, N. V, & Seddon, K. R. (2007). Ionic Liquids: "Designer" Solvents for Green Chemistry. In *Methods and Reagents for Green Chemistry* (pp. 103–130). https://doi.org/https://doi.org/10.1002/9780470124086.ch5
- Pretti, C., Chiappe, C., Baldetti, I., Brunini, S., Monni, G., & Intorre, L. (2009). Acute toxicity of ionic liquids for three freshwater organisms: Pseudokirchneriella subcapitata, Daphnia magna and Danio rerio. *Ecotoxicology and Environmental Safety*, 72(4), 1170–1176. https://doi.org/10.1016/j.ecoenv.2008.09.010
- Qian, P., Swainsbury, D. J. K., Croll, T. I., Castro-Hartmann, P., Divitini, G., Sader, K., & Hunter, C. N. (2021). Cryo-EM Structure of the Rhodobacter sphaeroides Light-Harvesting 2 Complex at 2.1 Å. *Biochemistry*, *60*(44), 3302–3314. https://doi.org/10.1021/acs.biochem.1c00576
- Qin, M., Zhong, F., Sun, Y., Tan, X., Hu, K., Zhang, H., Kong, M., Wang, G., & Zhuang, L. (2020). Effect of cation substituent of dodecanesulfate-based anionic surface active ionic liquids on micellization: Experimental and theoretical studies. *Journal of Molecular Liquids*, 303, 112695. https://doi.org/https://doi.org/10.1016/j.molliq.2020.112695
- Rahali, S., Zarrougui, R., Marzouki, M., & Ghodbane, O. (2020). Electrodeposition of silver from the ionic liquid Butylpyridinium dicyanamide. *Journal of Electroanalytical Chemistry*, 871. https://doi.org/10.1016/j.jelechem.2020.114289
- Rogers, R. D., & Seddon, K. R. (2003). Ionic Liquids--Solvents of the Future? *Science*, 302(5646), 792–793. https://doi.org/10.1126/science.1090313
- Ropel, L., Belvèze, L. S., Aki, S. N. V. K., Stadtherr, M. A., & Brennecke, J. F. (2005). Octanol–water partition coefficients of imidazolium-based ionic liquids. *Green Chemistry*, 7(2), 83–90. https://doi.org/10.1039/B410891D
- Roy, K., Kar, S., & Das, R. N. (2015). *Understanding the basics of QSAR for applications in pharmaceutical sciences and risk assessment*. Academic press.
- Ruokonen, S.-K., Sanwald, C., Robciuc, A., Hietala, S., Rantamäki, A. H., Witos, J., King, A. W. T., Lämmerhofer, M., & Wiedmer, S. K. (2018). Correlation between Ionic Liquid

- Cytotoxicity and Liposome-Ionic Liquid Interactions. *Chemistry (Weinheim an Der Bergstrasse, Germany)*, *24*(11), 2669–2680. https://doi.org/10.1002/chem.201704924
- Rüther, T., Bhatt, A. I., Best, A. S., Harris, K. R., & Hollenkamp, A. F. (2020). Electrolytes for Lithium (Sodium) Batteries Based on Ionic Liquids: Highlighting the Key Role Played by the Anion. *Batteries & Supercaps*, *3*(9), 793–827. https://doi.org/https://doi.org/10.1002/batt.202000022
- Samorì, C., Campisi, T., Fagnoni, M., Galletti, P., Pasteris, A., Pezzolesi, L., Protti, S., Ravelli, D., & Tagliavini, E. (2015). Pyrrolidinium-based Ionic Liquids: Aquatic Ecotoxicity, Biodegradability, and Algal Subinhibitory Stimulation. ACS Sustainable Chemistry and Engineering, 3(8), 1860–1865. https://doi.org/10.1021/acssuschemeng.5b00458
- Samorì, C., Malferrari, D., Valbonesi, P., Montecavalli, A., Moretti, F., Galletti, P., Sartor, G., Tagliavini, E., Fabbri, E., & Pasteris, A. (2010). Introduction of oxygenated side chain into imidazolium ionic liquids: Evaluation of the effects at different biological organization levels. *Ecotoxicology and Environmental Safety*, 73(6), 1456–1464. https://doi.org/https://doi.org/10.1016/j.ecoenv.2010.07.020
- Sangster, J. M. (1997). Octanol-water partition coefficients: fundamentals and physical chemistry (Vol. 1). John Wiley & Sons.
- Saphon, S., Jackson, J. B., Lerbs, V., & Witt, H. T. (1975). The functional unit of electrical events and phosphorylation in chromatophores from Rhodopseudomonas sphaeroides. *Biochimica et Biophysica Acta (BBA) - Bioenergetics*, 408(1), 58–66. https://doi.org/https://doi.org/10.1016/0005-2728(75)90158-9
- Saphon, S., Jackson, J. B., & Witt, H. T. (1975). Electrical potential changes, H+ translocation and phosphorylation induced by short flash excitation in Rhodopseudomonas sphaeroides chromatophores. *Biochimica et Biophysica Acta (BBA) Bioenergetics*, 408(1), 67–82. https://doi.org/https://doi.org/10.1016/0005-2728(75)90159-0
- Sazanov, L. A., & Hinchliffe, P. (2006). Structure of the hydrophilic domain of respiratory complex I from Thermus thermophilus. *Science (New York, N.Y.)*, *311*(5766), 1430–1436. https://doi.org/10.1126/science.1123809
- Schägger, H., Link, T. A., Engel, W. D., & von Jagow, G. (1986). Isolation of the eleven protein subunits of the bc1 complex from beef heart. *Methods in Enzymology*, *126*, 224–237. https://doi.org/10.1016/s0076-6879(86)26024-3
- Schmid, R., & Junge, W. (1975). Current-voltage studies on the thylakoid membrane in the

- presence of ionophores. *Biochimica et Biophysica Acta (BBA) Biomembranes*, 394(1), 76–92. https://doi.org/https://doi.org/10.1016/0005-2736(75)90206-0
- Schweigert, N., Hunziker, R. W., Escher, B. I., & Eggen, R. I. (2001). Acute toxicity of (chloro-)catechols and (chloro-)catechol-copper combinations in Escherichia coli corresponds to their membrane toxicity in vitro. *Environmental Toxicology and Chemistry*, 20(2), 239–247.
- Shah, A., Jain, M., Lad, V. N., Ray, D., Aswal, V. K., & Malek, N. I. (2020). Selective accumulation of dyes and curcumin in a macroscopic complex coacervates composed of morpholinium based ester functionalized ionic liquid and sodium salicylate. *Journal of Molecular Liquids*, 317, 114140. https://doi.org/https://doi.org/10.1016/j.molliq.2020.114140
- Shah, A., & Malek, N. I. (2021). Selective Sequestration of Charged Dyes and Drug in the ionic Liquid Based Complex Coacervates. *Journal of Ionic Liquids*, *1*(2), 100006. https://doi.org/https://doi.org/10.1016/j.jil.2021.100006
- Sharma, V. K., & Mukhopadhyay, R. (2018). Deciphering interactions of ionic liquids with biomembrane. *Biophysical Reviews*, *10*(3), 721–734. https://doi.org/10.1007/s12551-018-0410-y
- Shi, H., Zhang, X., Sundmacher, K., & Zhou, T. (2021). Model-based optimal design of phase change ionic liquids for efficient thermal energy storage. *Green Energy* & *Environment*, *6*(3), 392–404. https://doi.org/https://doi.org/10.1016/j.gee.2020.12.017
- Shimada, S., Shinzawa-Itoh, K., Baba, J., Aoe, S., Shimada, A., Yamashita, E., Kang, J., Tateno, M., Yoshikawa, S., & Tsukihara, T. (2017). Complex structure of cytochrome c–cytochrome c oxidase reveals a novel protein–protein interaction mode. *The EMBO Journal*, 36(3), 291–300. https://doi.org/https://doi.org/10.15252/embj.201695021
- Singh, S. K., & Savoy, A. W. (2020). Ionic liquids synthesis and applications: An overview. *Journal of Molecular Liquids*, 297, 112038. https://doi.org/10.1016/j.molliq.2019.112038
- Singharoy, A., Maffeo, C., Delgado-Magnero, K. H., Swainsbury, D. J. K., Sener, M., Kleinekathöfer, U., Vant, J. W., Nguyen, J., Hitchcock, A., Isralewitz, B., Teo, I., Chandler, D. E., Stone, J. E., Phillips, J. C., Pogorelov, T. V., Mallus, M. I., Chipot, C., Luthey-Schulten, Z., Tieleman, D. P., ... Schulten, K. (2019). Atoms to Phenotypes: Molecular Design Principles of Cellular Energy Metabolism. *Cell*, 179(5), 1098-1111.e23. https://doi.org/10.1016/j.cell.2019.10.021
- Sosnowska, A., Laux, E., Keppner, H., Puzyn, T., & Bobrowski, M. (2020). Relatively high-

- Seebeck thermoelectric cells containing ionic liquids supplemented by cobalt redox couple. *Journal of Molecular Liquids*, *316*. https://doi.org/10.1016/j.molliq.2020.113871
- Stepnowski, P., & Zaleska, A. (2005). Comparison of different advanced oxidation processes for the degradation of room temperature ionic liquids. *Journal of Photochemistry and Photobiology A: Chemistry*, *170*(1), 45–50. https://doi.org/https://doi.org/10.1016/j.jphotochem.2004.07.019
- Steudte, S., Stepnowski, P., Cho, C.-W., Thöming, J., & Stolte, S. (2012). (Eco)toxicity of fluoro-organic and cyano-based ionic liquid anions. *Chemical Communications* (*Cambridge, England*), 48(75), 9382–9384. https://doi.org/10.1039/c2cc34955h
- Sun, F., Huo, X., Zhai, Y., Wang, A., Xu, J., Su, D., Bartlam, M., & Rao, Z. (2005). Crystal structure of mitochondrial respiratory membrane protein complex II. *Cell*, *121*(7), 1043–1057. https://doi.org/10.1016/j.cell.2005.05.025
- Sun, Y., Xu, X., Qin, M., Pang, N., Wang, G., & Zhuang, L. (2019). Dodecyl sulfate-based anionic surface-active ionic liquids: synthesis, surface properties, and interaction with gelatin. *Colloid and Polymer Science*, 297(4), 571–586. https://doi.org/10.1007/s00396-019-04473-x
- Swainsbury, D. J. K., Hawkings, F. R., Martin, E. C., Musiał, S., Salisbury, J. H., Jackson, P. J., Farmer, D. A., Johnson, M. P., Siebert, C. A., Hitchcock, A., & Hunter, C. N. (2023). Cryo-EM structure of the four-subunit Rhodobacter sphaeroides cytochrome bc(1) complex in styrene maleic acid nanodiscs. *Proceedings of the National Academy of Sciences of the United States of America*, 120(12), e2217922120. https://doi.org/10.1073/pnas.2217922120
- Symersky, J., Osowski, D., Walters, D. E., & Mueller, D. M. (2012). Oligomycin frames a common drug-binding site in the ATP synthase. *Proceedings of the National Academy of Sciences*, *109*(35), 13961–13965. https://doi.org/10.1073/pnas.1207912109
- Takamiya, K., & Dutton, L. (1977). The influence of transmembrane potentials of the redox equilibrium between cytochrome c2 and the reaction center in Rhodopseudomonas sphaeroides chromatophores. *FEBS Letters*, 80(2), 279–284. https://doi.org/https://doi.org/10.1016/0014-5793(77)80457-2
- Tomida, D. (2018). *Thermal Conductivity of Ionic Liquids*. https://doi.org/10.5772/intechopen.76559
- Trumpower, B. L. (2002). A concerted, alternating sites mechanism of ubiquinol oxidation by the dimeric cytochrome bc(1) complex. *Biochimica et Biophysica Acta*, *1555*(1–3), 166–173. https://doi.org/10.1016/s0005-2728(02)00273-6

- Tullo, A.H. The time is now for ionic liquids. Chem. Eng. News 2020, 98, 24.
- Ventura, S. P. M., Gardas, R. L., Gonçalves, F., & Coutinho, J. A. P. (2011).
 Ecotoxicological risk profile of ionic liquids: octanol-water distribution coefficients and toxicological data. *Journal of Chemical Technology & Biotechnology*, 86(7), 957–963. https://doi.org/https://doi.org/10.1002/jctb.2606
- Ventura, S. P. M., Gonçalves, A. M. M., Sintra, T., Pereira, J. L., Gonçalves, F., & Coutinho, J. A. P. (2013). Designing ionic liquids: the chemical structure role in the toxicity. *Ecotoxicology*, 22(1), 1–12. https://doi.org/10.1007/s10646-012-0997-x
- Verkhovskaya, M. L., Belevich, N., Euro, L., Wikström, M., & Verkhovsky, M. I. (2008). Real-time electron transfer in respiratory complex I. *Proceedings of the National Academy of Sciences*, *105*(10), 3763–3767. https://doi.org/10.1073/pnas.0711249105
- Vinothkumar, K. R., Zhu, J., & Hirst, J. (2014). Architecture of mammalian respiratory complex I. *Nature*, *515*(7525), 80–84. https://doi.org/10.1038/nature13686
- Vorobyov, I., Olson, T. E., Kim, J. H., Koeppe, R. E., Andersen, O. S., & Allen, T. W. (2014). Ion-Induced Defect Permeation of Lipid Membranes. *Biophysical Journal*, *106*(3), 586–597. https://doi.org/https://doi.org/10.1016/j.bpj.2013.12.027
- Vraneš, M., Tot, A., Jovanović-Šanta, S., Karaman, M., Dožić, S., Tešanović, K., Kojić, V., & Gadžurić, S. (2016). Toxicity reduction of imidazolium-based ionic liquids by the oxygenation of the alkyl substituent. *RSC Advances*, *6*(98), 96289–96295. https://doi.org/10.1039/C6RA16182K
- Wang, L.-S., Wang, L., Wang, G., Li, Z.-H., & Wang, J.-J. (2009). Effect of 1-butyl-3-methylimidazolium tetrafluoroborate on the wheat (Triticum aestivum L.) seedlings. *Environmental Toxicology*, 24(3), 296–303. https://doi.org/https://doi.org/10.1002/tox.20435
- Wang, X., Ohlin, C. A., Lu, Q., Fei, Z., Hu, J., & Dyson, P. J. (2007). Cytotoxicity of ionic liquids and precursor compounds towards human cell line HeLa. *Green Chemistry*, 9(11), 1191–1197. https://doi.org/10.1039/B704503D
- Wei, H.-L., Wang, Y.-T., Hong, Y.-Y., & Zhu, M.-J. (2021). Pretreatment of rice straw with recycled ionic liquids by phase-separation process for low-cost biorefinery. *Biotechnology and Applied Biochemistry*, 68(4), 871–880. https://doi.org/10.1002/bab.2007
- Weldemhret, T. G., Bañares, A. B., Ramos, K. R. M., Lee, W.-K., Nisola, G. M., Valdehuesa, K. N. G., & Chung, W.-J. (2020). Current advances in ionic liquid-based pre-treatment and depolymerization of macroalgal biomass. *Renewable Energy*, 152,

- 283–299. https://doi.org/https://doi.org/10.1016/j.renene.2020.01.054
- Welton, Thomas. (1999). Room-Temperature Ionic Liquids. Solvents for Synthesis and Catalysis. *Chemical Reviews*, *99*(8), 2071–2084. https://doi.org/10.1021/cr980032t
- Welton, Tom. (2018). Ionic liquids: a brief history. *Biophysical Reviews*, *10*(3), 691–706. https://doi.org/10.1007/s12551-018-0419-2
- Weyhing-Zerrer, N., Gundolf, T., Kalb, R., Oßmer, R., Rossmanith, P., & Mester, P. (2017).
 Predictability of ionic liquid toxicity from a SAR study on different systematic levels of pathogenic bacteria. *Ecotoxicology and Environmental Safety*, 139, 394–403.
 https://doi.org/https://doi.org/10.1016/j.ecoenv.2017.01.055
- Wikstrom, M. K. (1977). Proton pump coupled to cytochrome c oxidase in mitochondria. *Nature*, 266(5599), 271–273. https://doi.org/10.1038/266271a0
- Wilkes, J. S. (2002). A short history of ionic liquids From molten salts to neoteric solvents. *Green Chemistry*, *4*(2), 73–80. https://doi.org/10.1039/b110838g
- Witt, H.T. (1974), PRIMARY ACTS OF ENERGY CONSERVATION IN THE FUNCTIONAL MEMBRANE OF PHOTOSYNTHESIS. Annals of the New York Academy of Sciences, 227: 203-206.https://doi.org/10.1111/j.1749-6632.1974.tb14385.x
- Wu, G., Liu, Y., Liu, G., & Pang, X. (2020). The CO2 Absorption in Flue Gas Using Mixed Ionic Liquids. In *Molecules* (Vol. 25, Issue 5). https://doi.org/10.3390/molecules25051034
- Xia, Y., Liu, D., Dong, Y., Chen, J., & Liu, H. (2018). Effect of ionic liquids with different cations and anions on photosystem and cell structure of Scenedesmus obliquus. *Chemosphere*, *195*, 437–447. https://doi.org/10.1016/j.chemosphere.2017.12.054
- Xu, J., Liu, B., Hou, H., & Hu, J. (2017). Pretreatment of eucalyptus with recycled ionic liquids for low-cost biorefinery. *Bioresource Technology*, *234*, 406–414. https://doi.org/10.1016/j.biortech.2017.03.081
- Yang, G., Song, Y., Wang, Q., Zhang, L., & Deng, L. (2020). Review of ionic liquids containing, polymer/inorganic hybrid electrolytes for lithium metal batteries. *Materials* and Design, 190. https://doi.org/10.1016/j.matdes.2020.108563
- Yang, H., Zhang, L., Chen, L., Zhou, C., Yu, X., Yagoub, A. E.-G. A., & Ma, H. (2018). Effect of ionic liquid based imidazolium as an additive on the formation of polymer/salt aqueous biphasic systems. *Journal of Molecular Liquids*, *256*, 1–8.
- Yang, X. H., & Trumpower, B. L. (1986). Purification of a three-subunit ubiquinolcytochrome c oxidoreductase complex from Paracoccus denitrificans. *The Journal of Biological Chemistry*, 261(26), 12282–12289.

- Yang, Z., & Huang, Z.-L. (2012). Enzymatic synthesis of sugar fatty acid esters in ionic liquids. Catalysis Science & Technology, 2(9), 1767–1775. https://doi.org/10.1039/C2CY20109G
- Yin, D., Sun, J., Liu, Y., & Liu, B. (2020). Novel Benzothiazole Ionic Liquids as Catalysts for the Synthesis of Parabens. *Russian Journal of Organic Chemistry*, *56*(8), 1476–1483. https://doi.org/10.1134/S1070428020050205
- Zanchet, L., da Trindade, L. G., Bariviera, W., Nobre Borba, K. M., Santos, R. D. M., Paganin, V. A., de Oliveira, C. P., Ticianelli, E. A., Martini, E. M. A., & de Souza, M. O. (2020). 3-Triethylammonium propane sulfonate ionic liquids for Nafion-based composite membranes for PEM fuel cells. *Journal of Materials Science*, 55(16), 6928–6941. https://doi.org/10.1007/s10853-020-04454-4
- Zante, G., Braun, A., Masmoudi, A., Barillon, R., Trébouet, D., & Boltoeva, M. (2020).
 Solvent extraction fractionation of manganese, cobalt, nickel and lithium using ionic liquids and deep eutectic solvents. *Minerals Engineering*, 156, 106512.
 https://doi.org/https://doi.org/10.1016/j.mineng.2020.106512
- Zhang, C., Du, Z., Wang, J., Wang, J., Zhou, T., Li, B., Zhu, L., Li, W., & Hou, K. (2018). Exposed zebrafish (Danio rerio) to imidazolium-based ionic liquids with different anions and alkyl-chain lengths. *Chemosphere*, 203, 381–386. https://doi.org/https://doi.org/10.1016/j.chemosphere.2018.03.178
- Zhang, C., Zhang, S., Zhu, L., Wang, J., Wang, J., & Zhou, T. (2017). The acute toxic effects of 1-alkyl-3-methylimidazolium nitrate ionic liquids on Chlorella vulgaris and Daphnia magna. *Environmental Pollution*, 229, 887–895. https://doi.org/https://doi.org/10.1016/j.envpol.2017.07.055
- Zhang, L., Yu, R., Zhang, X., & Zhang, D. (2021). Ionic Liquid–Based Dispersive Liquid–Liquid Micro-extraction of Five Organophosphorus Pesticides in Coarse Cereals. *Food Analytical Methods*, *14*(1), 10–17. https://doi.org/10.1007/s12161-020-01851-y
- Zhang, S., Sun, N., He, X., Lu, X., & Zhang, X. (2006). Physical Properties of Ionic Liquids: Database and Evaluation. *Journal of Physical and Chemical Reference Data*, *35*(4), 1475–1517. https://doi.org/10.1063/1.2204959
- Zhao, H., & Toe, C. (2020). "Water-like" ammonium-based ionic liquids for lipase activation and enzymatic polymerization. *Process Biochemistry*, 98, 59–64. https://doi.org/https://doi.org/10.1016/j.procbio.2020.07.016
- Zhao, R., Jiang, S., Zhang, L., & Yu, Z. (2019). Mitochondrial electron transport chain, ROS generation and uncoupling (Review). *Int J Mol Med*, *44*(1), 3–15.

- https://doi.org/10.3892/ijmm.2019.4188
- Zheng, Y., Zheng, M., Ma, Z., Xin, B., Guo, R., & Xu, X. (2015). 8 Sugar Fatty Acid Esters (M. U. Ahmad & X. B. T.-P. L. Xu (eds.); pp. 215–243). Elsevier. https://doi.org/https://doi.org/10.1016/B978-1-63067-044-3.50012-1
- Zhou, H., Chen, L., Wei, Z., Lu, Y., Peng, C., Zhang, B., Zhao, X., Wu, L., & Wang, Y. (2019). Effect of Ionic Composition on Physicochemical Properties of Mono-Ether Functional Ionic Liquids. In *Molecules* (Vol. 24, Issue 17). https://doi.org/10.3390/molecules24173112